Preface

The experimental work described in this dissertation for the Masters degree was carried out in the School of Chemistry and Physics, University of KwaZulu-Natal, Westville campus from June 2012 to November 2014, under the close supervision of Dr Bernard Omondi Owaga (University of KwaZulu–Natal).

These studies represent original work by the author and have not otherwise been submitted in any form for degree or diploma to any tertiary institution. Where use has been made of the work of others it is duly acknowledge in the text.

This dissertation has been prepared according to the format outlined in the guidelines from the Faculty of Science and Agriculture of UKZN, (FHDR Approved 13 March 2007).

Declaration 1–Plagiarism

I Sizwe Joshua Zamisa declare that

1. The research reported in this thesis, except where otherwise indicated, and is my original research.
2. This thesis has not been submitted for any degree or examination at any other university.
3. This thesis does not contain other persons' data, pictures, graphs or other information, unless specifically acknowledged as being sourced from other persons.
4. This thesis does not contain other persons' writing, unless specifically acknowledge as being sourced from the researchers. Where other written sources have been quoted, then:
    a. Their words have been re–written but the general information attributed to them has been referenced
    b. Where their exact words have been used, then their writing has been placed in italics and inside quotation marks and referenced
5. This thesis does not contain text, graphics or tables copied and pasted from the internet, unless specifically acknowledge, and the source being detail in the thesis and in the references sections.

Signed ……

Declaration 2–Scientific Communications

Details of contribution to publications that form part and include research presented in this thesis.

Presentation

Parts of this work have been presented in two international conferences**.**

List of conferences

1. INORG2013 international conference Durban, South Africa between 30 June and 4 July 2013.

   Title of paper presented: **Synthesis and structural investigation of silver(I)-1,3,5-triaza-phosphaadamantane complexes**

   Authors: Sizwe J. Zamisa, Bernard Owaga

2. ICOMC2014, Sapparo, Japan,

   Title of paper presented: **Coordination complexes of silver(I) salts with tertiary phosphines - interesting structural studies**

   Authors: Bernard Owaga and Sizwe J. Zamisa

Signed ……..

Abstract

Novel discrete complexes and coordination polymers of silver(I) and the water soluble 1,3,5-triaza-7-phosphaadamantane (PTA) or N-methyl-1,3,5-triaza-7-phosphaadamantane (PTAMe) have been isolated from the reactions of various silver(I) salts (AgX; X = CN^-, CO_3^{2-}, NO_3^-, $O_2CCH_3^-$, $O_2CCF_3^-$, ClO_4^-, $O_3SCF_3^-$, $O_3SCCH_3^-$, BF_4^-) with PTA or PTAMe giving a total of 15 compounds. The Ag-PTA coordination compounds are named **DCC$_{1-3}$** for discrete complexes, **CP$_{1-5}$** for one dimensional coordination polymers and **CN$_{1-5}$** for two dimensional coordination networks while the Ag-PTAMe coordination compounds are named **m-CP$_{1-4}$** for one dimensional coordination polymers. The synthesized silver(I) coordination compounds were analysed using Nuclear Magnetic Resonance (NMR) spectroscopy, infrared spectroscopy (IR), Electron Spray Ionization Mass Spectrometry (ESI-MS), thermogravimetric analysis (TGA) and differential scanning calorimetry (DSC). Coordination of PTA and PTAMe via the phosphorus and nitrogen atoms of the PTA moieties was confirmed by ^{1}H-, and ^{31}P-NMR. IR spectroscopic studies confirmed the presence of ligands and the silver(I) salt counter ions used whilst the ESI-MS results showed m/z peaks that are attributed to the products, fragmentation of the polymeric species and the formation of multiple charged ionic species. Thermal stability studies (TGA and DSC) revealed that the silver(I)-PTA coordination compounds were thermally stable up to approximately 210 °C.

$[Ag(PTA)(\mu^2\text{-}O_2CCH_3)]_n.2H_2O$ (**CP$_2$**) and $[Ag(PTA)(\mu^1\text{-}O_2CCF_3)]_n$ (**CP$_3$**) formed double stranded, ladder-like structures in which the carboxylate anions bridge Ag(I) centres in a μ^2-O_2 and μ^1-O_2 fashions resulting in short and long Ag…Ag separation, respectively. $[Ag_2(\mu^2\text{-}O_2CCF_3)_2(\mu^1\text{-}O_2CCF_3)(PTAMe)]_n$ (**m-CP$_3$**) has a 1D single stranded coil-like structure which contains PTAMe groups coordinating via the phosphorus atom only. The polymer propagates via the trifluoroacetate groups which bridge the Ag(I) centres in an alternating μ_2-O_2 and μ_1-O_2 bridging modes. The two bridging modes of the trifluoroacetate groups also resulted in the formation of alternating segments displaying Ag…Ag interactions and non-Ag…Ag interactions along the coil-like polymer. 2D coordination networks $[Ag(PTA)(H_2O)]_n(NO_3)_n$ (**CN$_1$**) and $[Ag_2(PTA)_2(H_2O)]_n(O_3SCF_3)_{2n}$ (**CN$_2$**) have stacked 2D corrugated sheet-like structures with

channels filled with uncoordinated anions between the stacked sheets. The 2D networks contained PTA groups that displayed an alternating *P*-,*N*-,*N*'- coordination mode which is responsible for the growth of the polymer. O-H…O, O-H…N, C-H…O, C-H…N and C-H…F types of hydrogen bonding were observed in most crystal structures.

This work also included the preparation of a silver(I)-PTA coordination compound containing ancillary ligands such as 4-nitrophenol from the solvothermal reaction of $AgNO_3$, PTA and 4-nitrophenol (4-NP). In an attempt to grow crystals for structural determination, a discrete, tri-coordinated silver-PTA complex $[Ag(PTA)_3][4\text{-}NP]_{10}$ (**DCC$_3$**) crystallized in a monoclinic system that co-crystallized along with ten molecules of 4-nitrophenol and a two-dimensional silver(I)-PTA sheet-like polymer $[Ag_2(PTA)_2(\mu_1\text{-}NO_3)(H_2O)](NO_3)(4\text{-}NP)(H_2O)$ (**CN$_5$**) co-crystallized with the 4-NP molecules positioned in between the sheets were obtained.

Acknowledgements

First and foremost, I thank my heavenly Father for all his blessings he has brought upon me.

I thank my one and only supervisor Dr Bernard Omondi Owaga for his support, encouragement and guidance throughout this research work. I not only thank him for his academic support but for all the life's lessons too. You are my mentor, my brother and I would not have done it without you, Boss.

I thank all my lab mates at the School of Chemistry and Physic especially Ekemini Akpan, Eric Njogu, Wisedom Munzeiwa and the members of the nanochemistry group for sharing ideas and helping me improve my presentation skills whenever I had to give PowerPoint presentations.

I thank my brothers (Siphiwe Zamisa and Mfanelo Zamisa), my parents (Mrs Topile Zamisa and Mr Sipho Zamisa) and my daughter (Nozipho) for their never-ending love and support throughout all my studies. I hope I made you guys proud as you read this.

Special thanks goes to my lover (Nomvula Madlala) who was there for me through the good and bad times. Thanks for bearing with me and giving me strength to keep on pushing especially during the lengthy write-up. I love you very much.

I also thank the UKZN's College of Agriculture, Engineering and Science for their financial support during this work.

Table of contents

List of tables

List of figures

Abbreviations

1D	One dimensional
2D	Two dimensional
3D	Three dimensional
CP	Coordination polymers
CN	Coordination networks
PTA	1,3,5-Triaza-7-phosphaadamantane
PTAMe	l-Methyl-3,5-diaza-l-azonia-7-phosphaadamantane
PTAMeI	l-Methyl-3,5-diaza-l-azonia-7-phosphaadamantane iodide
NMR	Nuclear Magnetic Resonance
ESI-MS	Electron Spray Ionisation Mass Spectrometry
ESI(+)	Electron Spray Ionisation in positive mode
TGA	Thermogravimetric Analysis
DSC	Differential Scanning Calorimetry
SC-XRD	Single Crystal X-ray Diffractometer
IR	Infrared spectroscopy
vs	Very strong
s	Strong
m	Medium
w	Weak
br	Broad

Chapter 1

1 Introduction and literature background

2.1 Introduction

The synthesis of novel compounds with unique or enhanced physical and chemical properties for the improvement of any system, is still a major and on-going area of research.[1] The novelty of this area is usually centred on crystal engineering which aids in understanding the structure-property relationship of compounds in their solid state. This in turn enables the fine tuning of properties such as solubility,[2] magnetism,[3] luminescence[4] and porosity[5] by altering certain molecules of the structure.[6] In inorganic chemistry, crystal engineering has led to the formation of different classes of coordination compounds that include discrete compounds,[7] coordination polymers [7a, b, 8] and coordination networks.[7d, 9] According to Batten *et al.*, the difference between these coordination compounds is the dimensionality that the complexes possess.[10] Discrete compounds are formed by coordination bonds that do not result in the formation of polymeric compounds; thus zero dimensional (0D) structures are obtained. Coordination polymers on the other hand, can have varied dimensionality such as one dimensional (1D), two dimensional (2D) or three dimensional (3D) structures.[10] Coordination polymers and networks usually consist of transition metal ions and organic ligands which are linked together by covalent or non-covalent bonds to form multi-dimensional molecular architectures with different topologies.[10] One of the key elements that leads to the formation of coordination polymers and networks is the organic bridging ligand used. The ligand normally contains donor atoms that coordinate to transition metal atoms with unsaturated coordination environment to form various multi-dimensional structures as shown in Scheme 1.[11] Other factors that contribute towards the topology of coordination compounds include the anion from metal salt precursor, the stoichiometric ratio of metal to ligand used, and the reaction conditions. The impact of the different factors is explained in greater detail in Section 2.3.1.

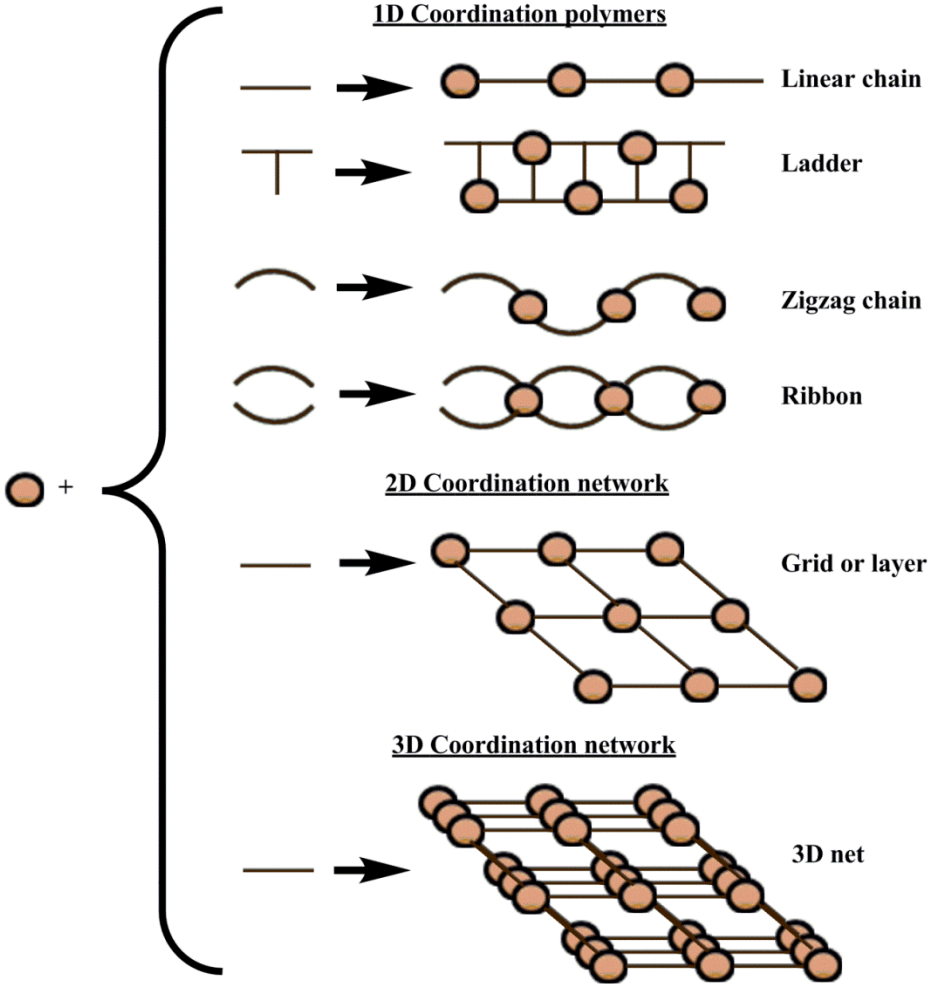

Scheme 1: The different structures of some coordination polymers and networks. The nodes and the lines represent the metal ions and the bridging ligands respectively.

Besides using coordination bonding to construct multidimensional molecular architectures, strong intermolecular interactions such as hydrogen bonding or π-π interactions can also lead to the formation of 3D structures also known as supramolecular architectures.[1] Stacking of aromatic molecular entities such as bipyridine,[12] and phenanthroline,[13] is usually the driving force for the formation of π-π interactions and this result in improved stability of such coordination compounds both in solid and solution states.[13a] On the other hand, the presence of ligands with hydrogen-donor or hydrogen-acceptor groups and polar solvents often drives hydrogen bonding between coordination entities and solvent molecules. Crystal engineering is utilized to strategically combine intermolecular interactions with discrete complexes, coordination polymers or 2D coordination networks into multi-dimensional supramolecular architectures.[13a]

2.2 Aims of the project

This work is aimed at using the concept of crystal engineering to prepare and comprehensively analyze the crystal structures of silver(I)-1,3,5-triaza-7-phosphaadamantane coordination compounds containing various anions to understand the influence of anions and hydrogen bonding interactions on the molecular architecture. We also varied the nature of PTA by alkylating one of the nitrogen atoms of PTA to prepare 1-methyl-3,5-diaza-1-azonia-7-phosphatricyclo[3.3.1.1]decane iodide (PTAMeI) which serves as controlling mechanism for the formation of multi-dimensional molecular architectures. To the best of our knowledge no alkylated-PTA silver(I) based coordination compounds have been structurally reported before; thus extending the novelty of this work.

The following is a summary of the goals set for this project:

- To synthesize and characterize the main ligands which are PTA and PTAMeI.
- To synthesize and characterize silver(I)-based coordination compounds using the main ligands, whilst varying the silver(I) salt precursor.
- To investigate the crystal structures of the silver(I)-based coordination compounds and examining their thermal properties.

Chapters 1 and 2 focus on literature background and experimental procedures respectively, while Chapter 3 covers the rationale behind the synthesis of all the silver(I)-based coordination compounds including the elucidation of spectroscopic data collected, thermal stability determinations and finally the analyses of crystal structures obtained in this work. The conclusions drawn based on all the findings are given in Chapter 4 and the raw data of this work is situated in the appendix section.

2.3 Literature review

Silver(I) coordination compounds have a d^{10} electronic configuration; thus making them diamagnetic. They are also known to possess various possible coordination geometries ranging from two-coordinate (linear) to eight-coordinate (tetragonal prism). The different coordination modes that silver(I) complexes adopt are summarized in Table 1.[14]

Table 1: Possible coordination numbers and geometries of silver(I) coordinaiton compounds

Coordination number	Coordination geometry
2	Linear
3	T-shaped
3	Triangular
4	Square planar
4	Tetrahedral
5	Trigonal bipyramidal
5	Tetragonal pyramidal
6	Octahedral
6	Trigonal prism
7	Pentagonal bipyramidal
8	Tetragonal prism

One of the key factors that influence the coordination environment of silver(I) complexes is the steric demand of ligands whereby bulky ligands favour the formation of low coordination numbers. In contrast, less sterically demanding ligands result in complexes with higher coordination numbers. For example, Fitchett *et al.* reported 1D coordination polymers with linear two coordinate geometric environment around silver(I) metal centres using sterically demanding chiral heterocyclic ligands[15] as opposed to tetra-coordinated silver(I) complexes with relatively less sterically demanding phosphine ligands reported by Santini and co-workers.[16] The flexibility of the coordination environment around silver(I) metal centres together with ligands possessing various coordination abilities, yields molecular architectures with diverse dimensionalities.[14a, 17]

2.3.1 Factors that influence the topology of coordination compounds

The choice of ligands to be used in the synthesis of coordination compounds not only has an impact on the coordination environment of metal ion centres but it also affects the overall molecular architecture of the product obtained.[17] Some of the features that ligands possess which allow them to manipulate the overall structure include the shape or possible conformations a ligand can take, the number, the orientation and the type of donor atoms present on a ligand.

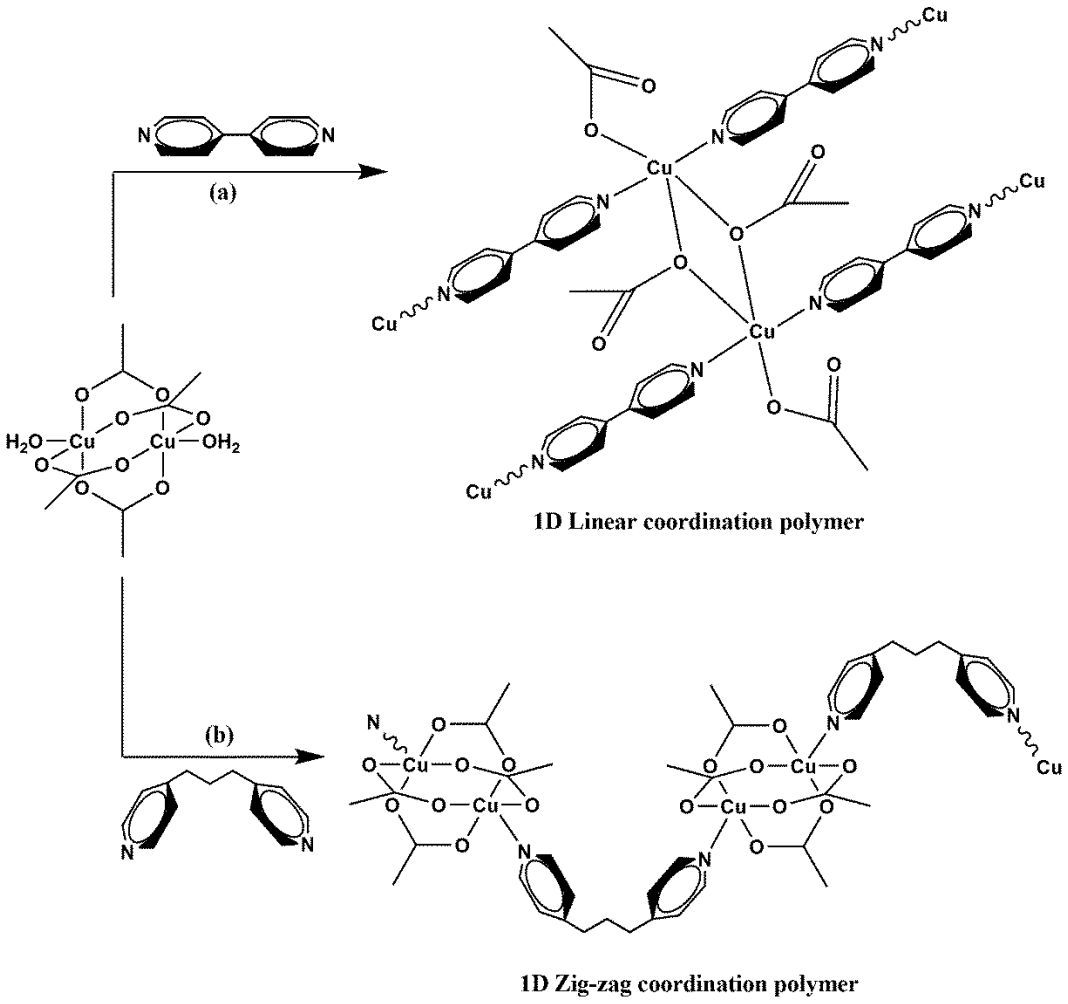

Scheme 2: Construction of structurally different copper(II) based coordination polymers using (a) 4,4'-bipyridine and (b) 1,3-bis(4-pyridyl)propane

From Scheme 2 it was noted that the shape of the bridging ligands can influence the outcome of the overall structure of the copper(II) based coordination polymers. In route (a), 4,4'-bipyridine was used. This is a rigid, linear ligand; thus the resultant copper(II) coordination polymer obtained by Zamisa *et al.* was a 1D linear structure.[12] In contrast, the use of a

flexible ligand such as 1,3-bis(4-pyridyl)propane in route (b) led to the formation of a 1D zig-zag copper(II) based coordination polymer.[18]

The number of donor atoms on a ligand can contribute and often determine the dimensionality of the product. Usually ligands with a single donor atom such as trialkyl-substituted phosphines,[19] tend to lead to the formation of discrete coordination compounds. However, oligomers and polymeric structures containing one donor atom have been reported by Bowmaker and co-workers whereby the ancillary ligand thiocyanate from the silver(I) salt acted as the bridging ligand.[20] Ligands that contain two or more donor atoms have the ability to form either discrete or polymeric compounds and this is determined by the orientation of the donor atoms which affects the denticity of ligands.

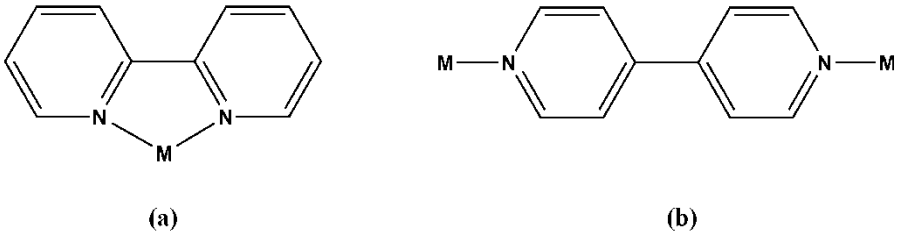

Figure 1: Denticity of (a) 2,2'-bipyridine and (b) 4,4'-bipyridine where M represents any metal

For an example, the two isomers of bipyridine, mainly 2,2'-bipyridine and 4,4'-bipyridine have different denticities whereby 2,2'-bipyridine is bidentate and hinders formation of multidimensional polymeric compounds as shown in Figure 1(a).[13a, 21] In contrast, 4,4'-bipyridine is monodentate and can form polymeric compounds by linking two metal centres as shown in Figure 1(b). [22] On the other hand, the use of ligands with different donor atoms gives rise to the possibility of forming multinuclear compounds. This is demonstrated by Zhang and co-workers, whereby Schiff base ligands with an oxygen donor atom are used to construct silver(I) coordination networks by bridging the metal centres via the terminal oxygen and γ-carbon atoms of the ligand.[23]

The choice of the metal salt precursor used also affects the structure of coordination polymers. Metal salts contain anions which can either be coordinating or non-coordinating. Coordinating anions are present in the inner coordination sphere and form an integral part in coordination polymers and networks. This often result in a neutral coordination compound and examples of coordinating anions include cyanide[24], thiocyanide[25] and halides.[26] On

the other hand, non-coordinating anions are present in the outer coordination sphere and result in the formation of cationic coordination compounds. Examples of non-coordinating anions include boron tetrafluoride[27] and phosphorus hexafluoride.[21] However, anions such as nitrate,[28] carbonate,[29] carboxylates[26a, 30] and perchlorate[31] often display capabilities of either being coordinating or non-coordinating.[32] According to Su and co-workers the coordinating ability of weakly coordinating anions under similar conditions increases in the following approximate order: phosphorus hexafluoride, perchlorate, boron tetraflouride < triflate < carboxylate < nitrate.[33] The coordination abilities of these anions are altered by the reaction conditions used to synthesize coordination compounds[34] which include the stoichiometric ratio of the metal precursor to the bridging ligand and the solvent used.[32, 34]

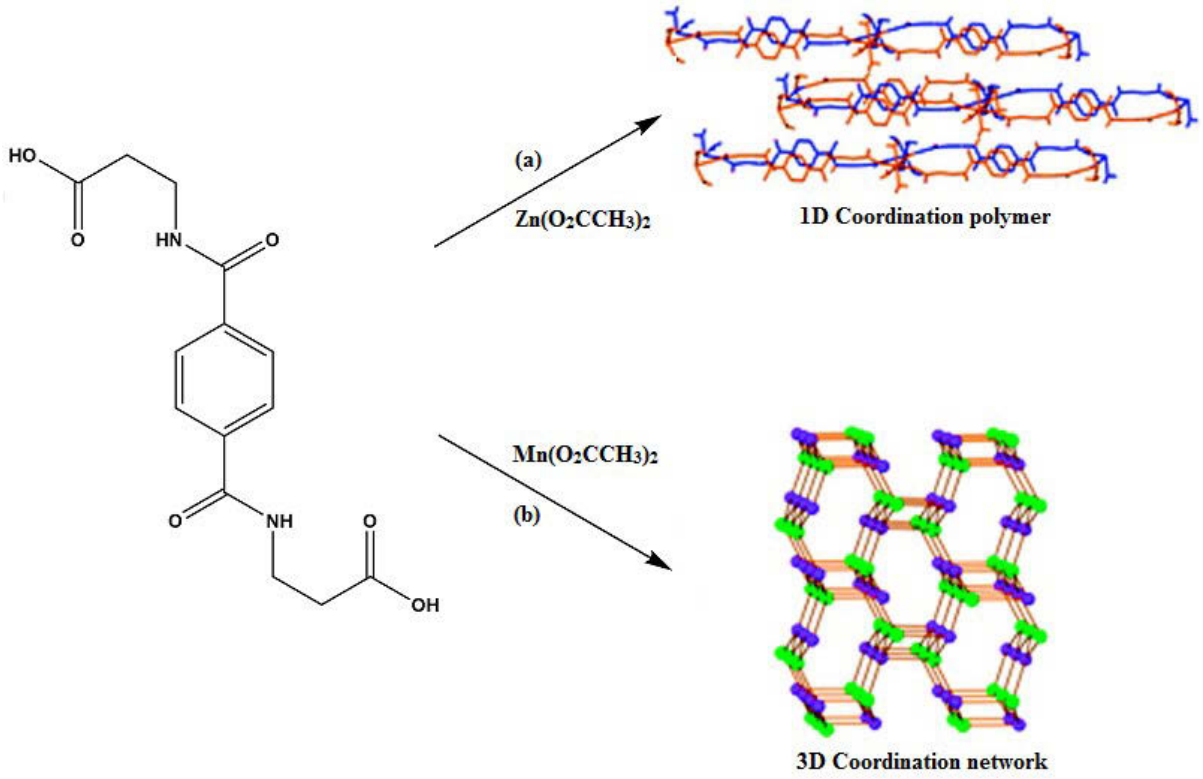

Figure 2: Synthesis of structurally distinct (a) manganese-based 3D coordination network and (b) zinc-based 1D coordination polymer

Morrison *et al.* reported that the molecular architecture of coordination compounds is affected by the radius of the metal ion. The reaction of the pseudopeptic ligand with manganese acetate and zinc acetate (as shown in Figure 2 as route (a) and (b), respectively) led to the formation of a manganese-based 3D coordination network and a zinc-based 1D coordination polymer.[35]

2.3.2 Silver(I) coordination compounds containing 1,3,5-triaza-7-phosphaadamante

The use of tertiary phosphine ligands that contain nitrogen donor atoms has proven to be useful in the synthesis of coordination compounds, particularly in the self-assembly of coordination polymers and networks by applying the Hard and Soft Acids and Bases (HSAB) theory.[33] For example, Ag^{+} is a soft acid and will preferentially coordinate to a soft base donor atom such as phosphorus and introducing a hard acid metal such as Sn^{2+} will result in the formation of a multinuclear compound since Sn^{2+} will preferentially coordinate to a hard base donor atom such as nitrogen. Some examples of the nitrogen-containing phosphine ligands include 3,6-bis(diphenylphosphino)Pyridazine ($DPPP_x$), 2,6-bis(diphenylphosphino)pyridine ($DPPP_y$) and 1,3,5-triaza-7-phosphaadamantane (PTA) are shown in Figure 3 .[8, 33, 36]

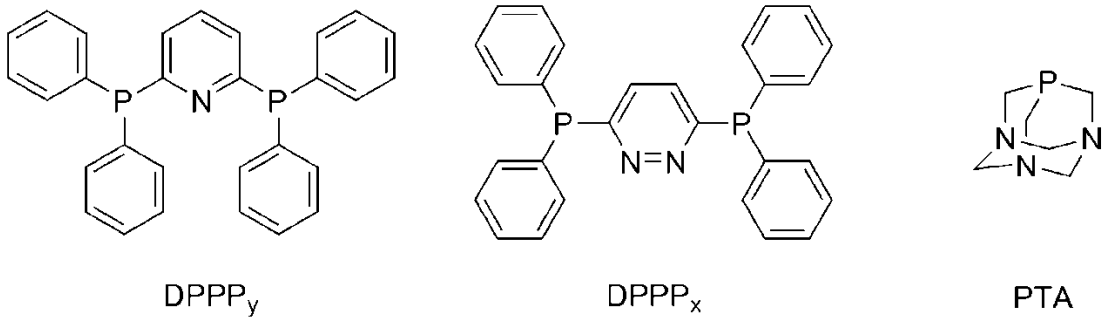

Figure 3: Examples of nitrogen-containing phosphine ligands mentioned in text

From the "building block methodology" point of view, for the construction of water-soluble coordination polymers, the use of water-soluble "building blocks" is essential.[37] One of the compounds that fit the criteria perfectly is PTA. It is a water soluble 3D cage-like amino-phosphine which has been greatly investigated in recent years due to the good solubility of transition metal PTA complexes in water; thus paving the way for possible applications in aqueous phase catalysis and medicine.[36b] PTA has one phosphorus and three nitrogen donor atoms which can be used to coordinate to the metal centres and this leads to the investigation of the structure and application of phosphorus- and nitrogen-linked coordination polymers.[8] The electronic properties of phosphine type ligands indicate that they possess both σ-donor and π-acceptor traits. This means that the ligand can donate electrons inductively to the metal via the σ bond and can perform back donation of electrons from the metallic centre to the empty anti-bonding orbitals of the ligand. This is very important since it aids in the

stabilization of metal complexes with low oxidation state.[36b, 38] The degree of π-acceptance and σ-donation relies strongly on the substituents of the ligand.[38] The extent of back-donation (or back bonding) is lowered by the presence of the alkyl substituents; thus one can then hypothesize that the PTA is of this nature.[36b, 38]

The design and synthesis of PTA containing coordination compounds is a popular area of research due to the various possible coordination modes of PTA which are shown in Figure 4 where M represents any metal.[8-9, 21, 39]

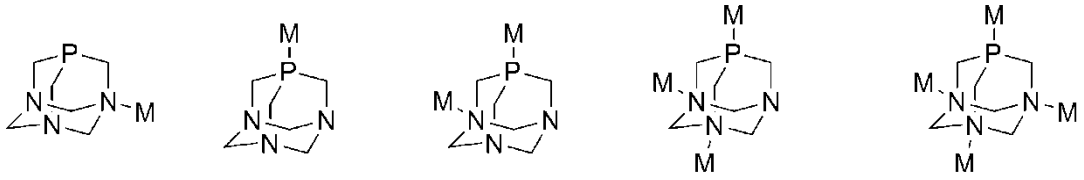

Figure 4: Possible coordination modes of PTA

Discrete complexes are often obtained when the metal coordination mode of PTA is via N- or *P*- only as shown Figure 4a and 4b, respectively.[39a, 40] The first copper complexes bearing the PTA ligand was reported in 2007, whereby $Cu(NO_3)_2$ and PTA were reacted in acidic aqueous solution at room temperature to yield a protonated copper(I) compound $[Cu(PTAH)_4](NO_3)_5$. After treating the acidic complex with sodium hydroxide in water, the deprotonated PTA derivative copper(I) compound $[Cu(PTA)_4](NO_3)$ was formed as shown in Figure 5a.[39a] The alternating *P*-,*N*- coordination mode of PTA often leads to the formation of 1D ladder-like copper coordination polymers whilst the azide anion in this case, links together two metal centres of the two Cu-PTA backbone strands (see Figure 5b).[7b]

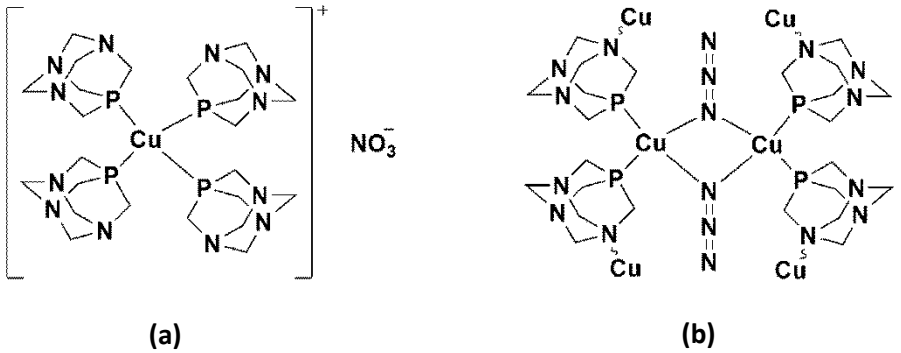

Figure 5: Copper-PTA based coordination compounds

Silver is in the same group in the periodic table of elements as copper and hence one can anticipate that silver should display similar properties as copper. We shall now look at the discrete and polymeric silver(I) PTA coordination compounds. To achieve discrete silver(I) PTA coordination compounds, two requirements have to be met. Firstly, the coordination mode of PTA has to be either *P*- or *N*- only since these coordination modes do not promote the formation of polymeric compounds and secondly, the ancillary ligand used should not bridge metal centres.[21, 33] Smolenski and co-workers have successfully met the above mentioned requirements by using 2,2'-bipyridine to inhibit the formation and growth of multidimensional coordination polymers. The coordination mode of *P*- only also prevented the formation of a polymeric compound; thus a discrete tetra-coordinated silver(I) complex was obtained (Figure 6).[21]

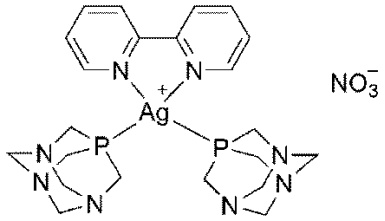

Figure 6: Discrete silver(I)-PTA coordination compound

One dimensional silver(I)-PTA coordination polymers are normally formed by the alternating *P*-,*N*- coordination mode of PTA with the ancillary ligand preventing growth in other directions.[8] For an example, $[Ag(benzoate)(\mu\text{-}PTA)]_n$ reported by Lis and workers displayed the alternating *P*-,*N*- coordination mode of PTA which led to the formation of a zig-zag 1D coordination polymer with the benzoate ancillary ligand coordinating to the tri-coordinate silver(I) metal centre via one oxygen atom (Figure 7a).[8] Another instance was reported by Smolenski and co-workers whereby a similar compound shown in Figure 6 was obtained but differs by having an alternating *P*-,*N*- coordination mode of PTA which resulted in the formation of a linear 1D coordination polymer (Figure 7b).[21]

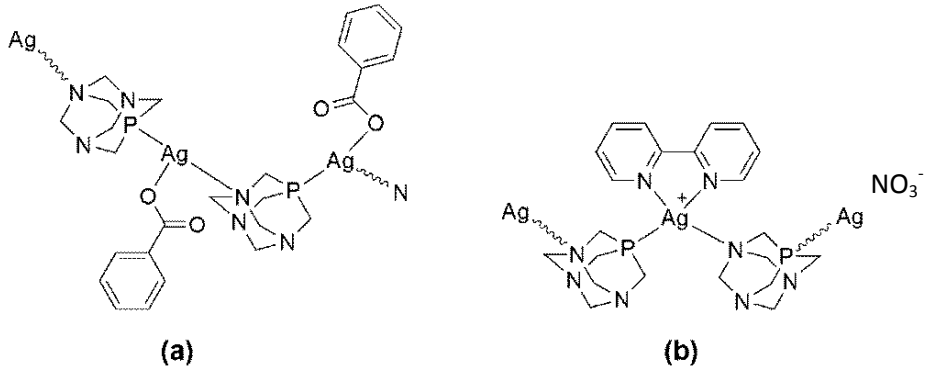

Figure 7: Representations of 1D silver(I)-PTA coordination polymers explained in the text.

Two dimensional silver(I)-PTA coordination networks are normally formed in two ways. Firstly, the coordination mode of PTA needs to be *P*-,*N*-,*N*'- with the silver(I) metal centres having a tetrahedral geometry and the ancillary ligand not having any bridging capabilities.[41] For example, Fabian *et al.* were among the first to report the *P*-,*N*-,*N*'-coordination mode of PTA with a coordinated water on a tetra-coordinated silver(I) metal centre which led to the formation of a 2D coordination network (Figure 8b).[41] The second route of forming 2D coordination networks is by using an ancillary ligand that can bridge metal centres in one dimension whilst the alternating *P*-,*N*- coordination mode of PTA results in the growth of the polymer along another dimension. Lis and co-workers have reported this combination of *P*-,*N*- coordination of PTA with the bridging ability of the ancillary terephthalate ligand to form 2D coordination networks (Figure 8a).[8]

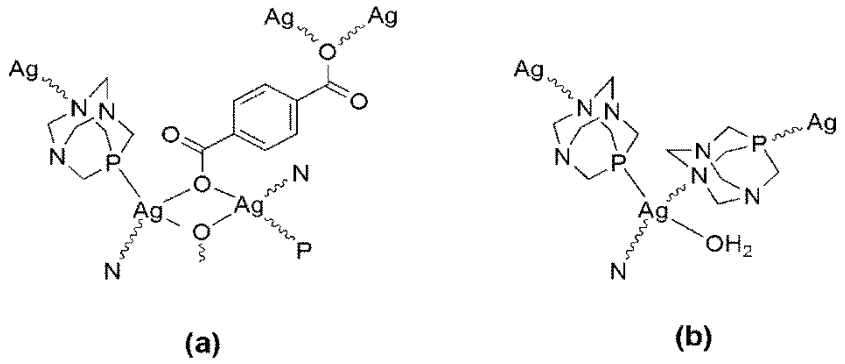

Figure 8: Representations of 2D silver(I)-PTA coordination networks explained in the text. The nitrate moiety in (b) is omitted for clarity.

Three dimensional silver(I)-PTA coordination networks are constructed by combining the *P*-,*N*-,*N*'- coordination mode of PTA (results in growth of a polymer in two dimensions) with the bridging ability of the ancillary ligand. This is what was reported by Kirillov *et al.* when the bridging biphenyl-4,4'-dicarboxylate ancillary ligand was used (Figure 9).[9a]

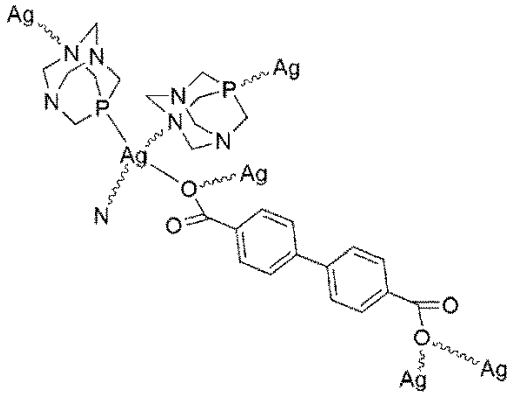

Figure 9: Representations of a 3D silver(I)-PTA coordination network explained in the text

1.3.3 N-alkylated PTA compounds

Alkylation of PTA via the nitrogen atom has received great attention over recent years in the effort of fine tuning properties such as the solubility of PTA.[42] Alkylation is achieved by reacting an alkyl halide with PTA and depending on the nature of the substituent, the solubility of the resultant compound will vary from that of PTA whereby short alkyl substituents lead to compounds with greater solubility in water as opposed to substituents with long alkyl groups.[2, 42] The use of PTA derivatives in coordination chemistry is useful in crystal engineering whereby nitrogen atoms can be made unavailable for coordination by alkylation; thus controlling the number of nitrogen atoms available for coordination. One of the PTA derivatives we are interested in, is N-methyl-1,3,5-triaza-7-phosphaadamantane (PTAMe) as shown in Figure 10.

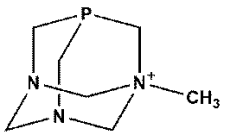

Figure 10: Diagram of PTAMe with the anion omitted for clarity

Copper(I) coordination compounds containing PTAMe have been reported by Porchia and co-workers whereby only discrete complexes were obtained.[42] However, no silver(I) coordination compounds containing alkylated PTA derivatives have been reported. Thus one of the objectives of this work is to investigate the silver(I) compounds containing alkylated PTA derivatives.

1.3.4 Synthesis of coordination compounds

Synthetic technique is a major factor that governs the formation of coordination compounds. The choice of a synthetic technique is normally based on the stability of the precursors under certain reaction conditions. These techniques include solvothermal, mechanochemical and ambient temperature.[43]

1.3.4.1 Solvothermal technique

Solvothermal technique involves the metal precursor and the ancillary ligand being dissolved in an appropriate solvent and heated under reflux or placed in a sealed digestion bomb and heated to elevated temperatures for a set period of time.[43b] Then slow cooling is applied to afford crystalline compounds.[43a] At times the resultant compound forms upon recrystallization of the crude product followed by controlled evaporation rate of the solvent.[43a] This technique often results in the retention of guest molecules such as solvent within the coordination framework structure.[43a] Attempts to remove the guest molecules by controlled heating sometimes leads to the loss of crystallinity of the coordination framework due to the fact that the guest molecules form an integral part of the coordination polymer. The disadvantage of using this technique is that thermally sensitive precursors and ligands cannot be used.[43a]

1.3.4.2 Mechanochemical technique

Mechanochemical technique is a green approach to the synthesis of coordination polymers since it uses minimum or no solvent at all.[43c] The general synthetic procedure involves the reactants being ground using a pestle and mortar or a ball mill to produce coordination polymers of high yields due to the fact that they are prepared in one pot reaction.[26b] It is relatively quick and easy technique as compared to solvothermal methods. The one disadvantage to using this technique at times is the difficulty of structural investigation of products by single crystal X-ray diffraction (SCXRD) due to the lack of solubility of products.[26b] Mechanochemical techniques are subdivided into three categories which are neat grinding, grinding-annealing and liquid assisted grinding.[26b] Neat grinding is the most basic form of mechanosynthesis and involves grinding of the reactants at ambient temperature and in the presence of air. When using neat grinding, the reactivity is favoured for organic ligands and metal precursors that are solvated.[26b] It is suggested that the solvent molecules acts as a liquid phase when liberated during grinding which then facilitates mechnochemical reactions and the formation of porous structures by host-guest inclusion in product.[26b] Grinding-annealing is a two-step mechanosynthesis which involves neat grinding followed by heating to expel solvent or gas molecules and results in the formation of a new product.[26b] It is during the heating stage whereby a subsequent reaction occurs that leads to a product that is different from that obtained from neat grinding. Lastly, liquid

assisted grinding is similar to neat grinding but a small amount of a liquid phase is added to facilitate a mechanochemical reaction.[26b] Liquid assisted grinding is often used for co-crystal synthesis and as compared to neat grinding, it does not form amorphous impurities.[26b]

1.3.4.3 Ambient temperature technique

Ambient temperature technique avoids decomposition of reactants at elevated temperatures. Stirring reactants at room temperature or carefully layering a solution containing ligand over a solution containing metal in a test tube to allow slow diffusion of the reactants to produce polymeric compounds are examples of ambient temperature technique.[44]

1.3.5 Characterization of silver(I)-PTA coordination compounds

Silver(I)-PTA coordination compounds are normally characterized using standard characterization techniques due to their excellent solubility. This allows them to be analysed using solution Nuclear Magnetic Resonance (NMR) spectroscopy experiments such as ^{1}H NMR and ^{31}P NMR. NMR is useful in determining whether coordination of PTA onto silver(I) metal centres occurred via the phosphorus or nitrogen atoms. When there is coordination via the phosphorous atom, there is usually a shift of the phosphorous peak to higher frequencies in ^{31}P NMR spectra which is different to uncoordinated PTA. The phosphorus peak appears as a broad singlet with no J coupling observed between Ag and P nuclei. This is due to the fast ligand exchange which is typical of silver monophosphine coordination compounds.[8-9] If there is coordination via PTA's nitrogen atoms, then two doublets are usually observed in the ^{1}H NMR spectra which correspond to the diastereotropic methylene protons between the nitrogen atoms. Infrared (IR) spectroscopy provides complimentary information which confirms the presence of both PTA and ancillary ligands in the product.[8-9] For the determination of molecular weight of silver(I)-PTA coordination compounds, a soft ionization source such as electron spray ionization mass spectrometer in the positive mode (ESI-MS^{+}) is normally used.[8-9] In solution, silver coordination compounds are known to dissociate to give smaller compounds that are often solvated; thus mixtures of monomers, oligomers and coordination entities containing solvent molecules are observed in the mass spectra and that molecular ion peaks, particularly for coordination

polymers and networks are not always observed but rather the fragments of the parent molecule.[45] For an example, Kirillov and co-workers reported a fragment of a 3D coordination network $[Ag_2(\mu_2\text{-bpca})(\mu_3\text{-PTA})_2]_n \cdot 2nH_2O$ with 771 m/z corresponding to the monomer $[Ag_2(PTA)_2(Hbpca)]^+$.[9a]. Other peaks observed in the mass spectra include 421 m/z and 264 m/z which correspond respectively to $[Ag(PTA)_2]^+$ and $[Ag(PTA)]^+$,[9a] are found in similar coordination compounds containing silver(I) and PTA.[46] The structural determinations of silver(I)-PTA coordination compounds is done using single crystal x-ray diffraction (SC-XRD) which allows for the investigation of molecular architecture, reveals coordination environment, intermolecular interactions (such as hydrogen bonding that can lead to the formation of supramolecular architectures) and metal-metal interactions (which are observed if the distance between two silver(I) metal centres are smaller than the ionic diameter of silver).[2, 46-47]

1.3.6 Applications of PTA based silver(I) coordination compounds

Silver coordination compounds are known for their use in medicine as antimicrobial agents but over the years, the discovery of antibiotics has led to the shift of interest on the use of silver compounds.[45] However, the increasing resistance of microorganisms towards antibiotics has sparked renewed research interest on the use silver compounds because at a molecular level, silver targets cell membrane and interacts with enzymes and proteins including DNA.[45] Banti and co-workers reported a novel silver(I) iodide coordination compound (containing triphenylphosphine ligands) which proved to be bioactive since it can interact with DNA and influence enzyme activity.[48] Although the detailed mechanism of action is still unknown, it is postulated that there is little probability that cells can develop resistance when using silver coordination compounds as antimicrobial agents.[45]

1.4 References

[1] D. Braga, L. Maini, M. Polito, L. Scaccianoce, G. Cojazzi and F. Grepioni, *Coordination Chemistry Reviews*, **2001**, *216–217*, 225-248.

[2] D. A. Krogstad, K. E. Gohmann, T. L. Sunderland, A. L. Geis, P. Bergamini, L. Marvelli and V. G. Young, *Inorganica Chimica Acta*, **2009**, *362*, 3049-3055.

[3] Q.-W. Li, J.-L. Liu, J.-H. Jia, J.-D. Leng, W.-Q. Lin, Y.-C. Chen and M.-L. Tong, *Dalton Transactions*, **2013**, *42*, 11262-11270.

[4] M. D. Allendorf, C. A. Bauer, R. K. Bhakta and R. J. T. Houk, *Chemical Society Reviews*, **2009**, *38*, 1330-1352.

[5] a) T. M. Reineke, M. Eddaoudi, M. O'Keeffe and O. M. Yaghi, *Angewandte Chemie International Edition*, **1999**, *38*, 2590-2594; b) T. M. Reineke, M. Eddaoudi, M. Fehr, D. Kelley and O. M. Yaghi, *Journal of the American Chemical Society*, **1999**, *121*, 1651-1657; c) M. Eddaoudi, H. Li and O. M. Yaghi, *Journal of the American Chemical Society* **2000**, *122*, 1391-1397.

[6] a) S. R. Batten, *Current Opinion in Solid State and Materials Science*, **2001**, *5*, 107-114; b) M. Kato, T. Fujihara, D. Yano and A. Nagasawa, *Crystal Engineering Communication*, **2008**, *10*, 1460-1466; c) P. Erk, H. Hengelsberg, M. F. Haddow and R. van Gelder, *Crystal Engineering Communication*, **2004**, *6*, 475-483.

[7] a) A. Biswas, S. Mondal, L. Mandal, A. Jana, P. Chakraborty and S. Mohanta, *Inorganica Chimica Acta*, **2014**, *414*, 199-209; b) Ł. Jaremko, A. M. Kirillov, P. Smoleński and A. J. L. Pombeiro, *Crystal Growth & Design*, **2009**, *9*, 3006-3010; c) D. N. Akbayeva, L. Gonsalvi, W. Oberhauser, M. Peruzzini, F. Vizza, P. Brüggeller, A. Romerosa, G. Sava and A. Bergamo, *Chemical Communications*, **2003**, 264-265; d) M.-C. Brandys and R. J. Puddephatt, *Chemical Communications*, **2001**, 1508-1509.

[8] A. Lis, M. F. C. Guedes da Silva, A. M. Kirillov, P. Smoleński and A. J. L. Pombeiro, *Crystal Growth & Design*, **2010**, *10*, 5244-5253.

[9] a) A. M. Kirillov, S. W. Wieczorek, M. F. C. Guedes da Silva, J. Sokolnicki, P. Smoleński and A. J. L. Pombeiro, *Crystal Engineering Communication*, **2011**, *13*, 6329; b) J.-Y. Li, Z. Yan, Z.-P. Ni, Z.-M. Zhang, Y.-C. Chen, W. Liu and M.-L. Tong, *Inorganic Chemistry*, **2014**, 53, 4039–4046.

[10] S. R. Batten, N. R. Champness, X.-M. Chen, J. Garcia-Martinez, S. Kitagawa, L. Ohrstrom, M. O'Keeffe, M. P. Suh and J. Reedijk, *Crystal Engineering Communication*, **2012**, *14*, 3001-3004.

[11] K. Katagiri, T. Sakai, M. Hishikawa, H. Masu, M. Tominaga, K. Yamaguchi and I. Azumaya, *Crystal Growth & Design*, **2013**, *14*, 199-206.

[12] S. J. Zamisa, P. Ndungu and B. Omondi, *Acta Crystallographica Section C*, **2013**, *69*, 1100-1103.

[13] a) B.-H. Ye, M.-L. Tong and X.-M. Chen, *Coordination Chemistry Reviews*, **2005**, *249*, 545-565; b) Y.-Q. Zheng, J.-L. Lin and J. Sun, *Zeitschrift für anorganische und allgemeine Chemie*, **2001**, *627*, 1059-1065; c) Y.-Q. Zheng, J. Sun and J.-L. Lin, *Zeitschrift für anorganische und allgemeine Chemie*, **2000**, *626*, 816-818.

[14] a) W.-Y. Sun and Z.-S. Bai in *Supramolecular chemistry of silver*, *Vol.* (Ed. M. Harmata), John Wiley & Sons, Inc, Canada, **2010**, 329-355; b) P. J. Steel and C. M. Fitchett, *Coordination Chemistry Reviews*, **2008**, *252*, 990-1006.

[15] C. M. Fitchett and P. J. Steel, *Dalton Transactions*, **2006**, 4886-4888.

[16] C. Santini, M. Pellei, G. Papini, B. Morresi, R. Galassi, S. Ricci, F. Tisato, M. Porchia, M. P. Rigobello, V. Gandin and C. Marzano, *Journal of Inorganic Biochemistry*, **2011**, *105*, 232-240.

[17] X.-M. Chen in *Chapter 10 - Assembly Chemistry of Coordination Polymers*, *Vol.* Eds.: R. Xu, W. Pang and Q. Huo), Elsevier, Amsterdam, **2011**, 207-225.

[18] S. R. Batten, *Current Opinion in Solid State and Materials Science*, **2001**, 107-114

[19] M. Bardají, O. Crespo, A. Laguna and A. K. Fischer, *Inorganica Chimica Acta*, **2000**, *304*, 7-16.

[20] G. A. Bowmaker, C. Di Nicola, Effendy, J. V. Hanna, P. C. Healy, S. P. King, F. Marchetti, C. Pettinari, W. T. Robinson, B. W. Skelton, A. N. Sobolev, A. Tabacaru and A. H. White, *Dalton Transactions*, **2013**, *42*, 277-291.

[21] P. Smolenski, S. W. Jaros, C. Pettinari, G. Lupidi, L. Quassinti, M. Bramucci, L. A. Vitali, D. Petrelli, A. Kochel and A. M. Kirillov, *Dalton Transactions*, **2013**, *42*, 6572-6581.

[22] H. Kajiro, A. Kondo, K. Kaneko and H. Kanoh, *International Journal of Molecular Sciences*, **2010**, *11*, 3803-3845.

[23] Q.-L. Zhang, B.-X. Zhu, Y.-Q. Zhang, Z. Tao, J. K. Clegg, L. F. Lindoy and G. Wei, *Crystal Growth & Design*, **2011**, *11*, 5688-5695.

[24] B. Lou and F. He, *New Journal of Chemistry*, **2013**, *37*, 309-316.

[25] a) W. J. Belcher, C. A. Longstaff, M. R. Neckenig and J. W. Steed, *Chemical Communications*, **2002**, 1602-1603; b) V. P. Singh, A. Singh and S. Singh, *Journal of Applied Polymer Science*, **2008**, *110*, 1336-1343.

[26] a) T. R. Crompton, *Comprehensive organometallic analysis*, Plenum press, New York and London, **1987**, p; b) L. R. MacGillary in *Toward mehanochemical synthesis of metal-organic frameworks: From coordination polymers and lattice inclusion compounds to porous materials*, *Vol.* (Ed. L. R. MacGillary), John Wiley & Sons, Inc., New Jersey, **2010**, 267-295.

[27] C. Panattoni and E. Frasson, *Acta Crystallographica*, **1963**, *16*, 1258.

[28] a) D. Sun, N. Zhang, G. G. Luo, R. B. Huang, L. S. Zheng, *Acta Crystallographica Section C*, **2010**, C66, m75-m78; b) A. Pramanik and G. Das, *Crystal Engineering Communication*, **2010**, *12*, 401; c) Z.-Y. Zhang, Z.-P. Deng, L.-H. Huo, H. Zhao and S. Gao, *Polyhedron*, **2013**, *59*, 38-47.

[29] a) D. A. Krogstad, K. E. Gohmann, T. L. Sunderland, A. L. Geis, P. Bergamini, L. Marvelli and V. G. Young Jr, *Inorganica Chimica Acta*, **2009**, *362*, 3049-3055; b) C. A. McAuliffe, *Transition metal complexes of phosphorus, arsenic and antimony ligands*, The Macillan Press LTD, London, **1973.**

[30] G. Meyer, D. Naumann and L. Wesemann, *Inorganic Chemistry in Focus II*, Wiley-Vch Verlag GmbH &co., Weinheim, **2005.**

[31] a) G.-F. Hou, Y.-H. Yu, X. Wang, J.-S. Gao, B. Wen, X.-D. Wang and P.-F. Yan, *Journal of Coordination Chemistry*, **2013**, *66*, 3402-3411; b) R. Chutia, S. K. Dey and G. Das, *Crystal Engineering Communication*, **2013**, *15*, 9641-9647.

[32] D. Braga, S. L. Giaffreda, F. Grepioni and M. Polito, *Crystal Engineering Communication*, **2004**, *6*, 459-462.

[33] C.-Y. Su, C.-L. Chen, J.-Y. Zhang and B.-S. Kang in *Silver(I) coordination polymers*, *Vol.* Eds.: M.-C. Hong and L. Chen), John Wiley & Sons, **2009**, 111-141.

[34] C. J. Adams, H. M. Colquhoun, P. C. Crawford, M. Lusi and A. G. Orpen, *Angewandte Chemie International Edition*, **2007**, *46*, 1124-1128.

[35] C. N. Morrison, A. K. Powell and G. E. Kostakis, *Crystal Growth & Design*, **2011**, *11*, 3653-3662.

[36] a) S.-M. Kuang, Q.-G. Wang, T. C. W. Mak, Z.-Z. Zhang and Q.-G. Wang, *Chemical Communications*, **1998**, 581-582; b) A. D. Phillips, L. Gonsalvi, A. Romerosa, F. Vizza and M. Peruzzini, *Coordination Chemistry Reviews*, **2004**, *248*, 955-993.

[37] J. T. Perry, J. A. Perman and M. J. Zaworotko, *Chemical Society Reviews*, **2009**, *38*, 1400-1417.

[38] C. Flener Lovitt, G. Frenking and G. S. Girolami, *Organometallics*, **2012**, *31*, 4122-4132.

[39] a) A. M. Kirillov, P. Smoleński, M. F. C. Guedes da Silva and A. J. L. Pombeiro, *European Journal of Inorganic Chemistry*, **2007**, *2007*, 2686-2692; b) L. Jaremko, A. M. Kirillov, P. Smolenski, T. Lis and A. J. Pombeiro, *Inorganic Chemistry*, **2008**, *47*, 2922-2924.

[40] P. Smoleński, L. Benisvy, M. F. C. Guedes da Silva and A. J. L. Pombeiro, *European Journal of Inorganic Chemistry*, **2009**, *2009*, 1181-1186.

[41] F. Mohr, L. R. Falvello and M. Laguna, *European Journal of Inorganic Chemistry*, **2006**, *2006*, 3152-3154.

[42] M. Porchia, F. Benetollo, F. Refosco, F. Tisato, C. Marzano and V. Gandin, *Journal of Inorganic Biochemistry*, **2009**, *103*, 1644-1651.

[43] a) S. Feng and L. Guanghua in *Chapter 4 - Hydrothermal and Solvothermal Syntheses*, *Vol.* Eds.: R. Xu, W. Pang and Q. Huo), Elsevier, Amsterdam, **2011**, 63-95; b) L.-Y.

Du, W.-J. Shi, L. Hou, Y.-Y. Wang, Q.-Z. Shi and Z. Zhu, *Inorganic Chemistry*, **2013**, *52*, 14018-14027; c) A. L. Garay, A. Pichon and S. L. James, *Chemical Society Reviews*, **2007**, *36*, 846-855.

[44] a) M. Bertelli, L. Carlucci, G. Ciani, D. M. Proserpio and A. Sironi, *Journal of Materials Chemistry*, **1997**, *7*, 1271-1276; b) L. Carlucci, G. Ciani, D. M. Proserpio and S. Rizzato, *Journal of Solid State Chemistry*, **2000**, *152*, 211-220; c) C.-S. Liu, Z. Chang, J.-J. Wang, L.-F. Yan, X.-H. Bu and S. R. Batten, *Inorganic Chemistry Communications*, **2008**, *11*, 889-892; d) M.-L. Tong, S.-L. Zheng and X.-M. Chen, *Chemistry – A European Journal*, **2000**, *6*, 3729-3738.

[45] K. M. Fromm, *Applied Organometallic Chemistry*, **2013**, *27*, 683-687.

[46] F. Tisato, L. Crociani, M. Porchia, P. D. Bernardo, F. Endrizzi, C. Santini and R. Seraglia, *Rapid Communications in Mass Spectrometry*, **2013**, *27*, 2019-2027.

[47] R. Huang and B. J. Frost, *Inorganic Chemistry*, **2007**, *46*, 10962-10964.

[48] C. N. Banti, L. Kyros, G. D. Geromichalos, N. Kourkoumelis, M. Kubicki and S. K. Hadjikakou, *European Journal of Medicinal Chemistry*, **2014**, *77*, 388-399.

Chapter 2

2. Experimental

2.1 Materials and method

Hexamine, formaldehyde solution (37%), sodium hydroxide, tetrakis(hydroxymethyl)phosphonium chloride (80%), silver(I)nitrate, silver(I)trifluoroacetate, silver(I)acetate, silver(I)perchlorate, silver(I)thiocyanide, silver(I)triflate, silver(I)methanesulphonate, silver(I)tetrafluoroborate, potassium silver(I)cyanide (54%), methyliodide, deuterated dimetylsulphonate (d_6-DMSO), deuterated water (D_2O), acetonitrile, methanol, ethanol, chloroform and acetone were all of reagent grade, obtained from Sigma Aldrich and used without any purification. PTA and PTAMeI were synthesized according to literature.[1] All solution ^{1}H NMR, ^{13}C NMR and ^{31}P NMR experiments were done using Bruker 400 MHz NMR spectrometer at a temperature of 298 K. ^{1}H NMR spectra are expressed in parts per million (ppm), referenced internally to residual proton impurity in the deuterated solvents. ^{31}P NMR experiments were decoupled from 1H and the ^{31}P nuclei chemical shifts were referenced relative to an 85% H_3PO_4 aqueous solution [multiplicity (s = singlet; d = doublet; dd = doublet of doublets; t = triplet; and m = multiplet)]. All IR spectra were recorded using PerkinElmer precisely ATR universal Spectrum 100 FT-IR spectrometer with the wavenumber range set from 4000 to 400 cm^{-1}. A background of air was used. High Resolution Electron Spray Ionization (HR-ESI) mass spectra of all products were recorded in positive ion mode using Waters Micro mass LCT Premier coupled with a Time Of Flight (TOF) mass analyser. Thermogravimetric analyses were done using SDT Q600 V20.9, DSC – TGA standard module with purge gas being air set at 50.0 ml/min, initial temperature set at 25 $^{\circ}C$, final temperature was set at 800 $^{\circ}C$ and the rate of heating was set to 10 $^{\circ}C$\min.

2.2 Experimental procedure

2.2.1. Synthesis of PTA

Crushed ice (12.41 g) and $P(CH_2OH)_4Cl$ (23,80 g; 0.125 mol) were transferred to a 500 ml beaker. A 50% w/w aqueous solution containing NaOH (6.39 g, 0.16 mol) was slowly added to the beaker using an addition funnel while stirring. The solution was allowed to warm to room temperature. Then formaldehyde (18.75 g, 0.625 mol) and hexamine (14.00 g; 0.100 mol) were added to the beaker and the contents of the beaker were stirred overnight. The solution was then transferred to two large evaporating dishes and placed in a fumehood for for ease of evaporation until the solution became approximately 90% solid. The solid was filtered through a Buchner funnel, washed with aliquots of cold ethanol (3 x 15 ml) and allowed to dry in air. Then the solid was dissolved in chloroform (40 ml), filtered under gravity through a filter paper, followed by removal of chloroform by roto-evaporation. The crude product was recrystallized in hot ethanol followed by slow cooling to room temperature which resulted in the formation of a white crystalline solid. Yield = 10.2 g (65%), M.P. = 260 °C (decomposition);); ^{1}H NMR (D_2O): δ 4.59-4.50 ppm (2d, 6H, (N-CH_{ax}-N) PTA H's, (N-CH_{eq}-N) PTA H's, J = 12.89 and 13.01 Hz), δ 4.06 ppm (d,6H, (N-CH_2-P) PTA H's, J = 9.0 Hz); ^{13}C NMR (D_2O): δ 73 ppm, δ 51 ppm; ^{31}P NMR (D_2O): δ -98.6 ppm (br s, PTA)

2.2.2 Synthesis of PTAMeI

PTA (3.00 g, 19.2 mmol) was transferred to a 100 ml round-bottomed flask and dissolved in acetone (60 ml). CH_3I (2.76 g; 19.2 mmol) was added to the round-bottom flask and refluxed for one hour during which white precipitate formed. The solution was filtered through a Biichner funnel and the white solid was washed with acetone (3 x 15 ml). The crude product is recrystallized from hot methanol (50 ml) and cooling in an ice bath which gave white, flaky crystals. The product was filtered under vacuum and air dried. Yield = 80 % (4.61 g); M.P. = 204 °C; ^{1}H NMR: (D_2O): δ 5.02-4.91 ppm (2d, 4H, N-$CH_{2(ax)}$-N^+ and N-$CH_{2(eq)}$-N^+, ^{2}J = 11.9 Hz), δ 4.43 ppm (d, 2H, P-CH_2-N^+, J = 6.7 Hz), δ 4.67-4.51 ppm (2d, 2H, N-CH_2-N, ^{2}J = 11.9 Hz), δ 4.04-3.91 ppm (m, 4H, P-CH_2-N), δ 2.82 ppm (s,3H, -CH_3); ^{31}P NMR (D_2O): δ -85.76 ppm (s, PTAMe)

2.2.3 Synthesis of $[Ag(PTA)_3(CN)]2H_2O$ (DCC_1)

54% $KAg(CN)_2$ (3.00 g; 8.14 mmol) was dissolved in 3 ml of distilled water and added to a solution containing PTA (3.84 g; 8.14 mmol) in 20 ml of methanol. The clear resultant solution was refluxed for 30 minutes then the volume was reduced by rotary evaporator to approximately 5 ml. Acetonitrile (40 ml) of was added to produce a cloudy solution which was decanted into a clean round bottom flask. The solvent was removed by rotary evaporator to give a white solid which was isolated by vacuum filtration, washed with (2 × 5 ml) of cold ethanol and dried in-vacuo. X-ray quality crystals were obtained by taking an aliquot of cloudy solution after the addition of acetonitrile and leaving it to stand overnight at room temperature. Yield = 96 %; M.P = 220 °C (decomposition); IR (in cm^{-1}): 3212 (br), 2901 (w), 2106 (w), 1676 (w), 1445 (w), 1410 (w), 1293 (m), 1240 (m), 1098 (w), 1037 (w), 1012 (m), 968 (s), 946 (m), 896 (m), 800 (m), 743 (m), 723 (m), 649 (w), 580 (s), 557 (m), 447 (m), 396 (m); ^{1}H NMR (D_2O): δ 4.63-4.55 ppm (2d, 6H, (N-CH_{ax}-N) PTA H's, (N-CH_{eq}-N) PTA H's, J = 13.0 and 13.2 Hz), δ 4.11 ppm (d,6H, (N-CH_2-P) PTA H's, J = 6.0 Hz); ^{13}C NMR (D_2O): δ 152 ppm, δ 71 ppm, δ 49 ppm; ^{31}P NMR (D_2O): δ -90.421 ppm (br s, PTA); ESI(+)-MS (selected peaks with relative abundance > 10 %): 631 m/z $[Ag(PTA)_3(CN)+Na+3H]^{4+}$ (90 %), 557 m/z $[Ag(PTA)_2.AgCN+H]^{2+}$ (40 %), 429 m/z $[Ag(PTA)_2+7H]^{8+}$ (100 %) and 368 m/z (50 %) $[Ag(PTA)+3H_2O+2Na+3H]^{6+}$

2.2.4 Synthesis of $[Ag(PTA)_2(PTAH)_2](2CO_3)$ (DCC_2)

Formic acid (0.3 ml; 8.0 mmol) was slowly added into a 100 ml conical flask containing silver(I) oxide (0.93 g; 4.0 mmol) in water (10 ml) to form silver(I) formate. The mixture was filtered under gravity to remove unreacted starting materials. PTA (1.26 g; 8.0 mmol) was dissolved in acetone (20 ml) and added drop-wise to the filtrate containing the dissolved silver salt. This led to the formation of a cloudy solution. After filtering the mixture, the product was formed upon slow evaporation of the filtrate. Yield = 9.7 % (0.09 g, based on Ag_2O); M.P. = 213 °C (decomposition); IR (in cm^{-1}): 2955 (w), 2464 (br), 1403 (m), 1339 (m), 1294 (s, br), 1118 (w), 1098 (w), 1024 (m), 1015 (m), 984 (m), 971 (m), 948 (m), 939 (m), 887 (w), 854 (m), 809 (m), 771 (m), 745 (w), 649 (w), 586 (w), 557 (m), 466 (w), 444 (w), 390 (w); ^{1}H NMR: (D_2O): δ 4.68-4.58 ppm (d, d,6H, (N-CH_{ax}-N) (N-CH_{eq}-N) PTA H's, ^2J = 13.1 and 13.3 Hz), δ 4.18 ppm (d,6H, (N-CH_2-P) PTA H's, ^2J = 4.7 Hz); ^{13}C NMR (D_2O): δ 171 ppm, δ 71 ppm, δ 50 ppm; ^{31}P NMR (D_2O): δ -82.6 ppm (br s, PTA); ESI(+)-

MS (selected peaks with relative abundance > 10 %): 461 m/z $[Ag(PTA)_2+H_2O+Na]^{2+}$ (20 %), 158 m/z $[PTA+H]^+$ (100 %), 101 m/z $[PTA\text{-}CH_2N(CH_2)CH_2]^+$ (20 %)

2.2.5 Synthesis of $[Ag(PTA)_3][4\text{-}NP]_{10}$ (DCC_3) and $[Ag_2(PTA)_2(\mu_1\text{-}NO_3)(H_2O)](NO_3)(4\text{-}NP)(H_2O)_n$ (CN_5)

In a 50 ml beaker, PTA (0.1048 g; 0.6669 mmol) was dissolved in a mixture containing 10 ml methanol, 10 ml acetonitrile and 1 ml H_2O. In separate 25 ml beakers, $AgNO_3$ (0.1150 g; 0.6769 mmol) was dissolved in 10 ml of acetonitrile and 4-nitrophenol was dissolved in 10 ml of methanol. The contents of the 25 ml beakers were combined in a 250 ml round-bottom flask to give a clear yellow solution. The PTA solution was then added to the round-bottom flask and the mixture was ultra-sonicated over a water bath for two minutes to ensure complete dissolution. The flask was then removed from the ultra-sonic water bath and the contents of the flask were refluxed at 100 °C for 24 hours. The solution turned from yellow to a fade black colour after the reflux time. The black solid was filtered off under gravity and the clear filtrate was kept in the dark for slow evaporation of the solvent. From the same filtrate, yellow block-like X-ray quality crystals of **DCC_3** and **CN_5** formed within four weeks and were harvested.

DCC_3 and **CN_5**: ^{1}H NMR (d_6-DMSO): δ 8.13-8.09 ppm (d, 2H, aromatic H's, ^3J = 3.04 Hz), δ 6.95-6.91 ppm (d, 2H, aromatic H's, ^3J = 3.04 Hz), δ 4.60-4.40 ppm (d, d, 2H, (N-CH_{ax}-N) PTA H's, (N-CH_{eq}-N) PTA H's, ^2J = 12.57 and 12.81 Hz), δ 4.23-4.23 ppm (d, 6H, (N-CH_2-P) PTA H's, (N-CH_{eq}-N) PTA H's, ^2J = 2.72 Hz). ^{31}P NMR (d_6-DMSO): δ -87.15 ppm (br s, PTA).

2.2.6 Synthesis of $[Ag(PTA)(NO_3)]_n$ (CP_1) and $[Ag(PTA)(H_2O)]_n(NO_3)_n$ (CN_1)

Silver(I) nitrate (1.08 g; 6.36 mmol) was dissolved in 15 ml of methanol in a 100 ml conical flask. In a clean 250 ml beaker, PTA (1.00 g, 6.36 mmol) was dissolved in 80 ml of methanol. The silver(I) nitrate solution was added to the PTA solution in the beaker. A white fluffy precipitate immediately formed and the contents of the flask were ultra-sonicated over a water bath for one hour at room temperature. The white precipitate was dissolved by the drop-wise addition of 25% aqueous ammonia solution and the resultant mixture was filtered under gravity to give a clear filtrate which was kept in the dark for slow evaporation of the

solvent. Colourless, block-like x-ray quality crystals of $[Ag(PTA)(NO_3)]_n$ (CP_1) formed within two weeks by slow evaporation of solvent and were harvested. Further evaporation of the solvent led to the production of x-ray quality crystals of $[Ag(PTA)_2(H_2O)]_n(NO_3)_n$ (CN_1) after an additional week.

$[Ag(PTA)(NO_3)]_n$ (CP_1): Yield = 29.4 % (0.32 g, based on $AgNO_3$); M.P = 213 °C (decomposition); IR (in cm^{-1}): 2946 (m), 1595 (w), 1280 (s), 1236(s), 1236 (s), 1102 (m), 1033 (m), 1008 (m), 968 (m), 947 (s), 896 (m), 790 (m), 749 (m), 725 (m), 599 (m), 577 (m), 563 (m), 454 (m), 398 (w); ^{1}H NMR: (d_6-DMSO): δ 4.608-4.391 ppm (d, d,6H, (N-CH_{ax}-N) PTA H's, (N-CH_{eq}-N) PTA H's, ^2J = 12.57 and 12.81 Hz), δ 4.233-4.226 ppm (d,6H, (N-CH_2-P) PTA H's, ^2J = 2.72 Hz).^{13}C NMR: δ 72.086-72.022 ppm, δ 50.132-50.076 ppm; ^{31}P NMR (d_6-DMSO): δ -85.862 ppm (br s, PTA); ESI(+)-MS (selected peaks with relative abundance > 10 %): 378 m/z $[(PTA)_2(NO_3)+2H]^+$ (100 %), 421 m/z $[Ag(PTA)_2]^+$ (95 %); 682 m/z $[Ag_2(PTA)_2(NO_3)+2H_2O+3H]^{4+}$ (20 %)

$[Ag(PTA)(H_2O)]_n(NO_3)_n$ (CN_1): Yield = 18 % (0.10 g, based on $AgNO_3$); M.P. = 217 °C (decomposition); IR (in cm^{-1}): 3233 (br), 2949 (w), 1672 (w), 1421 (m), 1376 (m), 1312 (s), 1288 (s), 1252 (m), 1231 (m), 1105 (m), 1040 (m), 1006 (m), 949 (s), 901 (m), 828 (m), 794 (m), 756 (m), 725 (w), 657 (w), 607 (m), 590 (m), 564 (m), 449 (m), 399 (m); ^{1}H NMR (400 MHz, d_6-DMSO): δ 4.590-4.389 ppm (d, d,6H, (N-CH_{ax}-N) PTA H's, (N-CH_{eq}-N) PTA H's, ^2J = 12.57 and 12.81 Hz), δ 4.234-4.227 ppm (d,6H, (N-CH_2-P) PTA H's, ^2J = 2.72 Hz). ^{31}P NMR (400 MHz, d_6-DMSO): δ -85.907 ppm (br s, PTA); ESI(+)-MS (selected peaks with relative abundance > 10 %): 421 m/z $[Ag(PTA)_2]^+$ (100 %), 378 m/z $[(PTA)_2(NO_3)+2H]^+$ (95 %)

2.2.7 Synthesis of $[Ag(PTA)_2(\mu\text{-}O_2CCH_3)]_n2H_2O$ (CP_2)

Silver(I) acetate (0.43 g; 2.58 mmol) was suspended in 20 ml of methanol in a 100 ml conical flask. In a clean 100 ml beaker, PTA (0.40 g; 2.58 mmol) was dissolved in 20 ml of methanol and added to the conical flask containing the silver(I) suspension to give a clear colourless solution. The solution was placed in an ultra-sonic water bath for one hour. A white precipitate formed after the set reaction time and it was dissolved by the drop-wise addition of 25% ammonia solution. The solution was ultra-sonicated over a water bath for a further 30 minutes and then filtered under gravity to give a clear filtrate which was kept in the

dark for slow evaporation of the solvent. Colourless blocks of x-ray quality formed within several days and were isolated by vacuum filtration and dried in-vacuo. Yield = 69 % (0.27 g, based on AgO_2CCH_3); M.P = 215 °C (decomposition); IR (in cm^{-1}): 3248 (br), 2926 (w), 1692 (m), 1534 (s), 1399 (s), 1340 (m), 1298 (m), 1280 (m), 1242 (m), 1108 (w), 1041 (w), 1015 (s), 975 (s), 959 (s), 950 (s), 920 (w), 796 (s), 753 (m), 729 (m), 656 (s), 606 (s), 583 (s), 565 (s), 448 (m), 397 (m); ^{1}H NMR: (D_2O): δ 4.706-4.562 ppm (d, d,6H, (N-CH_{ax}-N) PTA H's, (N-CH_{eq}-N) PTA H's, ^2J = 12.57 and 12.81 Hz), δ 4.317-4.314 ppm (d,6H, (N-CH_2-P) PTA H's, ^2J = 2.72 Hz), δ 1.943 ppm (s, 3H, -CH_3 from acetate group); ^{13}C NMR (D_2O): δ 71.050-70.992 ppm, δ 48.940-48.865 ppm, δ 23.085 ppm; ^{31}P NMR (D_2O): δ -78.004 ppm (br s, PTA); ESI(+)-MS (selected peaks with relative abundance > 10 %): 487 m/z $[Ag(PTA)_2(O_2CCH_3)+6H]^{5+}$ (30 %), 702 m/z $[Ag_2(PTA)_2(O_2CCH_3)_2+2Na+6H]^{8+}$ (60 %)

2.2.8 Synthesis of $[Ag(PTA)_2(\mu\text{-}O_2CCF_3)]_n$ (CP_3)

Silver(I) trifluroacetate (0.70 g; 3.18 mmol) was dissolved in 20 ml of methanol in a 100 ml conical flask. In a clean 100 ml beaker, PTA (0.50 g; 3.18 mmol) was dissolved in 20 ml of methanol and added to the conical flask containing the silver(I) solution that resulted in an immediate formation of a white needle like solid. The mixture was placed in an ultra-sonic water bath for one hour and the white precipitate was dissolved by the drop-wise addition of 25% ammonia solution. The solution was ultra-sonicated over water bath for a further 30 minutes and then filtered under gravity to give a clear filtrate which was kept in the dark for slow evaporation of the solvent. Colourless X-ray quality block-like crystals formed within several days and were isolated by vacuum filtration and dried in-vacuo. Yield = 63.3 % (0.44 g, based on AgO_2CCF_3); M.P. = 200 °C (decomposition); IR (in cm^{-1}): 2950 (w), 1654 (s), 1448 (w), 1419 (m), 1300 (w), 1285 (w), 1243 (m), 1181 (s), 1140 (m), 1107 (m), 1040 (w), 1015 (m), 992 (w), 973 (m), 951 (s), 898 (m), 835 (m), 809 (m), 793 (s), 751 (m), 721 (s), 653 (w), 604 (m), 578 (m), 565 (m), 519 (w), 451 (m), 398 (m); ^{1}H NMR: (400 MHz, D_2O): δ 4.714-4.570 ppm (d, d,6H, (N-CH_{ax}-N) PTA H's, (N-CH_{eq}-N) PTA H's, ^2J = 12.57 and 12.81 Hz), δ 4.323-4.318 ppm (d,6H, (N-CH_2-P) PTA H's, ^2J = 2.72 Hz); ^{19}F NMR (D_2O): δ -75.499 ppm; ^{31}P NMR (D_2O): δ -77.942 ppm (br s, PTA); ESI(+)-MS (selected peaks with relative abundance > 10 %): 343 m/z $[Ag(PTA)+3H_2O+Na+H]^{3+}$ (25 %), 438 m/z $[Ag(PTA)(O_2CCF_3)+K+3H]^{4+}$ (100 %), 495 m/z $[Ag(PTA)(O_2CCF_3)+2H_2O+2K+3H]^{5+}$ (45 %).

2.2.9 Synthesis of $[Ag(PTA)(O)]_n(ClO_4)$ (CP_4) and $[Ag(PTA)_2(H_2O)]_n(ClO_4)$ (CP_5)

Silver(I) perchlorate (0.50 g; 2.41 mmol) was dissolved in 20 ml of methanol in a 100 ml conical flask containing. In a clean 100 ml beaker, PTA (0.40 g; 2.55 mmol) was dissolved in 20 ml of methanol and added to the conical flask containing the silver(I) solution that resulted in an immediate formation of a white precipitate. The mixture was placed in an ultra-sonic water bath for one hour and the white precipitate was dissolved by the drop-wise addition of 25% ammonia solution. The solution was ultra-sonicated over a water bath for a further 30 minutes and then filtered under gravity to give a clear filtrate which was kept in the dark for slow evaporation the solvent. Colourless, block-like x-ray quality crystals of $[Ag(\mu\text{-}PTA)(O)]_n(ClO_4)$ (**CP_4**) formed within several days by slow evaporation of solvent and were harvested. Further evaporation of the solvent led to the production of colourless, block-like x-ray quality crystals of $[Ag(\mu\text{-}PTA)(PTA)(H_2O)]_n(ClO_4)$ (**CP_5**) after an additional week.

$[Ag(\mu\text{-}PTA)(O)]_n(ClO_4)$ (CP_4): Yield = 62 % (0.31 g, based on $AgClO_4$); M.P. = 218 °C (decomposition); IR: 2942 (w), 2877 (w), 1601 (w), 1441 (w), 1416 (w), 1179 (w), 1092 (m), 1064 (s), 1012 (s), 973 (m), 959 (m), 894 (m), 795 (m), 750 (m), 723 (m), 654 (w), 619 (m), 599 (m), 580 (m), 564 (m), 446 (m), 395 (w); ^{1}H NMR: (d_6-DMSO): δ 4.60-4.40 ppm (2d, 2H, (N-CH_{ax}-N) PTA H's, (N-CH_{eq}-N) PTA H's, ^2J = 12.57 and 12.81 Hz), δ 4.236-4.228 ppm (d,6H, (N-CH_2-P) PTA H's, ^2J = 2.80 Hz).^{13}C NMR: δ 72.18 ppm, δ 50.09 ppm; ^{31}P NMR (d_6-DMSO): δ -85.20 ppm (br s, PTA).

$[Ag(\mu\text{-}PTA)(PTA)(H_2O)]_n(ClO_4)$ (CP_5): Yield = 14 % (0.07 g, based on $AgClO_4$); M.P. = 224 °C (decomposition); IR: 3562 (w), 3176 (br), 2939 (w), 1642 (w), 1441 (w), 1423 (w), 1375 (w), 1290 (m), 1237 (m), 1073 (s, br), 1010 (m), 968 (m), 946 (m), 899 (m), 762 (m), 748 (m), 728 (m), 654 (w), 620 (m), 599 (m), 579 (m), 555 (m), 446 (m), 395 (w); ^{1}H NMR: (d_6-DMSO): δ 4.56-4.39 ppm (2d, 2H, (N-CH_{ax}-N) PTA H's, (N-CH_{eq}-N) PTA H's, ^2J = 12.60 and 12.85 Hz), δ 4.236-4.228 ppm (d,6H, (N-CH_2-P) PTA H's, ^2J = 2.56 Hz).^{13}C NMR (d_6-DMSO): δ 72.03 ppm, δ 49.88 ppm; ^{31}P NMR (d_6-DMSO): δ -86.27 ppm (br s, PTA). ESI(+)-MS (selected peaks with relative abundance > 10 %): 369 m/z $[Ag(PTA)(ClO_4)+4H]^{4+}$ (50 %), 488 m/z $[Ag(PTA)_2+H_2O+2Na+2H]^{5+}$ (40 %); 519 m/z $[Ag(PTA)_2+2K+H_2O+H]^{4+}$ (20 %), 605 m/z $[Ag(PTA)_2(ClO_4)+3H_2O+Na+6H]^{7+}$ (25 %), 758 m/z $[Ag(PTA)_3(ClO_4)+3H_2O+Na+2H]^{3+}$ (45 %).

2.2.10 Synthesis of Ag(PTA)(O_3SCF_3) (CN_2)

Silver(I) triflate (0.50 g; 1.9 mmol) was dissolved in 20 ml of methanol in a 100 ml conical flask. In a clean 100 ml beaker, PTA (0.31 g; 1.9 mmol) was dissolved in a 20 ml of methanol and added to the conical flask containing the silver(I) suspension. A white fluffy precipitate immediately formed and the contents of the flask were placed in an ultra-sonic water bath for one hour. The white precipitate was dissolved by the drop-wise addition of 25% aqueous ammonia solution and the resultant mixture was filtered under gravity to give a clear filtrate which was kept in a dark place under ambient conditions for slow evaporation the solvent. Colourless block-like crystals of x-ray quality formed within two weeks and were isolated by vacuum filtration and dried in-vacuo. Yield = 56.4 % (0.28 g, based on AgO_3SCF_3); M.P = 256 °C (decomposition); IR (in cm^{-1}): 2950 (w), 1418 (w), 1240 (s), 1231 (s), 1192 (m), 1174 (m), 1139 (m), 1110 (m), 1023 (m) 1010 (m), 953 (m), 945 (m), 903 (w), 811 (m), 796 (m), 757 (m), 734 (w), 630 (s), 612 (m), 580 (m), 561 (m), 516 (m), 457 (m), 445 (m), 401 (m); ^{1}H NMR: (d_6-DMSO): δ 4.678-4.509 ppm (2d, 6H, (N-CH_{ax}-N) PTA H's, (N-CH_{eq}-N) PTA H's, ^2J = 12.57 and 12.81 Hz), δ 4.228-4.221 ppm (d,6H, (N-CH_2-P) PTA H's, ^2J = 2.72 Hz). ^{31}P NMR (d_6-DMSO): δ -80.448 ppm (br s, PTA); ^{19}F NMR (D_2O): δ -75.512 ppm; ESI(+)-MS (selected peaks with relative abundance > 10 %): 352 m/z $[Ag(PTA)+CH_3CN+2Na]^{3+}$ (100 %), 510 m/z $[Ag(PTA)(O_3SCF_3)+Na+4H_2O+H]^{2+}$ (40 %), 519 m/z $[Ag(PTA)_2+2K+H_2O+H]^{4+}$ (50 %) and 588 m/z $[Ag(PTA)(O_3SCF_3)_2+Na+2H]^{2+}$ (45 %).

2.2.11 Synthesis of Ag(PTA)(O_3SCH_3) (CN_3)

Silver(I) methanesulfonate (0.50 g; 2.5 mmol) was suspended in 20 ml of methanol in a 100 ml conical flask. In a clean 100 ml beaker, PTA (0.39 g; 2.5 mmol) was dissolved in a 100 ml beaker containing 20 ml of methanol and added to the conical flask containing the silver(I) suspension. The solution was placed in an ultra-sonic water bath for one hour. A white precipitate formed after the set reaction time and it was dissolved by the drop-wise addition of 25% ammonia solution. The solution was ultra-sonicated over a water bath for a further 30 minutes and then filtered under gravity to give a clear filtrate which was kept in the dark for slow evaporation the solvent. The product was isolated as a microcrystalline solid. Yield = 68 % (0.34 g, based on AgO_3SCH_3); M.P. = 200 °C (decomposition); IR (in cm^{-1}):

3209 (br), 1674 (w), 1450 (w), 1419 (w), 1332 (w), 1296 (m), 1240 (m), 1205 (m), 1161 (m), 1063 (m), 1008 (m), 964 (s), 951 (m), 901 (m), 795 (m), 768 (m), 757 (m), 736 (m), 595 (s), 520 (m), 446 (m), 398 (m); ^{1}H NMR: (D_2O): δ 4.711-4.566 ppm (2d, 6H, (N-CH_{ax}-N) PTA H's, (N-CH_{eq}-N) PTA H's, ^{2}J = 12.57 and 12.81 Hz), δ 4.322-4.316 ppm (d,6H, (N-CH_2-P) PTA H's, ^{2}J = 2.72 Hz), δ 2.834 ppm (s, 3H, -CH_3 from methanesulphonate group); ^{31}P NMR (D_2O): δ -80.376 ppm (br s, PTA).

2.2.12 Synthesis of Ag(PTA)(BF_4) (CN_4)

Silver(I)tetrafluoroborate (0.50 g; 3.0 mmol) was dissolved in 20 ml of methanol in a 100 ml conical flask. In a clean 100ml beaker, PTA (0.48 g; 3.0 mmol) was dissolved in 20 ml of methanol and added to the conical flask containing the silver(I) solution. A white fluffy precipitate immediately formed and the contents of the flask were placed in an ultra-sonicate water bath for one hour. The white precipitate was dissolved by the drop-wise addition of 25% aqueous ammonia solution and the resultant mixture was filtered under gravity to give a clear filtrate which was kept in the dark for slow evaporation the solvent. The product was isolated as a microcrystalline solid. Yield = 74 % (0.37 g, based on $AgBF_4$); M.P.= 219 °C (decomposition); ^{1}H NMR: (d_6-DMSO): δ 4.60-4.40 ppm (2d, 2H, (N-CH_{ax}-N) PTA H's, (N-CH_{eq}-N) PTA H's, ^{2}J = 12.57 and 12.85 Hz), δ 4.233-4.226 ppm (d,6H, (N-CH_2-P), PTA H's, ^{2}J = 2.92 Hz).^{13}C NMR (d_6-DMSO): δ 72.11 ppm, 50.07 ppm; ^{31}P NMR (d_6-DMSO): δ -85.54 ppm (br s, PTA); ^{19}F NMR (d_6-DMSO): δ -148.20 ppm; ESI(+)-MS (selected peaks with relative abundance > 10 %): 403 m/z $[Ag(PTA)(BF_4)+5H+2Na]^{7+}$ (100 %)

2.2.13 Synthesis of $[Ag(PTAMe)(CH_3OH)(ClO_4)]_nClO_4$ (m-CP_1)

$AgClO_4$ (0.50 g, 2.4 mmol) was dissolved in 20 ml of methanol in a 100 ml conical flask. In a clean 250 ml beaker, PTAMeI (0.30g, 1 mmol) was dissolved in 100 ml of methanol and to it the silver(I) solution was added. A yellow precipitate of AgI(s) immediately formed and the supernant liquid became turbid. The mixture was swirled and filtered under gravity to produce a clear colourless filtrate which was kept in the dark for slow evaporation the solvent. X-ray quality block-like crystals of the product formed after several days within the same reaction solvent and were collected. Yield = 18 % (0.09 g, based on $AgClO_4$); M.P. = 200 °C (decomposition); IR: 3535 (br), 3265 (br), 2996 (w), 1618 (w), 1478 (w), 1459 (w), 1419 (w), 1305 (w), 1253 (m), 1036 (s), 1018 (s), 969 (m), 929 (m), 810 (m), 753 (m), 616 (s), 564 (m), 546 (w), 440 (m); ^{1}H NMR: (D_2O): δ 5.16-5.00 ppm (2d, 4H, N-$CH_{2(ax)}$-N^+ and

N-$CH_{2(eq)}$-N^+, ^2J = 11.61 Hz and 12.09 Hz), δ 4.76 ppm (2d, 2H, N-CH_2-N, ^2J = 14.21 Hz), δ 4.72 ppm (s, 2H, P-CH_2-N^+), δ 4.41-4.24 ppm (m, 4H, P-CH_2-N), δ 2.92 ppm (s,3H, -CH_3); ^{31}P NMR (D_2O): δ -65.20 ppm (br s, PTAMe)

2.2.14 Synthesis of Ag(PTAMe)(NO_3) (m-CP_2)

$AgNO_3$ (0.50 g, 2.9 mmol) was dissolved in 20 ml of methanol in a 100 ml conical flask. In a clean 250 ml beaker, PTAMeI (0.36g, 1.2 mmol was dissolved in 100 ml of methanol and to it the silver(I) solution was added. A yellow precipitate of AgI(s) immediately formed and the supernant liquid became turbid. The mixture was swirled and filtered under gravity to produce a clear colourless filtrate which was kept in the dark for slow evaporation the solvent. X-ray quality block-like crystals of the product formed after several days within the same reaction solvent and were collected. Yield = 22 % (0.11 g, based on $AgNO_3$); M.P. = 200 °C (decomposition); IR (cm^{-1}): 3391 (br),3021 (w), 2988 (w), 1641 (w), 1461 (m), 1316 (m), 1291 (s), 1247 (m), 1115 (m), 1095 (m), 928 (m), 893 (m), 865 (m), 820 (m), 788 (m), 755 (m), 726 (w), 576 (m), 559 (m), 449 (m), 397 (w); ^{1}H NMR: (d_6-DMSO): δ 4.99-4.89 ppm (2d, 4H, N-$CH_{2(ax)}$-N^+ and N-$CH_{2(eq)}$-N^+, ^2J = 11.41 Hz and 11.61 Hz), δ 4.58 ppm (d, 1H, N-$CH_{(ax)}$-N, ^2J = 13.41 Hz), δ 4.43 ppm (s, 2H, P-CH_2-N^+), δ 4.34 ppm (2d, 2H, N-CH_2-N, $^2J_{HH}$= 13.49 Hz), δ 4.09-3.89 ppm (m, 4H, P-CH_2-N), δ 2.92 ppm (s,3H, -CH_3); ^{31}P NMR (D_2O): δ -65.20 ppm (br s, PTAMe)

2.2.15 Synthesis of Ag(PTAMe)(O_2CCF_3) (m-CP_3)

AgO_2CCF_3 (0.50 g, 2.3 mmol) was dissolved in a 100 ml conical flask containing 20 ml of methanol. In a clean beaker, PTAMeI (0.27g, 0.9 mmol) was dissolved in a 250 ml beaker containing 100 ml of methanol and to it the silver(I) solution was added. A yellow precipitate of AgI(s) immediately formed and the supernant liquid became turbid. The mixture was swirled and filtered under gravity to produce a clear colourless filtrate which was kept in the dark for slow evaporation the solvent. X-ray quality block-like crystals of the product formed after several days within the same reaction solvent and were collected. Yield = 23 % (0.12 g, based on AgO_2CCF_3); M.P. = 203 °C (decomposition); IR (cm^{-1}): 2988 (w) 2942 (w), 1672 (s), 1463 (w), 1374 (m), 1332 (s), 1315 (s), 1300 (m), 1255 (m), 1187 (s), 1127 (m), 1117 (m), 1095 (m), 979 (m), 933 (m), 812 (m), 719 (m), 656 (w), 565 (m), 448 (m), 441 (m), 393 (w); ^{1}H NMR: (DMSO): δ 5.07-4.89 ppm (2d, 4H, N-$CH_{2(ax)}$-N^+ and N-

$CH_{2(eq)}$-N^+, ^2J = 11.37 Hz and 11.57 Hz), δ 4.70 ppm (s, 2H, P-CH_2-N^+), δ 4.52 ppm (d, 2H, N-$CH_{(eq)}$-N, ^2J = 13.97 Hz), δ 4.36-4.20 ppm (m, 4H, P-CH_2-N), δ 2.89 ppm (s,3H, -CH_3); ^{31}P NMR (d_6-DMSO): δ -68.38 ppm (br s, PTAMe)

2.2.16 Synthesis of Ag(PTAMe)(O_3SCF_3) (m-CP_4)

AgO_3SCF_3 (0.50 g, 1.9 mmol) was dissolved in a 100 ml conical flask containing 20 ml of methanol. In a clean 250 ml beaker, PTAMeI (0.24g, 0.80 mmol) was dissolved in 100 ml of methanol and to it the silver(I) solution was added. A yellow precipitate of AgI(s) immediately formed and the supernant liquid became turbid. The mixture was swirled and filtered under gravity to produce a clear colourless filtrate which was kept in the dark for slow evaporation of the solvent. X-ray quality block-like crystals of the product formed after several days within the same reaction solvent and were collected. Yield = 53 % (0.27 g, based on AgO_3SCF_3); M.P. = 204 °C (decomposition); IR (cm^{-1}): 3488 (br), 3009 (w), 2988 (w), 1635 (w), 1460 (w), 1301 (m), 1273 (m), 1243 (s), 1218 (m), 1160 (s), 1094 (m), 1019 (m), 975 (m), 930 (m), 898 (w), 813 (m), 753 (m), 630 (s), 575 (m), 561 (m), 516 (s), 445 (m), 406 (w); ^{1}H NMR: (D_2O): δ 5.14-4.98 ppm (2d, 4H, N-$CH_{2(ax)}$-N^+ and N-$CH_{2(eq)}$-N^+, ^2J = 12.13 Hz and 11.97 Hz), δ 4.70 ppm (s, 2H, P-CH_2-N^+), δ 4.52 ppm (d, 2H, N-$CH_{(eq)}$-N, ^2J = 13.97 Hz), δ 4.36-4.20 ppm (m, 4H, P-CH_2-N), δ 2.89 ppm (s,3H, -CH_3); ^{31}P NMR (D_2O): δ -65.27 ppm (br s, PTAMe), ^{19}F NMR (D_2O): δ -78.78ppm;

2.3 X-ray crystal structure determinations

Crystals of **DCC_{1-3}**, **CP_{1-5}**, **CN_1**, **CN_2**, **CN_5** and **m-CP_{1-3}** were selected and attached onto the tip of glass fibres using epoxy glue. The crystals were mounted on a Mitegen Micromount and centered in the X-ray beam by using a video camera. The crystal evaluation and data collection were done on a Bruker Smart APEX2 diffractometer with Mo Kα radiation (λ = 0.71073 Å) equipped with an Oxford Cryostream low temperature apparatus operating at 100(1) K for all samples except for m-CP_2 which was ran at 295 K. The initial cell matrix was determined from three series of scans consisting of twelve frames collected at intervals of 0.5° in a 6° range with the exposure time of ten seconds per frame. Each of the three series of scans was collected at different starting angles and the *APEX2* program suite was used to index the reflections.[2] The data collection involved using omega scans of 0.5° width

with an exposure time of 20 seconds per frame. The total number of images was based on results from the program *COSMO*[3] whereby the expected redundancy was to be 4.0 and completeness of 100% out to 0.75 Å. Cell parameters were retrieved using *APEX2*[2] and refined using *SAINT*[4] on all observed reflections. Data reduction was performed using the SAINT[4] software and the scaling and absorption corrections were applied using *SADABS*[5] multi-scan technique. The structures were solved by the direct method using the *SHELXS* program and refined. [6] The visual crystal structure information were performed using *ORTEP*-3[7], *Mercury*[8] and *DIAMOND*[9] system software. Non-hydrogen atoms were first refined isotropically and then by anisotropic refinement with full-matrix least squares method based on F^2 using *SHELXL*.[6] All hydrogen atoms were positioned geometrically, allowed to ride on their parent atoms and refined isotropically. The crystal data and structural refinement information are summarized in Tables 2 to 5. All the data was subjected to the online checkCIF evaluation criteria and the reports are provided in Appendix E.

Table 2: Crystallographic data and structural refinement details for **DCC_{1-3}** and **CP_1**

	DCC_1	**DCC_2**	**DCC_3**	**CP_1**
Empirical formula	$C_{19}\ H_{44}\ N_{10}\ O_4\ P_3\ Ag$	$C_{9.33}\ H_{17}\ N_4\ O_4\ P_{1.33}\ Ag_{0.33}$	$C_{16.42}\ H_{17.79}\ N_4\ O_{6.53}\ P_{0.63}\ Ag_{0.21}$	$C_6\ H_{12}\ N_4\ O_3\ P\ Ag$
Formula weight	677.42	326.52	417.88	327.04
Crystal system	Orthorhombic	Rhombohedral	Monoclinic	Monoclinic
Space group	*Pnma*	*R*3	$P2_1/c$	*Cm*
Unit cell dimensions	a = 11.9813(4) Å; α= 90°	a = 15.7992(12) Å; α = 90°	a = 21.4989(4) Å; α = 90°	a = 7.9133(10) Å; α = 90°
	b = 20.8423(7) Å; β = 90°	b = 15.7992(12) Å; β = 90°	b = 23.9573(4) Å; β = 104.854(1)°	b = 9.0276(10) Å; β= 105.5°
	c = 12.2359(4) Å ; γ = 90°	c = 13.1502(18) Å; γ = 120°	c = 17.7204(3) Å; γ = 90°	c = 7.0791(10) Å; γ = 90°
Volume	3055.52(18) $Å^3$	2842.7(5) $Å^3$	8822.0(3) $Å^3$	487.22(11) $Å^3$
Z	4	9	19	2
Density (calculated)	1.473 mg m^{-3}	1.717 mg m^{-3}	1.494 mg m^{-3}	2.229 mg m^{-3}
Absorption coefficient	0.859 mm^{-1}	0.779 mm^{-1}	0.377 mm^{-1}	2.226 mm^{-1}
***F*(000)**	1408	1518	4102	324
Crystal size	0.35 x 0.26 x 0.20 mm	0.36 x 0.24 x 0.22 mm	0.50 x 0.37 x 0.26 mm	0.16 x 0.10 x 0.09 mm
Theta range for data collection	1.93 to 28.32°	2.15 to 24.99°	0.980 to 28.314°	2.99 to 28.37°
Reflections collected	62216	15950	265749	5996
Index ranges	-15<=h<=15	-18<=h<=17	-28<=h<=26	-10<=h<=10
	-23<=k<=27; -16<=l<=16	-15<=k<=18; -15<=l<=15	-31<=k<=31; -23<=l<=23	-12<=k<=11; -9<=l<=9
Independent reflections	3898 [R(int) = 0.0356]	2198 [R(int) = 0.0209]	21928 [R(int) = 0.0248]	1231 [R(int) = 0.0246]
Completeness to theta = 28.37°	99.90%	100.00%	100.00%	99.80%
Max. and min. transmission	0.8470 and 0.7531	0.8473 and 0.7669	-	0.8248 and 0.7172
Data / restraints / parameters	3898 / 0 / 178	2198 / 1 / 176	21928 / 0 / 1262	1231 / 2 / 80
Goodness-of-fit on F2	1.108	1.057	0.7	1.039
Final R indices [I>2sigma(I)]	R1 = 0.0237, wR2 = 0.0551	R1 = 0.0158, wR2 = 0.0417	R1 = 0.0481, wR2 = 0.1142	R1 = 0.0101, wR2 = 0.0239
R indices (all data)	R1 = 0.0313, wR2 = 0.0577	R1 = 0.0159, wR2 = 0.0419	R1 = 0.0638, wR2 = 0.1307	R1 = 0.0101, wR2 = 0.0239
Absolute structure parameter	-	-0.025(13)	-	0.021(14)
Largest diff. peak and hole	0.428 and -0.389 e $Å^{-3}$	0.344 and -0.170 e $Å^{-3}$	1.884 and -0.921 e $Å^{-3}$	0.204 and -0.571 e $Å^{-3}$

Table 3: Crystallographic data and structural refinement details for **$CP_{2\text{-}5}$**

	CP_2	**CP_3**	**CP_5**	**CP_4**
Empirical formula	$C_{16}\ H_{38}\ N_6\ O_8\ P_2\ Ag_2$	$C_8\ H_{12}\ F_3\ N_3\ O_2\ P\ Ag$	$C_{12}\ H_{24}\ Cl\ N_6\ O_5\ P_2\ Ag$	$C_6\ H_{12}\ Cl\ N_3\ O_5\ P\ Ag$
Formula weight	720.2	378.05	537.63	380.48
Crystal system	Monoclinic	Monoclinic	Orthorhombic	Orthorhombic
Space group	*C*2/*c*	$P2_1/c$	$P2_12_12_1$	$P2_12_12_1$
Unit cell dimensions	a = 25.2513(6) Å; α = 90°	a = 6.9024(2) Å; α = 90°	a = 6.846(5) Å; α = 90°	a = 9.6090(3) Å; a= 90°
	b = 6.8455(2) Å; β = 123.123°	b = 15.1654(4) Å; β = 104.6990°	b = 13.618(5) Å; β = 90°	b = 10.88900(10) Å; b= 90°
	c = 17.7551(5) Å; γ = 90°	c = 12.1053(4) Å; γ = 90°	c = 21.803(5) Å; γ = 90°	c = 11.5910(2) Å; g= 90°
Volume	2570.37(12) $Å^3$	1225.68(6) $Å^3$	2032.7(17) $Å^3$	1212.79(4) $Å^3$
Z	4	4	4	4
Density (calculated)	1.861 mg m^{-3}	2.049 mg m^{-3}	1.757 mg m^{-3}	2.084 mg m^{-3}
Absorption coefficient	1.700 mm^{-1}	1.811 mm^{-1}	1.317 mm^{-1}	2.027 mm^{-1}
***F*(000)**	1456	744	1088	752
Crystal size	0.16 x 0.10 x 0.09 mm	0.63 x 0.58 x 0.29 mm	0.34 x 0.22 x 0.19 mm	0.27 x 0.17 x 0.17 mm
Theta range for data collection	1.93 to 28.44°	2.20 to 28.35°	1.76 to 27.97°	2.566 to 28.476°
Reflections collected	28016	19385	22481	33028
Index ranges	-33<=h<=33	-9<=h<=9	-12<=h<=12	-8<=h<=7,
	-9<=k<=9; -23<=l<=23	-20<=k<=17, -15<=l<=16	-14<=k<=14, -15<=l<=15	-11<=k<=15, -28<=l<=24
Independent reflections	3233 [R(int) = 0.0222]	3057 [R(int) = 0.0227]	3869 [R(int) = 0.1181]	3058 [R(int) = 0.0302]
Completeness to theta = 28.37°	99.80%	99.60%	82.60%	99.80%
Max. and min. transmission	0.8620 and 0.7726	0.6218 and 0.3950	0.7880 and 0.6631	0.724 and 0.611
Data / restraints / parameters	3233 / 4 / 171	3057 / 0 / 164	3869 / 0 / 140	3058 / 0 / 154
Goodness-of-fit on F2	0.979	1.058	1.68	1.076
Final R indices [I>2sigma(I)]	R1 = 0.0157, wR2 = 0.0395	R1 = 0.0528, wR2 = 0.1514	R1 = 0.1531, wR2 = 0.4219	R1 = 0.0178, wR2 = 0.0480
R indices (all data)	R1 = 0.0177, wR2 = 0.0410	R1 = 0.0538, wR2 = 0.1523	R1 = 0.1857, wR2 = 0.4415	R1 = 0.0184, wR2 = 0.0484
Absolute structure parameter	-	0.0163(15)	0.122(17)	0.010(5)
Largest diff. peak and hole	0.488 and -0.313 e $Å^{-3}$	5.855 and -2.091 e $Å^{-3}$	4.457 and -2.315 e $Å^{-3}$	0.522 and -0.736 e $Å^{-3}$

Table 4: Crystallographic data and structural refinement details for **CN_1** and **m-CP_{1-3}**

	CN_1	**m-CP_1**	**m-CP_2**	**m-CP_3**
Empirical formula	C_{12} H_{28} N_8 O_8 P_2 Ag_2	C_8 H_{19} Cl_2 N_3 O_9 P Ag	C_8 H_{18} N_5 O_7 P Ag	C_{13} H_{15} F_9 N_3 O_6 P Ag_2
Formula weight	690.1	511	435.11	726.99
Crystal system	Orthorhombic	Orthorhombic	Orthorhombic	Tetragonal
Space group	*Pbca*	*Pna*2_1	*P*$2_1$$2_1$$2_1$	*P*4_1
Unit cell dimensions	a = 11.129(3) Å; α = 90°	a = 15.8408(4) Å; α = 90°	a = 6.9435(12) Å; α = 90°	a = 11.3149(4) Å; α = 90°.
	b = 11.296(3) Å; β = 90°	b = 14.3962(4) Å; β = 90°	b = 8.1743(15) Å; β = 90°	b = 11.3149(4) Å; β = 90°.
	c = 16.832(4) Å; γ = 90°	c = 7.1173(2) Å; γ = 90°	c = 26.591(6) Å; γ = 90°	c = 17.0355(9) Å; γ = 90°.
Volume	2116.1(8) $Å^3$	1623.08(8) $Å^3$	1509.3(5) $Å^3$	2181.00(19) $Å^3$
Z	4	4	4	4
Density (calculated)	2.166 mg m^{-3}	2.091 mg m^{-3}	1.915 mg m^{-3}	2.214 mg m^{-3}
Absorption coefficient	2.063 mm^{-1}	1.720 mm^{-1}	1.484 mm^{-1}	1.982 mm^{-1}
***F*(000)**	1376	1024	876	1408
Crystal size	0.28 x 0.24 x 0.14 mm	0.33 x 0.16 x 0.16 mm	0.38 x 0.35 x 0.32 mm	0.71 x 0.28 x 0.26 mm
Theta range for data collection	2.42 to 28.37°	1.91 to 28.48°	2.61 to 24.99°	1.800 to 28.581°
Reflections collected	38151	36962	2369	12862
Index ranges	-14<=h<=14	-20<=h<=21	-5<=h<=8	-15<=h<=15
	-11<=k<=15; -22<=l<=21	-18<=k<=18; -9<=l<=9	-4<=k<=9; -24<=l<=22	-15<=k<=14; -22<=l<=22
Independent reflections	2638 [R(int) = 0.0253]	4076 [R(int) = 0.0279]	1795 [R(int) = 0.0181]	4566 [R(int) = 0.0212]
Completeness to theta = 28.37°	99.70%	99.30%	70.20%	93.6 %
Max. and min. transmission	0.7611 and 0.5959	0.7739 and 0.6022	0.6514 and 0.6046	0.632 and 0.332
Data / restraints / parameters	2638 / 0 / 153	4076 / 1 / 223	1795 / 0 / 197	4566 / 1 / 307
Goodness-of-fit on F2	1.105	1.016	1.154	1.049
Final R indices [I>2sigma(I)]	R1 = 0.0193, wR2 = 0.0498	R1 = 0.0147, wR2 = 0.0357	R1 = 0.0421, wR2 = 0.1042	R1 = 0.0164, wR2 = 0.0420
R indices (all data)	R1 = 0.0206, wR2 = 0.0509	R1 = 0.0152, wR2 = 0.0359	R1 = 0.0437, wR2 = 0.1051	R1 = 0.0170, wR2 = 0.0424
Absolute structure parameter	-	0.006(12)	0.45(6)	-0.009(8)
Largest diff. peak and hole	1.272 and -0.459 e $Å^{-3}$	0.432 and -0.298 e $Å^{-3}$	0.0000(6) e $Å^{-3}$	0.522 and -0.459 e $Å^{-3}$

Table 5: Crystallographic data and structural refinement details for $\mathbf{CN_2}$ and $\mathbf{CN_3}$

	$\mathbf{CN_2}$	$\mathbf{CN_3}$
Empirical formula	$C_{5.50}H_{0.12}F_3N_{3.50}O_3PSAg$	$C_{12}H_{19.33}N_6O_{7.33}P_{1.33}Ag_{1.33}$
Formula weight	391.12	550.12
Crystal system	Orthorhombic	Orthorhombic
Space group	*Pnma*	*Aba*2
Unit cell dimensions	a = 16.214(5) Å; α = 90.000(5)°	a = 6.9445(2) Å; α = 90°
	b = 6.733(5) Å; β = 90.000(5)°	b = 66.6807(16) Å; β = 90°
	c = 27.026(5) Å; γ = 90.000(5)°	c = 12.2203(3) Å; γ = 90°
Volume	2950(2) Å^3	5658.8(3) Å^3
Z	8	12
Density (calculated)	1.761 mg m^{-3}	1.937 mg m^{-3}
Absorption coefficient	1.650 mm^{-1}	12.822 mm^{-1}
F(000)	1493	3296
Crystal size	0.12 x 0.23 x 0.17 mm	0.180 x 0.15 x 0.12 mm
Theta range for data collection	1.465 to 28.286°	23.609 to 64.485°
Reflections collected	83708	27520
Index ranges	-21<=h<=21, -8<=k<=8, -36<=l<=36	-8<=h<=8 -78<=k<=78, -6<=l<=14
Independent reflections	3934 [R(int) = 0.0315]	2972 [R(int) = 0.1074]
Completeness to theta = 28.37°	99.4 %	81.6 %
Data / restraints / parameters	3934 / 0 / 164	2972 / 1 / 376
Goodness-of-fit on F2	2.436	1.089
Final R indices [I>2sigma(I)]	R1 = 0.1401, wR2 = 0.4622	R1 = 0.0362, wR2 = 0.0974
R indices (all data)	R1 = 0.1580, wR2 = 0.4995	R1 = 0.0363, wR2 = 0.0975
Absolute structure parameter	-	0.077(13)
Largest diff. peak and hole	0.437 and -0.598 e Å^{-3}	0.827 and -0.723 e Å^{-3}

2.4 References

[1] D. J. Daigle, *Inorganic Syntheses*, **1998**, *40.* 40-44.

[2] Bruker. *APEXII*. Bruker AXS Inc., Madison, Wisconsin, USA, **2009**.

[3] Bruker. *COMSO*. Bruker AXS Inc., Madison, Wisconsin, USA, **2009**.

[4] Bruker. *SAINT*. Bruker AXS Inc., Madison, Wisconsin, USA, **2009**.

[5] Bruker. *SADABS.* Bruker AXS Inc., Madison, Wisconsin, USA, **2009**.

[6] G. M. Sheldrick, *Acta Crystallographica*, **2008**, A64, 112-122.

[7] Farrugia, L. J. *Journal of Applied Crystallography*, **2012**, 45, 849-854.

[8] C. F. Macrae, P. R. Edgington, P. McCabe, E. Pidcock, G. P. Shields, R. Taylor, M. Towler, J. van de Streek, *Journal of Applied Crystallography*, **2006**, 39, 453-457.

[9] K. Brandenburg, H. Putz, *DIAMOND.* Crystal Impact GbR, Bonn, Germany, **2005**

Chapter 3

3. Results and discussion

3.1 Reactions of PTA with silver(I) salts

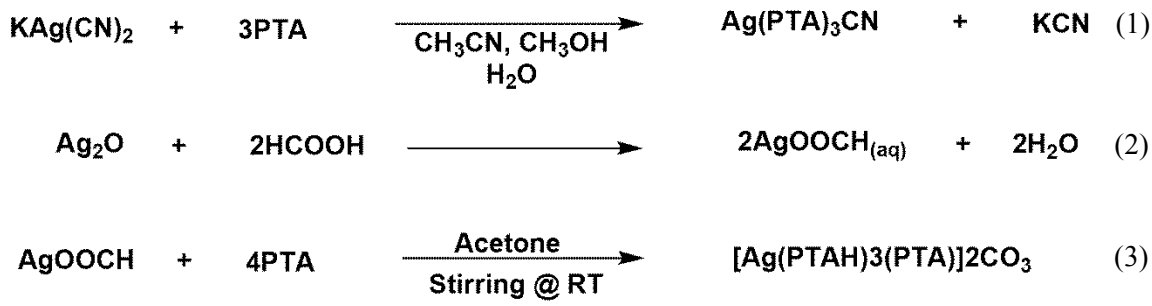

This section begins by discussing the reactions of PTA with various silver(I) salts. In an attempt to construct coordination architectures using a generalized synthetic procedure, part of the focus of this work was on the influence of the anions of Ag(I) salts on the topology and the metal geometry of coordination compounds.

The formation of discrete coordination compound **DCC$_1$** resulted from a solvothermal reaction of equimolar amounts of $KAg(CN)_2$ with PTA in a methanol-water medium producing a clear solution as shown in Equation 1. After reducing the volume of the solvent, addition of acetonitrile to this solution led to the precipitation of the product as white microcrystalline product in 96% yield. Discrete coordination compound **DCC$_2$** was formed in a two-step reaction as shown in Equations 2 and 3. In the first reaction, silver(I) oxide was reacted with formic acid (1:2 mole ratio) in an aqueous medium to give silver(I) formate. The second reaction involved a solution of acetone containing PTA being added drop-wise to the dissolved silver salt. After filtering the mixture, the product formed upon slow evaporation of the filtrate with low yield (10 %).

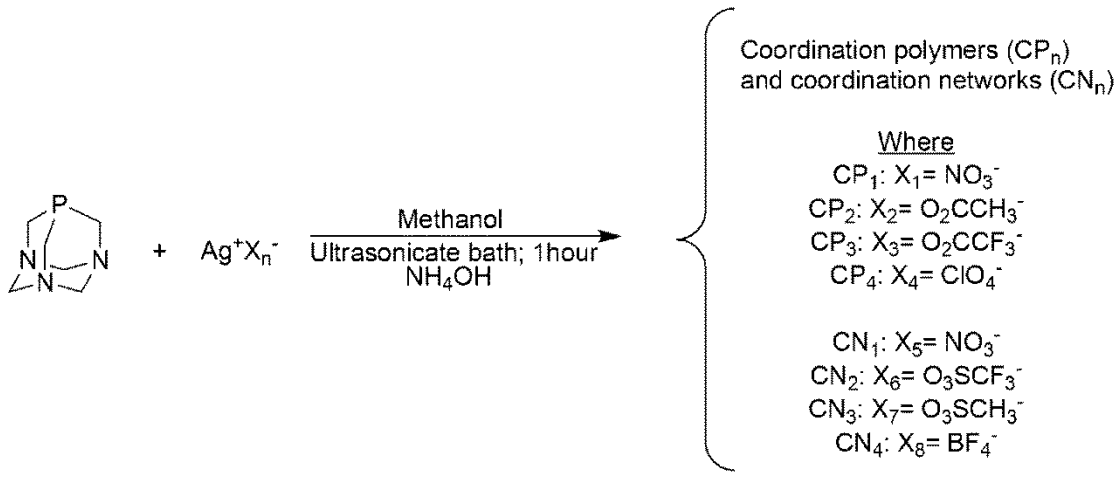

Scheme 3: Synthesis of silver(I)-PTA coordination polymers and networks

For silver(I) coordination polymers and networks, the counter-ions of the Ag(I) salts used were NO_3^- (for compound **CP$_1$** and **CN$_1$**), $H_3CCO_2^-$ (for compound **CP$_2$**) ClO_4^- (for **CP$_4$** and **CP$_5$**), $O_3SCF_3^-$ (for **CN$_2$**), $O_3SCH_3^-$ (for **CN$_3$**), BF_4^- (**CN$_4$**). These polymeric compounds were formed as a result of the reactions of PTA with the corresponding Ag(I) salt in equimolar amounts at ambient temperature in methanol as shown in Scheme 3. There was an immediate formation of a white precipitate, which was the desired silver(I)-PTA complexes as confirmed by ^{1}H, ^{13}C and ^{31}P NMR spectroscopy. Treatment of the reaction mixture with NH_3(aq) re-dissolved the white precipitate and X-ray quality crystals were obtained by slow evaporation of the mother liquor.

3.1.1 Spectroscopic studies of silver(I)-PTA coordination compounds

In order to understand and account for the successful coordination of PTA onto a silver(I) metal centre using solution NMR, it is essential to first understand the solution NMR of the free PTA. A short NMR study was done on free PTA in two different solvents D_2O and $CDCl_3$ because they have different polarities which were found to result in two distinct ^{1}H NMR spectra.

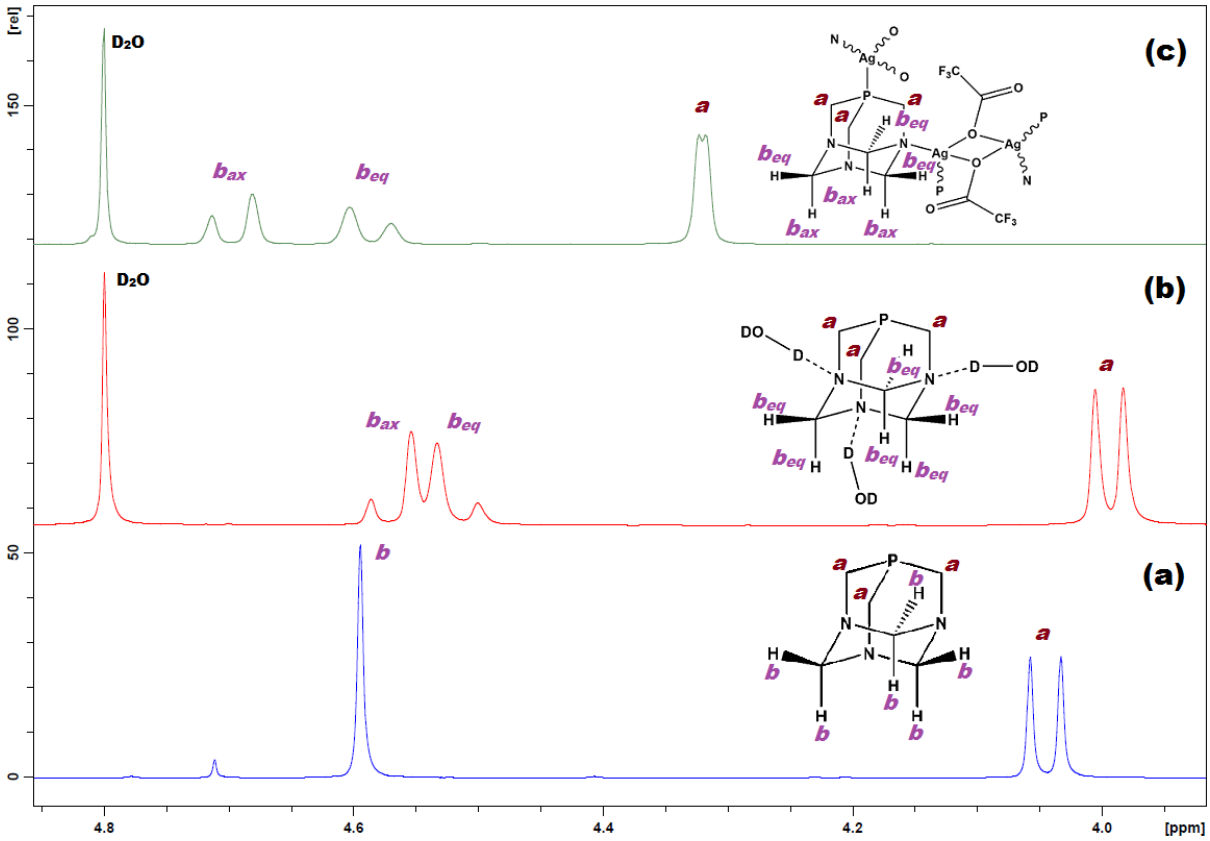

Figure 11: ^{1}H NMR spectrum of (a) free PTA in $CDCl_3$, (b) free PTA in D_2O and (c) **CP_3** in D_2O

The ^{1}H NMR spectra of PTA in $CDCl_3$ and D_2O are shown in Figure 11(a) and (b) respectively. The spectra reveal that free PTA exhibits two signals, one for the methylene protons between the phosphorus and nitrogen atoms (P-C**H**$_2$-N) and the other signal for the methylene protons between two nitrogen atoms (N-C**H**$_2$-N). The N-C**H**$_2$-N protons resonate at δ = 4.60 ppm and appear as a singlet in $CDCl_3$ signifying that methylene protons are equivalent. In $CDCl_3$ and D_2O, the P-C**H**$_2$-N protons (*a* in Figure 11a and Figure 11b) appear as a doublet which resonates between δ = 3.89-4.06 ppm for the free PTA. This is due to the fact that the phosphorus has the same spin as hydrogen; thus splitting the proton signal with $^{2}J_{P\text{-}H}$ values of 9.9 Hz and 9.0 Hz, respectively. The difference between the free PTA's ^{1}H NMR spectra in the two solvents lies in the N-C**H**$_2$-N protons. These appear as a singlet in $CDCl_3$ (*b* in Figure 11(a)) which signifies that methylene protons are equivalent. However, in D_2O the N-C**H**$_2$-N protons appear as two distinct doublets (b_{ax} and b_{eq} in Figure 11b) and this is due to the fact that D_2O is a protic polar solvent; thus it interacts with the nitrogen atoms of the PTA via hydrogen bonding. This interaction between the solvent molecule and the nitrogen atoms of the PTA influences the N-C**H**$_2$-N protons to become diastereotropic which then causes the axial and equatorial protons of the methylene group to

be non-equivalent resulting in the formation of an AB type spin which constitutes the two doublets observed in the ranges δ = 4.59-4.55 ppm and δ = 4.53-4.50 ppm with J_{AB} and J_{BA} values of 12.89 Hz and 13.01 Hz, respectively. $CDCl_3$ is not involved in any strong intermolecular hydrogen bonding with PTA, hence AB type spin is not observed but rather a singlet at δ 4.59 ppm. Figure 11(c) is a ^{1}H NMR spectrum of $[Ag(\mu\text{-}O_2CCF_3)(\mu\text{-PTA})]_n$ (**CP$_3$**) which is used as a representative spectrum for all the other synthesized Ag-PTA coordination compounds. It has similar features as the ^{1}H NMR spectrum of free PTA in D_2O since the N-C**H**$_2$-N protons exhibit the AB type spin. The difference is in the P-C**H**$_2$-N protons which appear slightly downfield at δ = 4.32 ppm and has a $^2J_{P\text{-}H}$ value of 2.08 Hz which is lower than that of free PTA (9.00 Hz in D_2O). This suggests that the phosphorus atom of PTA is coordinated to the Ag metal since the $^2J_{P\text{-}H}$ value is comparable to those published for Ag(I)-PTA compounds.[1] The N-C**H**$_2$-N protons exhibit AB type spin with J_{AB} and J_{BA} values of 12.97 Hz and 13.25 Hz respectively but the doublets appear slightly downfield between δ = 4.71-4.68 ppm and δ = 4.60-4.57 ppm, respectively. The separation of 0.11 ppm between the two distereotropic protons signals signifies that the N-C**H**$_2$-N protons have become even more non equivalent and this might not so much be caused by the intermolecular hydrogen bonding with the D_2O molecules but rather more of coordination via the PTA's nitrogen atom to the silver(I) metal centre. ^{1}H NMR results also provided evidence of the presence of the anion in compounds $[Ag(\mu_2\text{-}O_2CCH_3)(PTA)]_n$ (**CP$_3$**) and $[Ag(PTA)]_n(O_3SCH_3)_n$ (**CN$_3$**), whereby the singlet for the methyl group appears at δ = 1.94 ppm for the acetate group and δ = 2.83 ppm for the methanesulfonate group, respectively. ^{1}H NMR results also provided evidence of the presence of the 4-nitrophenol molecules in compounds $[Ag(PTA)_3][4\text{-NP}]_{10}$ (**DCC$_3$**) and $[Ag_2(PTA)_2(\mu_1\text{-}NO_3)][4\text{-NP}][H_2O][NO_3]$ (**CN$_5$**), whereby two sets of doublets for the aromatic protons appear at δ 6.93 ppm and δ 8.12 ppm with ^2J values of 3.0 Hz, respectively.

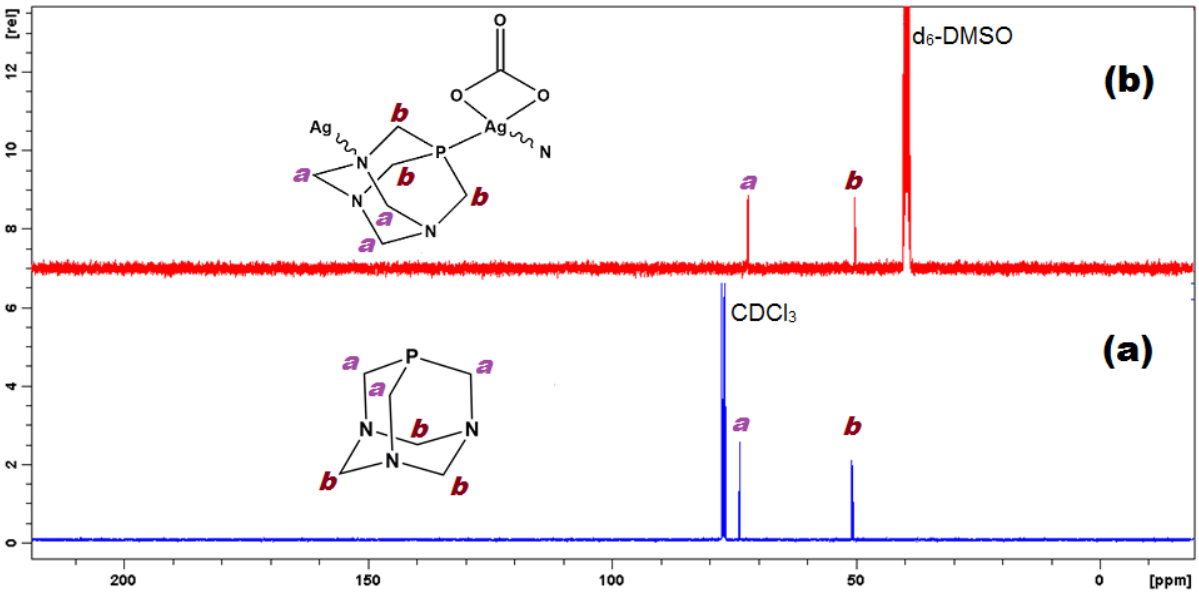

Figure 12: ^{13}C NMR of (a) [Ag(μ-PTA)(μ-NO_3)]$_n$ (**CP$_1$**) in d_6-DMSO and (b) PTA in $CDCl_3$

Figure 12(a) is a ^{13}C NMR spectrum of free PTA in $CDCl_3$ which shows two sets of signals. One of the signals is for the P-**C**H_2-N carbons **(**labelled as *b*) at δ 50.56-50.76 ppm and the other set resonating at δ = 73.71-73.74 ppm for the N-**C**H_2-N carbons **(**labelled as *a*). Figure 12(b) is a ^{13}C NMR spectrum of [Ag(*μ*-PTA)(NO_3)]$_n$ (**CP$_1$**) which as a representative spectrum for all the other synthesized Ag-PTA coordination compounds displayed similar sets of signals as the free PTA with the P-**C**H_2-N carbons resonating between δ = 50.56-50.76 ppm and the N-**C**H_2-N carbons resonating between δ = 73.71-73.74 ppm which provides evidence of the presence of PTA in the silver(I) complexes. In general, not much information with regards to coordination of PTA onto silver atom could be obtained using ^{13}C NMR except for cases where the presence of the anion is evident. The ^{13}C NMR spectra of, **CP$_3$** showed peaks at δ = 23.1 ppm for –**C**H_3 and δ = 181.4 ppm for –**C**=O from the acetate group; **CP$_4$** showed peaks at δ = 121.7 ppm for –**C**F_3 and δ = 181.4 ppm for –**C**=O from the trifluoroacetate group; **CN$_2$** showed peaks at δ = 121.7 ppm for –**C**F_3 from the trifluoromethanesulfonate group; **CN$_3$** showed peaks at δ = 23.1 ppm for –**C**H_3 from the methanesulfonate group; **DCC$_1$** showed peaks at δ = 152.4 ppm for –**C**N from cyanide group, and **DCC$_2$** showed peaks at δ = 170.8 ppm for carbonyl group from the carbonate ion.

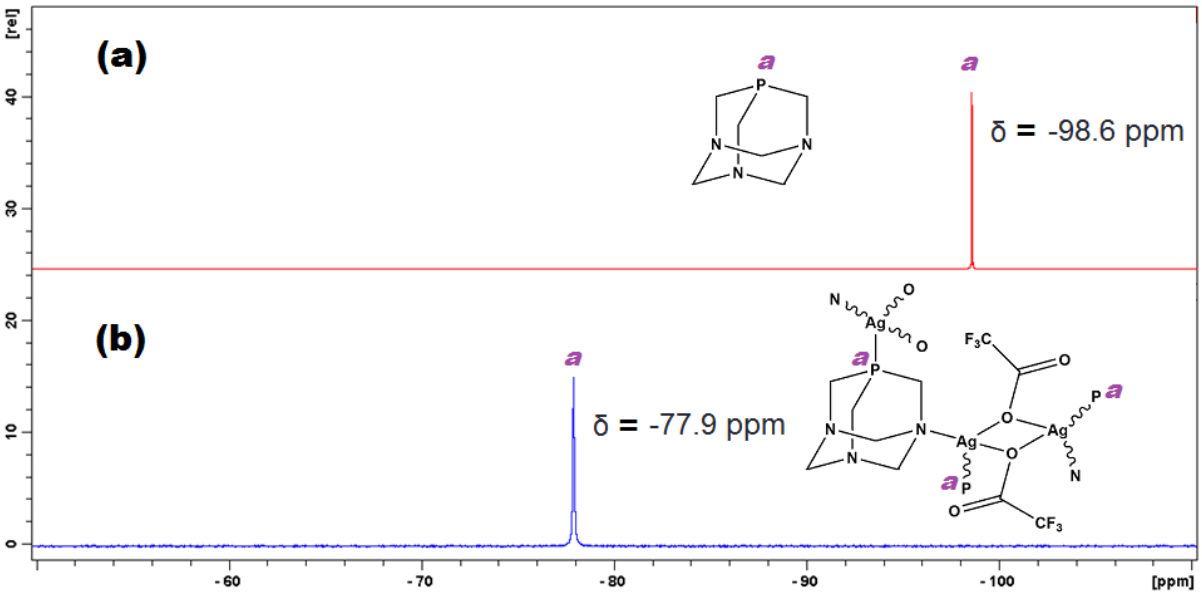

Figure 13: ^{31}P NMR of (a) PTA and (b) $[Ag(\mu\text{-PTA})(\mu\text{-}O_2CCF_3)]_n$ (**CP_3**)

Figure 13(a) shows the ^{31}P NMR spectrum of PTA in D_2O. The spectrum shows only one signal which appears as a sharp singlet resonating at δ -98.63 ppm. Figure 13(b) is the ^{31}P NMR spectrum of **CP_3** which is a representative spectrum for all the other Ag-PTA coordination compounds. The spectrum also shows one signal which resonates at a much higher frequency of δ -77.9 ppm when compared with that of free PTA and this is comparable to those of related silver(I)-PTA compounds in literature.[1] The signal appears as a broad singlet with ^{107}Ag-^{31}P and ^{109}Ag-^{31}P spin-spin coupling not observed in all cases because of the occurrence of fast ligand exchange which is typical of silver monophosphine coordination compounds.[1a] Therefore, based on ^{31}P NMR results, coordination of PTA via the phosphorus atom was confirmed. [1a]

Table 6: Characteristic NMR spectroscopic data for Ag(I)-PTA coordination compounds

Compound	δ (d, 6H,P-C**H**$_2$-N, ^{1}H)	δ (d, 3H, N-C**H$_{2(eq)}$**-N, ^{1}H)	δ (d, 3H, N-C**H$_{2(ax)}$**-N, ^{1}H)	δ (P, ^{31}P)
DCC$_1$	4.11 ($^2J_{P-H}$ = 6.0 Hz)	4.55 (J_{AB} = 13.2 Hz)	4.63 (J_{BA} = 13.0 Hz)	-90.4
DCC$_2$	4.18 ($^2J_{P-H}$ = 4.7 Hz)	4.58(J_{AB} = 13.3 Hz)	4.68 (J_{BA} = 14.0 Hz)	-82.6
CP$_1$	4.23 ($^2J_{P-H}$ = 2.8 Hz)	4.40 (J_{AB} = 12.8 Hz)	4.58 (J_{BA} = 12.6 Hz)	-85.9
CP$_2$	4.32 ($^2J_{P-H}$ = 1.1 Hz)	4.58 (J_{AB} = 13.2 Hz)	4.69 (J_{BA} = 13.0 Hz)	-78.0
CP$_3$	4.32 ($^2J_{P-H}$ = 2.1 Hz)	4.59 (J_{AB} = 13.2 Hz)	4.70 (J_{BA} = 13.0 Hz)	-77.9
CP$_4$	4.23 ($^2J_{P-H}$ = 2.8 Hz)	4.60 (J_{AB} = 12.6 Hz)	4.40 (J_{BA} = 12.8 Hz)	-85.2
CP$_5$	4.16 ($^2J_{P-H}$ = 2.6 Hz)	4.40 (J_{AB} = 12.9 Hz)	4.54 (J_{BA} = 12.6 Hz)	-86.3
CN$_1$	4.23 ($^2J_{P-H}$ = 2.9 Hz)	4.41 (J_{AB} = 13.0 Hz)	4.57 (J_{BA} = 12.7 Hz)	-85.9
CN$_2$	4.22 ($^2J_{P-H}$ = 3.2 Hz)	4.52 (J_{AB} = 12.7 Hz)	4.66 (J_{BA} = 12.4 Hz)	-80.4
CN$_3$	4.31 ($^2J_{P-H}$ = 2.1 Hz)	4.58 (J_{AB} = 13.2 Hz)	4.69 (J_{BA} = 12.9 Hz)	-80.4
CN$_4$	4.23 ($^2J_{P-H}$ = 2.9 Hz)	4.42 (J_{AB} = 12.8 Hz)	4.58 (J_{BA} = 12.6 Hz)	-85.5

Table 6 lists characteristic ^{1}H and ^{31}P NMR data for Ag-PTA coordination compounds. There are some observable trends where the discrete compounds **DCC$_1$** and **DCC$_2$** have higher $^2J_{P-H}$ values (6.0 Hz to 4.7 Hz) than those of coordination polymers and networks (3.2 Hz to 1.1 Hz). **CP$_2$** and **CP$_3$** contain carboxylate groups which, based on their similarities in NMR features, suggests that **CP$_2$** and **CP$_3$** may have similar molecular architectures as will be shown in section 3.1.3.

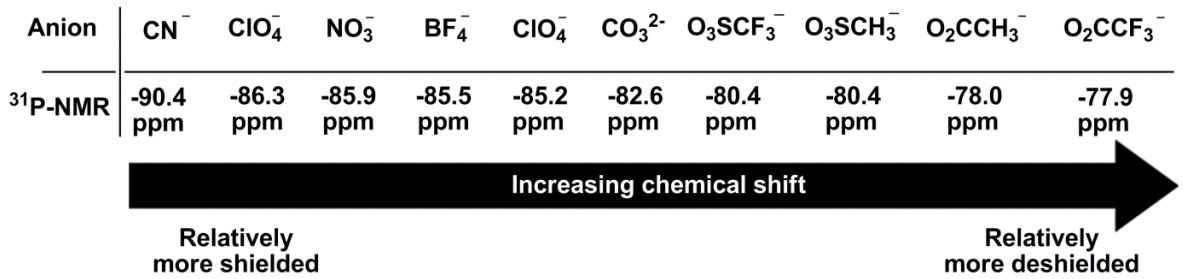

Figure 14: Influence of the anion on the chemical shifts of the peak in ^{31}P-NMR spectra of Ag-PTA coordination compounds

Figure 14 shows the effect of the Ag and the anion on the chemical shifts of the phosphorus peak in the ^{31}P NMR spectra of Ag-PTA coordination compounds. **CP$_4$** and **CP$_5$** contain the same perchlorate anion but the oxidation states of the metal centres are found to be Ag^{3+} and Ag^{+}, respectively. The phosphorus atom coordinated to the Ag^{3+} metal centre experiences a slightly more electron shielded environment with respect to the phosphorus atom that is

coordinated to the Ag^+ metal centre which experiences a more electron deshielded environment. The effect of the anions appears not to follow any particular trend in terms of the overall structure of the Ag-PTA coordination compounds. For example, the nitrate anion is present in both **CP_1** and **CN_1** but the two coordination compounds have different overall structures with the anion having different coordination modes, yet the chemical shifts of the peak observed in ^{31}P NMR spectra of **CP_1** and **CN_1** are the same (δ = -85.9 ppm). In general, the influence of the anions on the chemical shifts of the peak in ^{31}P NMR could be based on its electronic properties.

The IR spectra of all the silver(I)-PTA coordination compounds exhibit related features with typical vibrations due to the anions and PTA ligands. Hence, a number of characteristic bands in the range 2942-2950 cm^{-1} and 1100-900 cm^{-1} associated with $\nu(CH_2)$ and ν(C-X; X = P and N) vibrations within the PTA ligands were observed. **CP_1** and **CN_1** were both synthesized using $AgNO_3$ as the precursor; hence $\nu(NO_3)$ vibration bands are observed in the range 1420-1232 cm^{-1}. **CN_1** also contains a broad band attributed to the $\nu(H_2O)$ vibration mode lying between 3500 cm^{-1} and 3200 cm^{-1}. The broadness of the band is associated with the extensive hydrogen bonding interactions of the coordinated water molecule.[1c] **DCC_2**, **CP_2** and **CP_3** were synthesized using silver(I) carboxylate salts as precursors and their IR spectra contain two sets of high intensity vibration frequency appearing between 1654-1534 cm^{-1} and 1450-1399 cm^{-1} due to the asymmetric and symmetric modes of the carboxylate groups, respectively. **CP_2** also contains $\nu(H_2O)$ vibrations with a broad band lying between 3500-3200 cm^{-1} which is associated with the extensive hydrogen bonding interactions of the two waters of crystallization that are present in **CP_2**.[1a, b] **CN_3** and **CN_4** were both synthesized using silver(I) sulphonate salts as precursors and two sets of bands are associated with the high intensity ν(S=O) vibration appearing between 1240-1232 cm^{-1} and the medium intensity ν(S-O) vibration observed between 1010-1008 cm^{-1}. The IR spectrum of **DCC_1** displays a weak intensity band at 2106 cm^{-1} pertaining to ν(CN) vibration mode and a broad peak lying between 3500-3200 cm^{-1} which is associated with the extensive hydrogen bonding interactions of the two of waters crystallization present in **DCC_1**.

The ESI(+) mass spectrometry results of all the silver(I)-PTA coordination polymers synthesized in this work have a common characteristic feature in which the formation of multiple charged ion species with either solvent, sodium or potassium adducts are observed. The common ion species are listed in Table 7.

Table 7: Common ionic species in the ESI(+) mass spectra of silver(I)-PTA coordination compounds

m/z	Ionic species	Compound
330	$[Ag(PTA)+CH_3CN+Na+H]^{3+}$	**CP_1, CP_2**
368	$[Ag(PTA)+3H_2O+2Na+3H]^{6+}$	**DCC_1, CP_2, CP_4**
377	$[(PTA)_2+H_2O+2Na+3H]^{5+}$	**DCC_2, CP_4**
417	$[(PTA)_2+H_2O+2Na+K]^{3+}$	**DCC_1, DCC_2**
429	$[Ag(PTA)+H_2O+CH_3CN+Na]^{2+}$	**DCC_1, CP_2, CP_3**
461	$[Ag(PTA)_2+K]^{2+}$	**DCC_2, CP_1, CN_1**
575	$[Ag_2(PTA)_2+K+6H]^{10+}$	**DCC_1, CP_2, CP_3**
610	$[Ag_2(PTA)_2+CH_3CN+K]^{3+}$	**CP_{1-4}, CN_{1-4}**
684	$[Ag_3(PTA)_2+CH_3CN+H_5]^{8+}$	**CP_{1-4}, CN_{1-4}**
776	$[Ag_3(PTA)_2+CH_3CN+5H+4Na]^{12+}$	**CP_{1-4}, CN_{1-4}**
850	$[Ag_3(PTA)_3+3H_2O+H]^{4+}$	**CP_{1-4}, CN_{1-4}**

Despite the presence of common ions in all the silver(I)-PTA complexes, there are some unique features in each ESI(+) mass spectra.

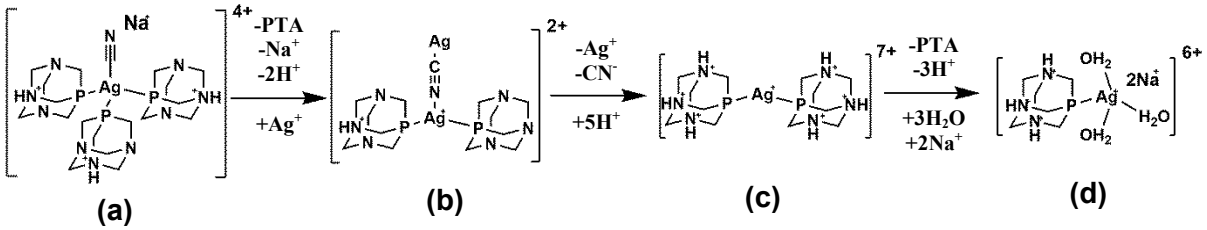

Figure 15: Proposed fragmentation pattern of **DCC_1**

Figure 15 shows the ions that are observed due to the fragmentation of **DCC_1**. The ESI(+) mass spectrum of discrete silver(I)-PTA coordination compound **DCC_1** was characterized by the presence of the peak at m/z 631 with 90 % abundance, corresponding to the sodiated $[Ag(PTA)_3(CN)+Na+3H]^{4+}$ species which confirms the formation of the desired tetra-coordinated silver(I) complex containing three PTA molecules as shown in Figure 15(a). A peak at 557 m/z with 40% abundance is attributed by the rearranged adduct

$[Ag(PTA)_2.AgCN+H]^{2+}$ species which is characteristic of the loss of one PTA molecule of DCC_1 as shown in Figure 15(b).[2] A peak at 429 m/z with 100 % abundance is attributed to the bis-substituted $[Ag(PTA)_2+7H]^{8+}$ species which resembles a loss of AgCN in ion species (b) as shown in Figure 15(c). Finally, the peak at 368 m/z with 50 % relative abundance is attributed to ionic species shown in Figure 15(d) which resembles the loss of one PTA molecule from the ionic species (c).

The ESI(+) mass spectrum of discrete silver(I)-PTA coordination compound **DCC_2** was characterized by the presence of the peaks at 101 m/z (20% abundance) and 115 m/z (<10% abundance) which correspond to fragmented PTA species $[PTA\text{-}CH_2N(CH_2)CH_2]^+$ and $[PTA\text{-}CH_2NCH_2]^+$ reported by Tisato *el al*.[2] A base peak at 158 m/z (100% abundance) corresponds to the protonated form of PTA $[PTA+H]^+$ species and a peak at 174 m/z with 30% abundance could be attributed to the methylated PTA $[PTAMe+2H]^{3+}$ species which could have formed by the combination of PTA and methyl radicals in the ionization chamber. A peak at 242 m/z (20% abundance) could be due to the inclusion of solvent to the silver-phosphazene species (221 m/z) reported by Tisato *et al.* which forms the new $[(Ag\text{-phosphazene})+2H_2O+5H]^{6+}$ species.[2] The peaks at 461 (20% abundance) and 620 (<10% abundance) are attributed sodiated bis-substituted and tri-substituted silver-PTA species $[Ag(PTA)_2+H_2O+Na]^{2+}$ and $[Ag(PTA)_3+H_2O+Na]^{2+}$, respectively. The peaks observed in the ESI(+) mass spectra of the rest of the silver(I)-PTA coordination compounds were attributed to the respective ionic species are listed in Table 8.

Table 8: Attributed peaks in the ESI(+) mass spectra of silver(I)-PTA coordination polymers and coordination networks

Compound	m/z (relative abundance)	Ionic species
CP_1	682 (20%)	$[Ag_2(PTA)_2(NO_3)+2H_2O+3H]^{4+}$
	421 (95%)	$[Ag(PTA)_2]^+$
CP_2	487 (30%)	$[Ag(PTA)_2(O_2CCH_3)+6H]^{5+}$
	702 (60%)	$[Ag_2(PTA)_2(O_2CCH_3)_2+2Na+6H]^{8+}$
CP_3	343 (25%)	$[Ag(PTA)+3H_2O+Na+H]^{3+}$
	495 (45%)	$[Ag(PTA)(O_2CCF_3)+2H_2O+2K+3H]^{5+}$
	438 (100%)	$[Ag(PTA)(O_2CCF_3)+K+3H]^{4+}$
CP_4	396 (50)	$[Ag(PTA)(ClO_4)+4H]^{4+}$
	488 (40)	$[Ag(PTA)_2+H_2O+2Na+2H]^{5+}$
	519 (20)	$[Ag(PTA)_2+2K+H_2O+H]^{4+}$
	605 (25)	$[Ag(PTA)_2(ClO_4)+3H_2O+Na+6H]^{7+}$
	758	$[Ag(PTA)_3(ClO_4)+3H_2O+Na+2H]^{3+}$
	610	$[Ag_2(PTA)_2+CH_3CN+K]^{3+}$
CN_1	421 (95%)	$[Ag(PTA)_2]^+$
CN_2	352	$[Ag(PTA)+CH_3CN+2Na]^{3+}$
	510 (40%)	$[Ag(PTA)(O_3SCF_3)+Na+4H_2O+H]^{2+}$
	519 (50%)	$[Ag(PTA)_2+2K+H_2O+H]^{4+}$
	588 (45%)	$[Ag(PTA)(O_3SCF_3)_2+Na+2H]^{2+}$
CN_4	352	$[Ag(PTA)+CH_3CN+2Na]^{3+}$
	403	$[Ag(PTA)(BF_4)+5H+2Na]^{7+}$

Table 9 lists some thermal properties of the synthesized silver(I)-PTA coordination compounds. **DCC_2, CP_1**, **CP_3**, **CN_2** and **CN_3** are non-solvated whereas **DCC_1** and **CP_2** are dihydrated and in these, the loss of the water molecules occurs at 78 °C and 70 °C, respectively. The loss of the water molecules in both **DCC_1** and **CP_2** occur as endothermic events with ΔH values of 172 kJ mol^{-1} and 92.5 kJ mol^{-1}, respectively. However, **CN_1** contains a coordinated water molecule which is lost at a higher temperature (121 °C) than that of **DCC_1** and **CP_2** (70-78 °C). All compounds appear to be thermally stable up temperatures of 210 °C that is despite the loss of water molecules observed in **DCC_1**, **CP_2** and **CN_1**. In the temperature range of 213 to 272 °C, decomposition of the Ag-PTA complexes (associated to the loss of PTA) occurs as an exothermic event.

Table 9: Summary of events from the thermal analysis of silver(I)-PTA coordination compounds

Compound	Anion	Solvent	Temperature/°C	
			Loss of solvent[a]	Decomposition[b]
DCC_1	CN	H_2O	78	272
DCC_2	CO_3	-	-	228
CP_1	NO_3	-	-	227
CP_2	O_2CCH_3	H_2O	70	233
CP_3	O_2CCF_3	-	-	220
CN_1	NO_3	H_2O	121	227
CN_2	O_3SCF_3	-	-	213
CN_3	O_3SCH_3	-	-	232

[a] Endothermic event; [b] Exothermic event

Figure 16 shows the TGA and DSC traces of **CN_1**. There is an interesting observation made in the TGA trace of **CN_1**. A sharp spike appears at the temperature of 224 °C indicating a very rapid weight increase of 7.442 % and the event is accompanied by sudden loss of a significant amount (about 80 % weight loss) of the sample mass. According to Nadler, the rise in weight (%) is due to combustion of the sample which leads to the very rapid evolution of hot gases such as $H_2O(g)$, $CO_x(g)$ and $NO_x(g)$ that applied a downward force on the sample; thus increasing the weight.[3] **CN_1** and **CP_1** have similar TGA traces and this could be due to the presence of the nitrate moiety in both **CP_1** and **CN_1**.

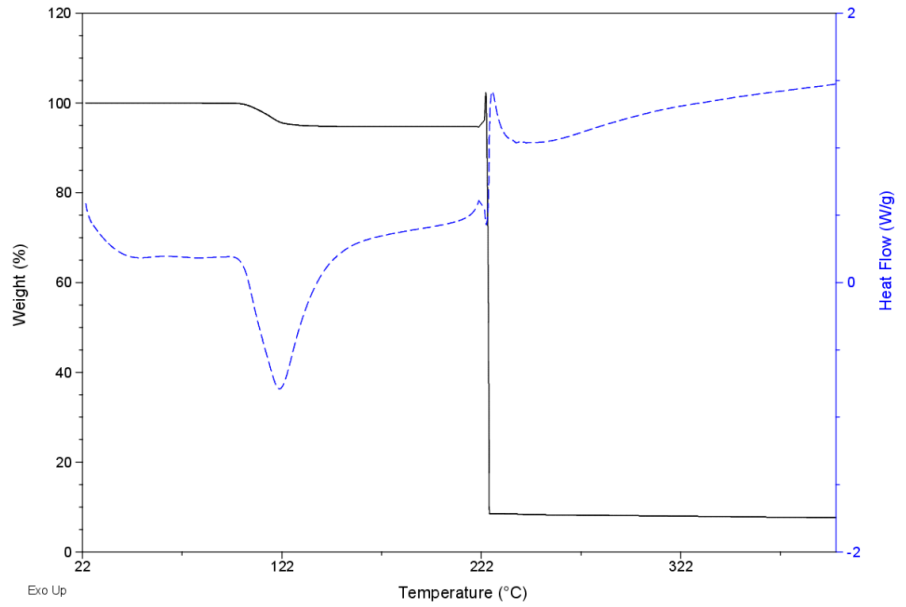

Figure 16: TGA and DSC traces of **CN_1**

3.1.2 Solid state structural analysis of Ag-PTA coordination compounds

This section outlines in detail the molecular and crystal structures of **DCC$_{1-3}$**, **CP$_{1-5}$** and **CN$_{1-3}$**. Also included is the discussion of hydrogen bonding patterns observed in each of the structures. As pointed out in the beginning of Chapter 3, different types of structures are formed; discrete complexes, coordination polymers and coordination networks. We start by discussing the molecular structures of the discrete complexes followed by those of coordination polymers.

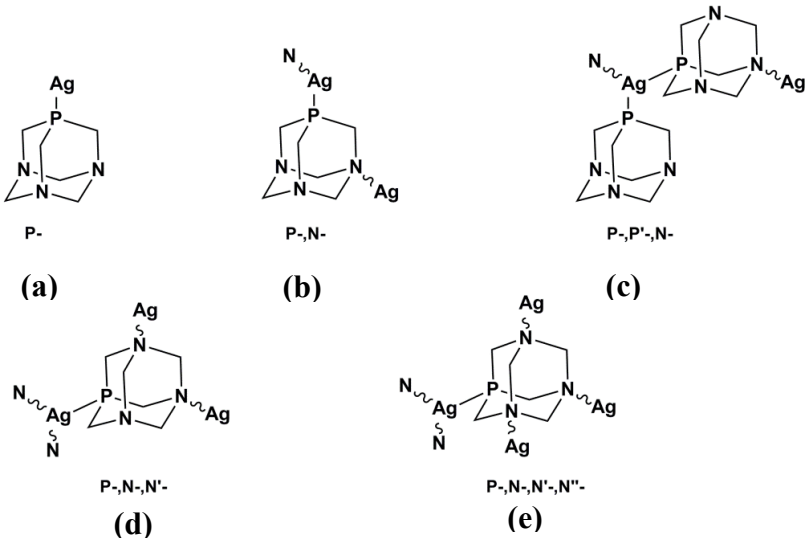

Figure 17: Coordination modes of Ag and PTA observed in the crystal structures of (a) discrete coordination compounds, (b-c) 1D coordination polymers and (d-e) 2D coordination networks

Figure 17 displays the different coordination modes of Ag and PTA observed in the crystal structures of Ag-PTA coordination compounds. The main difference between the discrete complexes and coordination polymers is mainly in the coordination mode of Ag atom to the donor atoms. In the discrete complexes **DCC$_{1-3}$**, the coordination was to the P atom only as shown in Figure 17(a) while for coordination polymers **CP$_{1-5}$** and coordination networks **CN$_{1-3}$**, there is coordination to P and N as depicted in (b), two P atoms and N atom as shown in (c), a P and two N atoms (d), and P and all three N atoms of the PTA as depicted in (e) of Figure 17. The anions also play a role in the formation of the overall molecular architecture of the various coordination compounds obtained. The diverse molecular architectures of the polymeric compounds include infinite 1D linear (**CP$_1$**), ladder-like (**CP$_2$** and **CP$_3$**), branched (**CP$_4$**) and zigzag (**CP$_5$**) coordination polymers, 2D corrugated sheet-like coordination networks (**CN$_1$** and **CN$_2$**) with cavities that are filled by the anions and a 2D non-corrugated sheet-like coordination network (**CN$_5$**).

3.1.2.1 Comparison of Ag-N, Ag-P and Ag-O bond distances in literature versus this work

We have carried out a search on the Cambridge Structural Database (CSD) for coordination compounds of silver(I) salts and PTA and derivatives for comparison reason. The search focuses on bond distances involving Ag(I) and three donor atoms, nitrogen, phosphorus from PTA and oxygen from either an oxidized phosphorus atom of the PTA, a solvent or from an anion.[4]

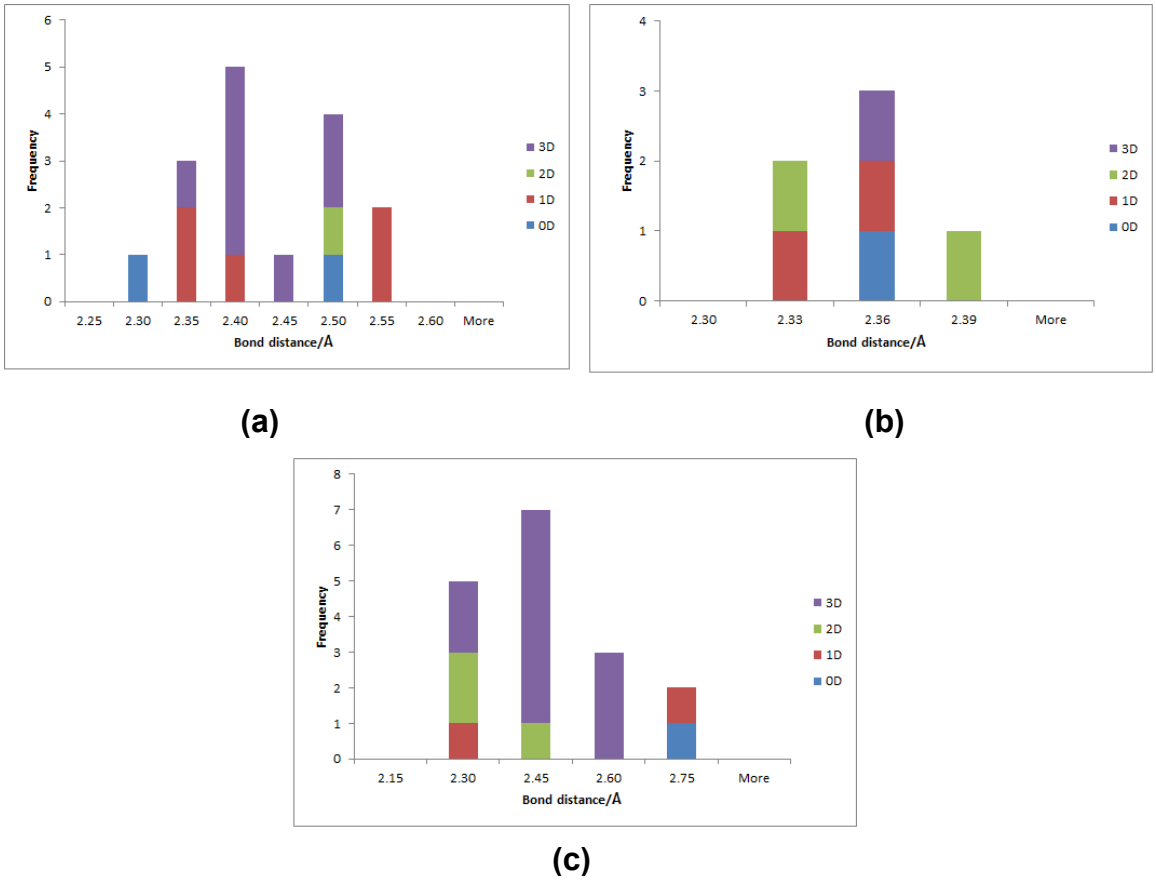

Figure 18: Distribution of (a) Ag-N, (b) Ag-P and (c) Ag-O bond distances from CSD search of crystal structures of silver(I) complexes containing PTA moieties

Figure 18 shows three histograms for the distribution of Ag-N, Ag-P and Ag-O bond distances of compounds from literature related to those in this study while Figure 19 shows some diagrams of Ag compounds containing PTA moieties from the CSD search. The search yielded a total of 41 hits which were split into 6 hits for Ag-P, 16 hits for Ag-N and 17 hits for Ag-O bond distances. The CSD ref codes of the hits are listed in Table 10.

Table 10: CSD ref codes of related Ag-PTA compounds and their frequecy of Ag-P, Ag-N and Ag-O bond distances

	Number of hits		
CSD ref code	**Ag-P**	**Ag-N**	**Ag-O**
ARODER	1	-	1
ARODIV	-	1	1
ARODOB	-	2	
ARODUH	1	1	1
AVEMIY	-	-	2
AVEMOE	-	2	2
BEVGEQ	1	2	
LEZLAF	1	4	3
LEZLEJ	-	1	1
OFUSEP	-	1	4
QARDIY	1	2	1
YEMYIZ	1	-	1

The histogram of the Ag-N bond distances has a bimodal distribution as shown in Figure 18(a) with the shortest bond distance being 2.256 Å observed in the coordination compound shown in Figure 19(a). The longest Ag-N bond distance of 2.541 Å is obtained in the coordination polymer shown in Figure 19(b) while the average Ag-N bond distance is 2.409 (82) Å. The histograms of the Ag-P and Ag-O bond distances have a right skewed distribution as shown in Figure 18(b) and (c).

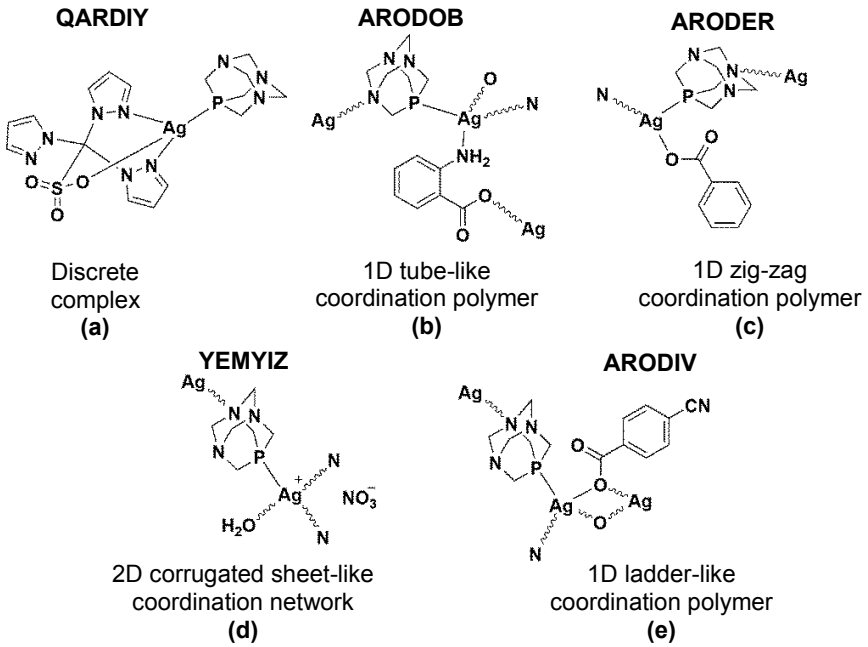

Figure 19: Structures of some Ag-PTA coordination from CSD

The shortest and longest Ag-P bond distances are 2.324 Å and 2.382 Å which are observed in compounds shown in Figure 19(c) and (d), respectively. The shortest and longest Ag-O bond

distances are 2.172 Å and 2.615 Å found in a 1D zig-zag coordination polymer and in a 1D ladder-like coordination as shown in Figure 19(c) and (e), respectively. The average Ag-P and Ag-O bond distances obtained from the CSD are 2.409(82) Å, 2.342(21) Å and 2.393(131) Å respectively.

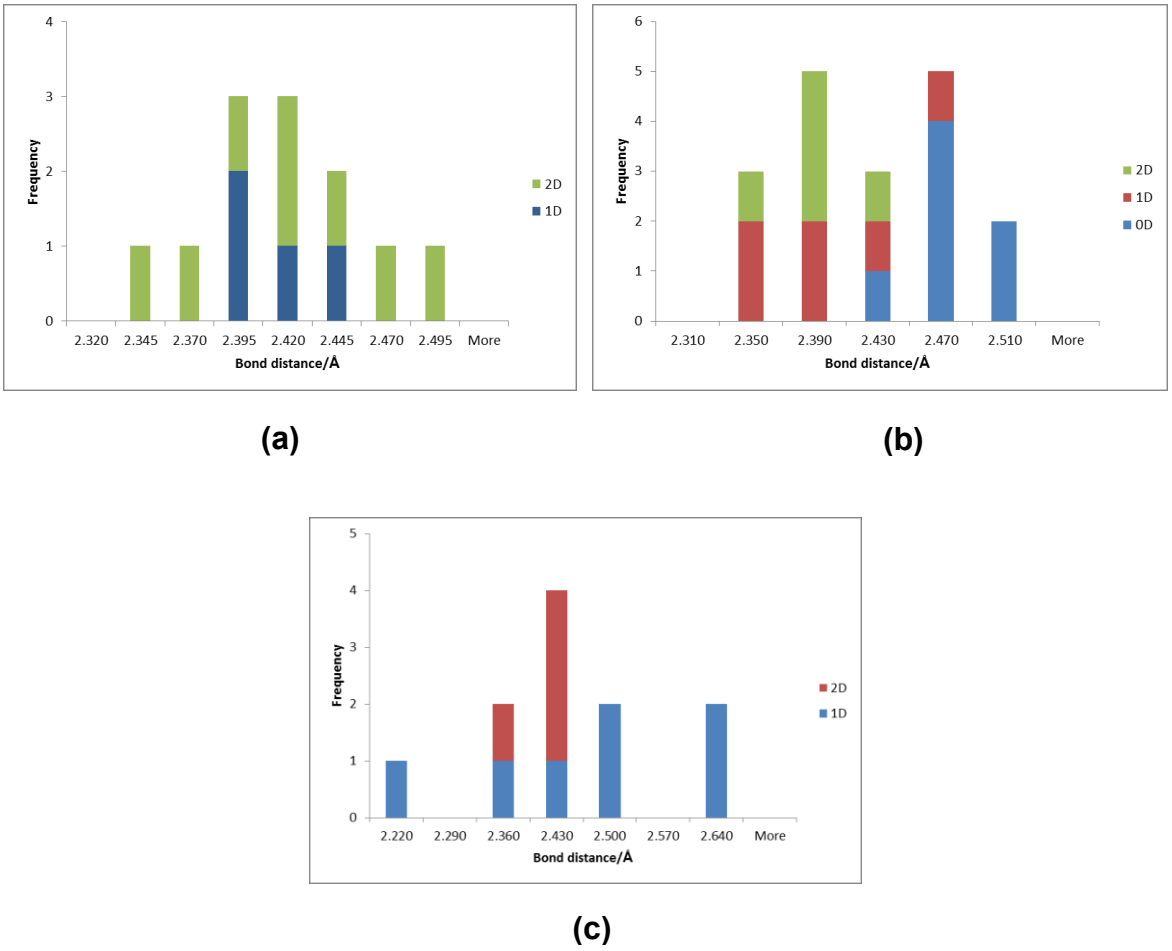

Figure 20: Distribution of (a) Ag-N, (b) Ag-P and (c) Ag-O bond distances from discrete complexes (0D), coordination polymers (1D) and coordination networks (2D) of Ag-PTA coordination compounds from our work

Histograms for the distribution of Ag-N, Ag-P and Ag-O bond distances of compounds reported in this study are given in Figure 20 while Figure 21 depicts some Ag-PTA coordination compounds. The histogram of the Ag-N bond distances as shown in Figure 20(a), has a right skewed distribution with the shortest Ag-N distance being 2.337 Å while the longest being 2.476 Å, which are evident in 2D coordination networks as shown in Figure 21(a) and Figure 21(b), respectively. The majority of the Ag-N bond distances lie between 2.39 Å and 2.44 Å and are mostly observed in 1D coordination polymers and 2D

coordination networks. Figure 20(b) shows the histogram of Ag-P bond distances which appears to have a bimodal distribution with the highest frequencies observed at 2.390 Å and 2.470 Å which are mostly found in coordination polymers and discrete complexes, respectively. The shortest and longest Ag-P bond distances are 2.3239(15) Å and 2.4728(6) Å and are statistically different at 5% probability. These are observed in coordination compounds shown in Figure 21(b) and (c), respectively. Lastly, a normal distribution with three extreme outliers is observed in the histogram of the Ag-O bond distances as depicted in Figure 20(c). The longest Ag-O bond distance of 2.22 Å is found in coordination compound shown in Figure 21(d) while the other outlier with the longest Ag-O bond distance of 2.584 Å is found in a 1D ladder-like coordination polymer shown in Figure 21(e). The rest of the Ag-O bond distances lie between 2.36 and 2.50 Å and have a bell shaped distribution for 1D coordination polymers and 2D coordination networks. The silver(I)-donor atom bond distances from CSD coincide with the average Ag-N, Ag-P and Ag-O bond distances reported in this work which were found to be 2.409 (31) Å, 2.411 (53) Å and 2.420 (125) Å respectively.

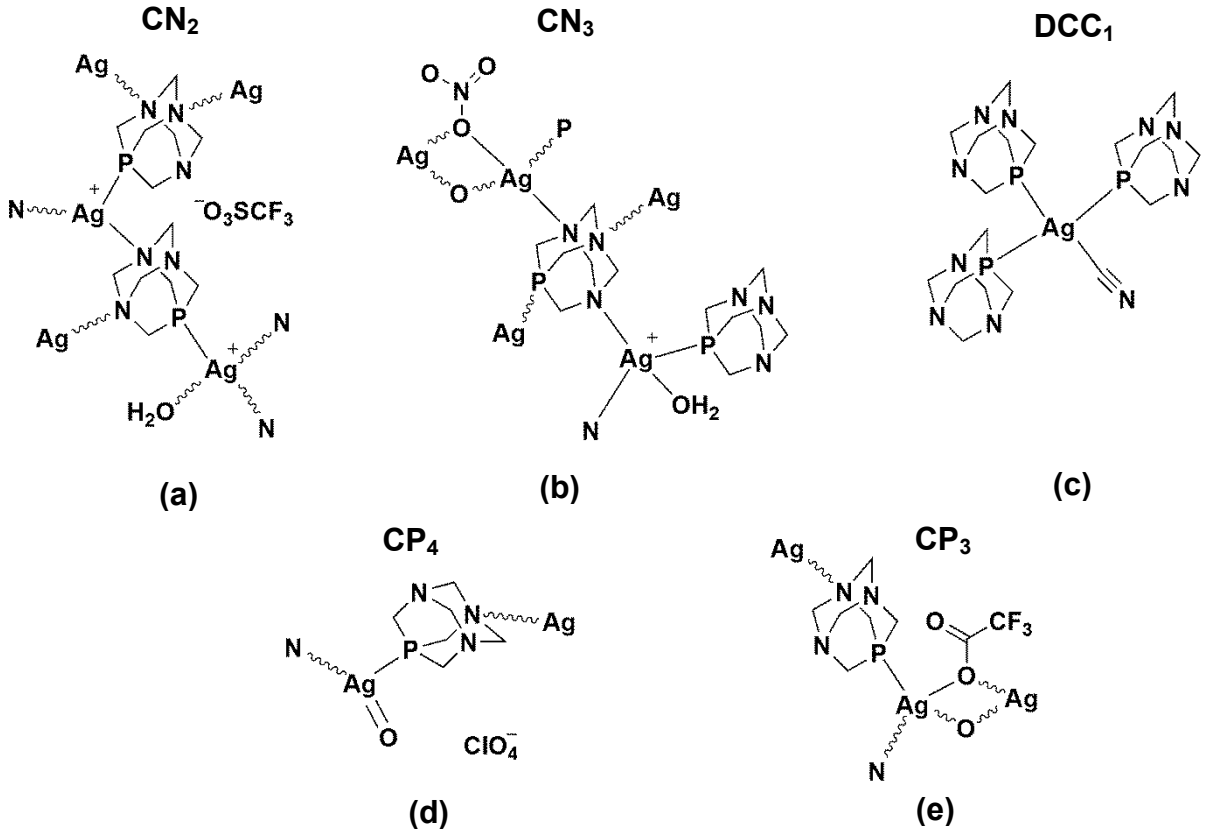

Figure 21: Structures of some Ag-PTA coordination compounds from our work

There are some trends observed concerning the silver(I)-donor atom bond distances in Figure 20. Statistically, the average Ag-P bond distances for discrete silver(I)-PTA complexes [2.470(125) Å], coordination polymers [2.379(35) Å] and networks [2.368(2) Å] are the same at 5% probability. Ag-O bond distances seems to be comparable to coordination polymers [2.428(133) Å] and networks]2.317(105) Å] except for one anomaly observed in **CP_4** with a slightly shorter Ag-O bond distance of 2.221(3) Å. In comparison between literature and this work, the shortest and longest Ag-O seem to generally occur in 1D zig-zag coordination and 1D ladder-like coordination polymers. As for the Ag-P and Ag-N bond distances, there appears to be no correlation between the Ag-donor atom bond distance and the overall molecular architecture.

3.1.2.2 Crystal structure of $[Ag(PTA)_3(CN)]4H_2O$ (DCC_1)

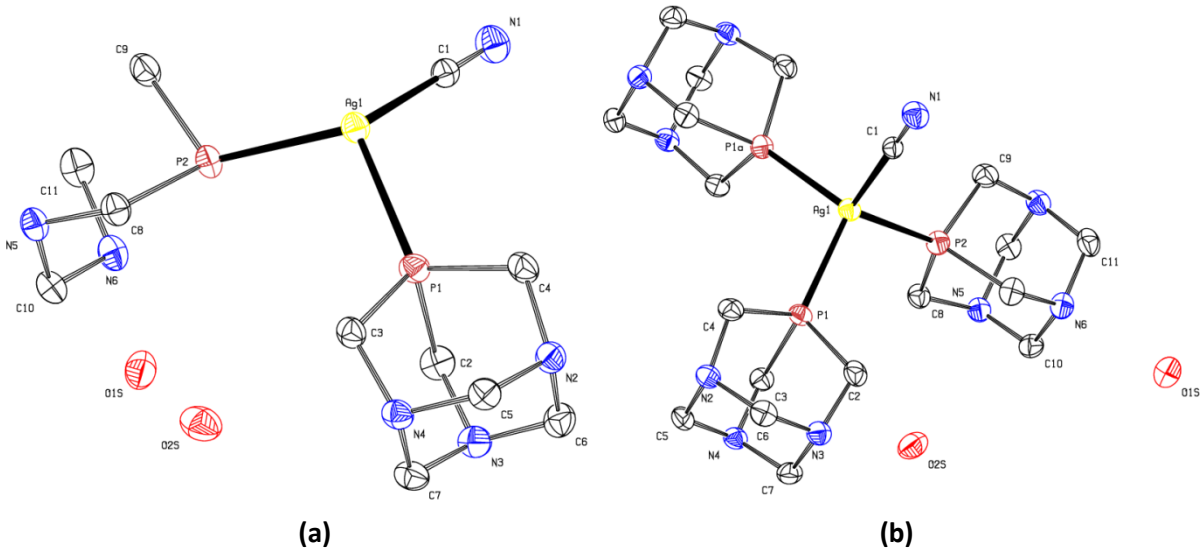

Figure 22: *ORTEP* diagrams of (a) the asymmetric unit and (b) complete molecular structure of DCC_1. All hydrogen atoms have been omitted for clarity and ellipsoids are drawn at 50% probability level

Figure 22 shows the *ORTEP* diagrams of (a) the asymmetric unit and (b) the complete molecular structure of **DCC_1** while Table 11 lists the selected bond parameters. **DCC_1** crystallizes in the orthorhombic *Pnma* space group. The asymmetric unit consists of a $[AgCN(PTA)_{3/2})]$ unit together with two water molecules and the complete molecule is generated by the symmetry code: x, $^3/_2$ - y, z. **DCC_1** is a neutral discrete complex in which the silver(I) metal centre is coordinated to three phosphorus atoms from three separate PTA

molecules and a carbon atom from the nitrile anion giving a distorted tetrahedral geometry around the metal centre with the bond angles around the Ag(1) atom ranging from 107.401(13)° to 111.07(3)°. The Ag-P bond distances are 2.4696(4) and 2.4728(6) Å while the Ag-C bond distance is 2.168(2) Å.

Table 11: Selected bond distances (Å) and angles (°) of **DCC_1**

C(1)-Ag(1)	2.168(2)	Ag(1)-P(2)	2.4728(6)
Ag(1)-P(1)	2.4696(4)	C(1)-N(1)	1.141(3)
N(1)-C(1)-Ag(1)	179.81(19)	P(1)#1-Ag(1)-P(1)	109.55(2)
C(1)-Ag(1)-P(1)	111.07(3)	C(1)-Ag(1)-P(2)	110.21(6)
		P(1)#1-Ag(1)-P(2)	107.401(13)

Symmetry codes: #1 = x, $^3/_2$ - y, z

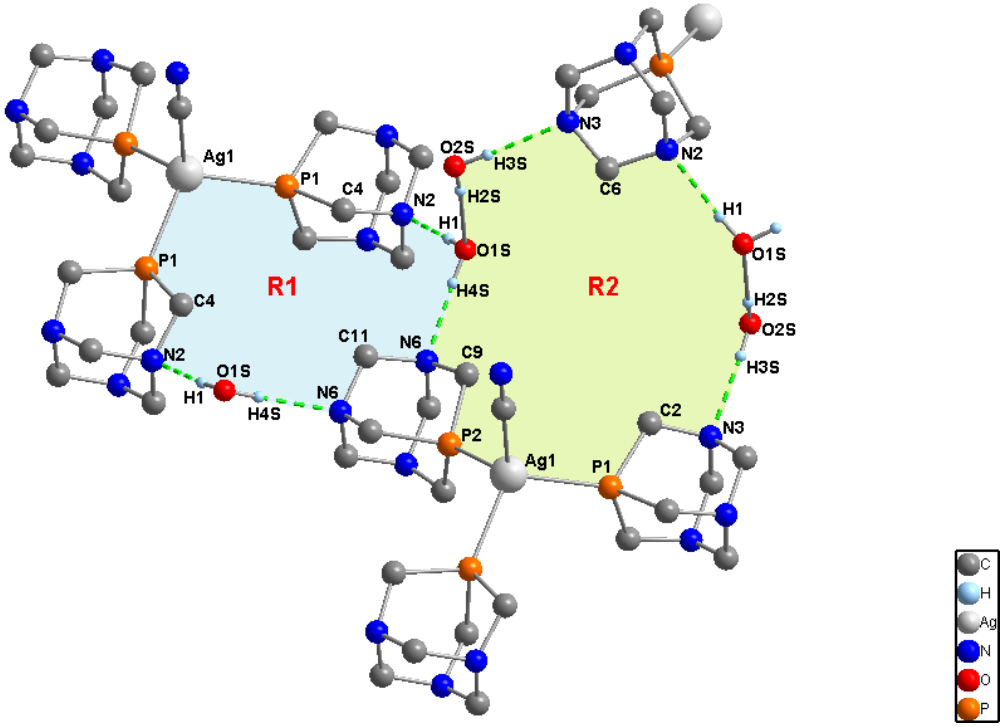

Figure 23: Hydrogen bonding networks observed in **DCC_1**. R1 and R2 represent graph-set descriptions $\boldsymbol{R_4^4(16)}$ and $\boldsymbol{R_6^6(20)}$, repectively.

A number of hydrogen bonds are observed in the crystal structure of **DCC_1**. Figure 23 and Figure 24 depict the hydrogen bonding networks observed and the crystal packing diagram, respectively while Table 12 lists hydrogen bonding parameters. Both water molecules and

the $[Ag(PTA)_3(CN)]$ molecules are involved in hydrogen bonding. The water molecule with O(1S) is involved in two different hydrogen bonds. In one, adjacent $[Ag(PTA)_3(CN)]$ molecules are linked through O-H…N hydrogen bonds involving N(2) and N(6) and forms chains that run along the crystallographic *c*-axis. In linking the two molecules in this manner, a ring described by the graph-set notation $R_4^4(16)$ is formed, R1 in Figure 23. In the second, O(1S) acts as a hydrogen acceptor and O(2S) acts as a hydrogen donor whilst O(2S) also links with N(3) of an adjacent $[Ag(PTA)_3(CN)]$ molecule through O-H…N hydrogen bonds. In doing so, a larger ring is formed, R2 in Figure 23 which can be described by graph-set notation $R_6^6(20)$. The water molecules including the discrete complexes are joined together via O-H…O and a O-H…N hydrogen bonds to form a 2D supramolecular architecture with a corrugated sheet topology as shown in Figure 24.

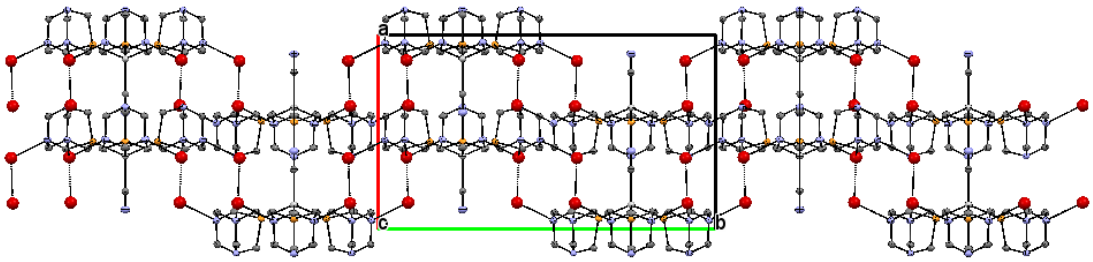

Figure 24: Hydrogen bonding patterns present in the crystal packing of **DCC_1** forming a two dimensional corrugated sheet-like supramolecular structure shown along the crystallographic *b*-axis

Table 12: Selected hydrogen bonding parameters in **DCC_1**

D-H…A	d(D-H)	d(H…A)	d(D…A)	<(DHA)
O(1S)-H(1)…N(2)#1	0.84	2.01	2.8520(18)	176
O(1S)-H(4S)…N(6)#2	0.85	1.99	2.8377(19)	174
O(2S)-H(3S)…N(3)#3	0.82	2.06	2.8795(19)	176
O(2S)-H(2S)…O(1S)	0.81	1.99	2.7940(18)	174

Symmetry codes: #1 = x, y, z-1; #2 = x, ½ -y,z; #3 = ½ -x,-y, z-½

3.1.2.3 Crystal structure of $[Ag(PTAH)_3(PTA)](CO_3)_2$ (DCC_2)

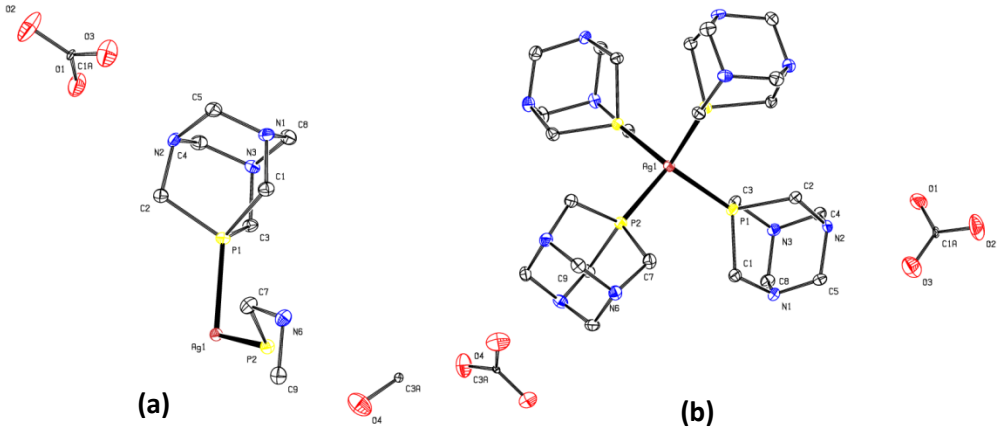

Figure 25: *ORTEP* diagram for (a) the asymmetric unit and (b) complete molecular structure of **DCC_2**. All hydrogen atoms have been omitted for clarity and ellipsoids are drawn at 50% probability level

DCC_2 crystallizes in the rhombohedral *R*3 space group. The asymmetric unit of **DCC_2** is shown in Figure 25(a) and contains the unit $[Ag(PTA)(PTAH)_{1/3}]$, one full molecule and one half molecule of the carbonate counter anion. The equivalent atoms that complete the molecule are generated by the symmetry code: 1-y, x-y, z. The complete molecular structure is shown in and Figure 25 (b) while the selected bond distances and angles are given in Table 13. The molecular structure of the **DCC_2** consists of a Ag atom that is coordinated to one neutral PTA molecule and three mono-protonated PTA molecules. The three mono-protonated PTA moieties together with the silver(I) metal centre result in a cationic complex with a charge of 4+ counter balanced by the two carbonate anions. The Ag(1) atom has a tetrahedral geometry with the bond angles around the Ag atom averaging 109°. The Ag-P(1) and Ag-P(2) bond distances are 2.4701(5) and 24680(9) Å, respectively. The P-Ag-P bond angles are comparable to those of other tetra-coordinated metal phosphine complexes such as $[Cu(PTA)_4][BF_4].6H_2O$ and $[Cu(PTAH)_4][NO_3]_5$ with an average P-Cu-P bond angle of 109.5°.[5]

Table 13: Selected bond distances (Å) and angles (°) of **DCC_2**

Ag(1)-P(2)	2.4680(9)	P(1)-Ag-P(2)	109.592(12)
Ag(1)-P(1)#1	2.4701(5)	P(1)-Ag-P(1)#1	109.350(12)

Symmetry codes: #1= -y+1, x-y, z

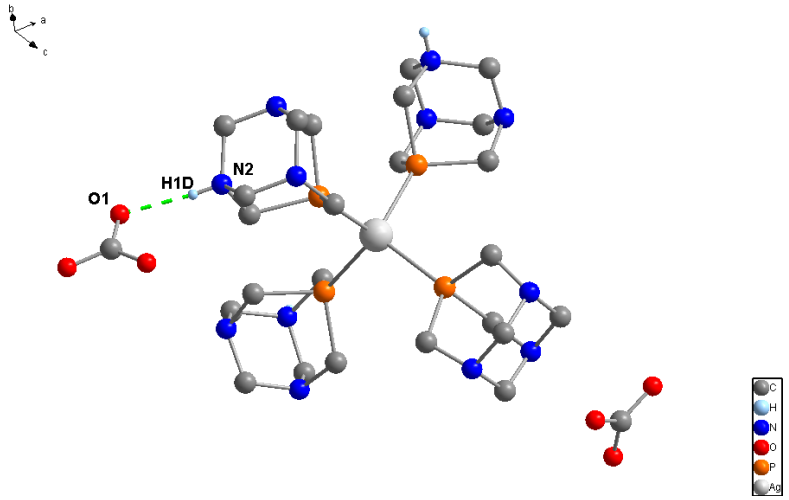

Figure 26: Intermolecular N-H…O hydrogen bonding observed in **DCC_2**

Figure 26 shows intermolecular hydrogen bonding between the $[Ag(PTAH)_3(PTA)]^{4+}$ units and the non-coordinating carbonate anions. The carbonate anions interact with the protonated N atoms of the PTA moieties via N-H…O hydrogen bonds with N…O distance of 2.737 Å and a N-H…O angle of 174° (symmetry code: $^1/_3$ -x+y, $^2/_3$ -x, z-$^1/_3$).

3.1.2.4 Crystal structure of $[Ag(PTA)_3][4\text{-}NP]_{10}$ (DCC_3)

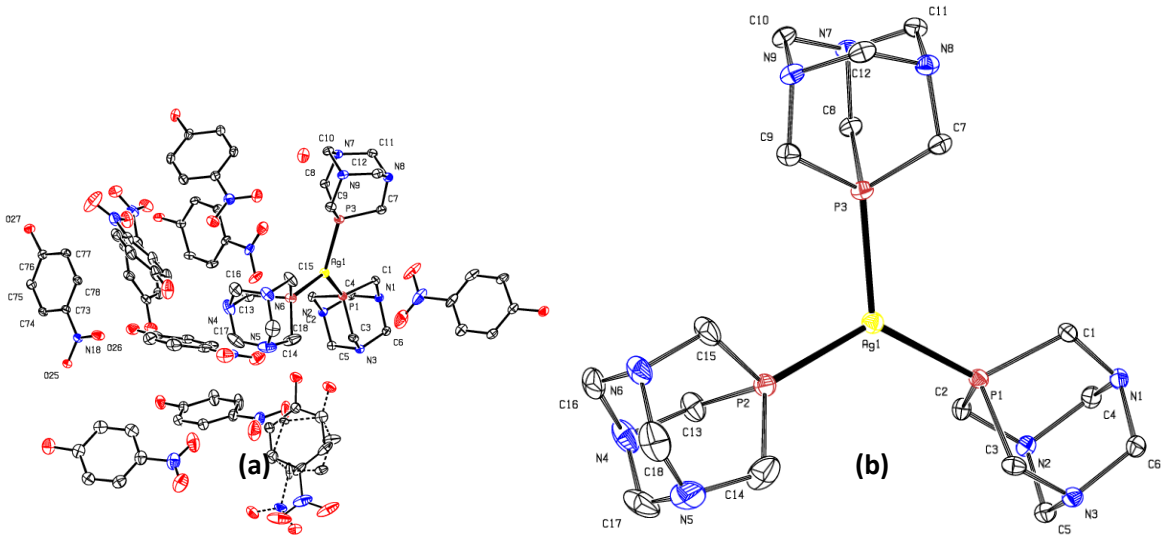

Figure 27: *ORTEP* diagram for (a) the asymmetric unit of **DCC_3** and (b) molecular structure of the tri-coordinated silver(I)-PTA complex with the 4-nitrophenol molecules omitted. All hydrogen atoms have been omitted for clarity and ellipsoids are drawn at 30% probability level.

DCC$_3$ crystallizes in a monoclinic $P2_1/c$ space group. Figure 27(a) and (b) depict the *ORTEP* diagram of the asymmetric unit of **DCC$_3$** and the molecular structure of the Ag-PTA complex, respectively, while Table 14 lists important bond distances and angles. The asymmetric unit consists of a tri-coordinated silver(I)-PTA unit [Ag(PTA)$_3$] and ten 4-nitrophenol molecules. The molecular structure of **DCC$_3$** reveals the coordination environment of the Ag metal centre being a distorted trigonal planar geometry in which the P-Ag-P bond angles are 110.91(3)°, 122.27(2)° and 126.81(2)° deviating from the ideal trigonal planar bond angle of 120°. The Ag(1)-P(1), Ag(1)-P(2) and Ag(1)-P(3) bond distances are 2.4148(7), 2.4410(7) and 2.4441(7) Å, respectively and are comparable to the Ag-P bond distances of a similar tri-coordinated silver-phosphine complex such as [Ag$_2$(dmpm)$_3$](BF$_4$)$_2$ with bond distances ranging from 2.425 to 2.477 Å.[6] One of the p-nitrophenol molecules displays a pseudorotational disorder with 75% : 25% occupancy.

Table 14: Selected bond distances (Å) and angles (°) of **DCC$_3$**

Ag(1)-P(1)	2.4148(7)	P(1)-Ag(1)-P(2)	126.81(2)
Ag(1)-P(2)	2.4410(7)	P(1)-Ag(1)-P(3)	122.27(2)
Ag(1)-P(3)	2.4441(7)	P(2)-Ag(1)-P(3)	110.91(3)

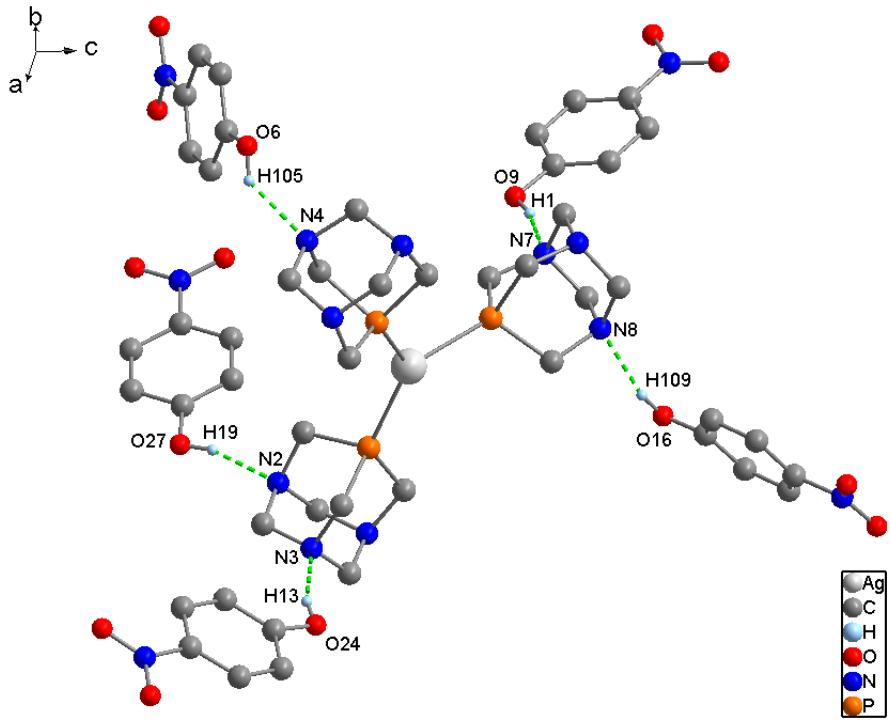

Figure 28: Representation of the intermolecular O-H…N hydrogen bonding (shown as dashed green bonds) between the tri-coordinated silver-PTA complex and the 4-nitrophenol molecules in **DCC$_3$**. The methylene and aromatic hydrogens have been omitted for clarity.

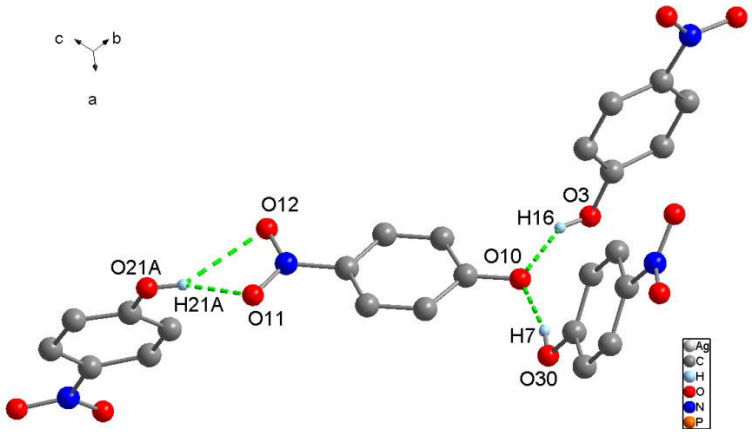

Figure 29: Representation of the intermolecular O-H…O hydrogen bonding (shown as dashed green bonds) between the 4-nitrophenol molecules in **DCC$_3$**. The silver-PTA complex and aromatic hydrogens have been omitted for clarity.

Figure 28 andFigure 29 depict the intermolecular hydrogen bonding patterns between the tri-coordinated silver-PTA complex and the 4-nitrophenol molecules while Table 15 lists the hydrogen bonding parameters observed in the crystal structure of **DCC$_3$**. The 4-nitrophenol molecules with oxygen atoms O(6), O(9), O(16), O(24) and O(27) interact with the PTA moieties of the complex through O-H…N hydrogen bonds as shown in Figure 28. The rest of the *p*-nitrophenol molecules with oxygen atoms O(21A), O(10), O(3) and O(30) exhibited O-H…O hydrogen bonds between the 4-nitrophenol molecules. H(21A) forms a bifurcated hydrogen bond with an adjacent 4-nitrophenol molecule that can be described by the graph-set notation $R_1^2(4)$ as shown in Figure 29.

Table 15: Selected hydrogen bonding parameters in **DCC$_3$**

D-H…A	d(D-H)	d(H…A)	d(D…A)	<(DHA)
O(9)-H(1)…N(7)#1	0.84	1.89	2.714(3)	166
O(30)-H(7)…O(10)	0.84	1.79	2.613(3)	167
O(15)-H(10A)…O(1S)#2	0.84	1.85	2.677(4)	170
O(24)-H(13)…N(3)#3	0.84	1.92	2.732(3)	162
O(3)-H(16)…O(10)#4	0.84	1.77	2.544(3)	152
O(27)-H(19)…N(2)#1	0.84	1.90	2.719(3)	164
O(21A)-H(21A)…O(11)	0.84	1.89	2.642(4)	148
O(21A)-H(21A)…O(12)	0.84	2.42	3.166(4)	149
O(6)-H(105)…N(4)	0.84	2.01	2.702(4)	139
O(16)-H(109)…N(8)#5	0.84	1.90	2.681(3)	153

Symmetry codes: #1 = x, $^3/_2$-y, z- ½; #2 = 1-x, 1-y, 1-z; #3 = x, ½ -y, ½ +z; #4 = x, $^3/_2$-y, ½ +z; #5 = x, y, z-1

3.1.2.5 Crystal structure of $[Ag(PTA)(NO_3)]_n$ (CP_1)

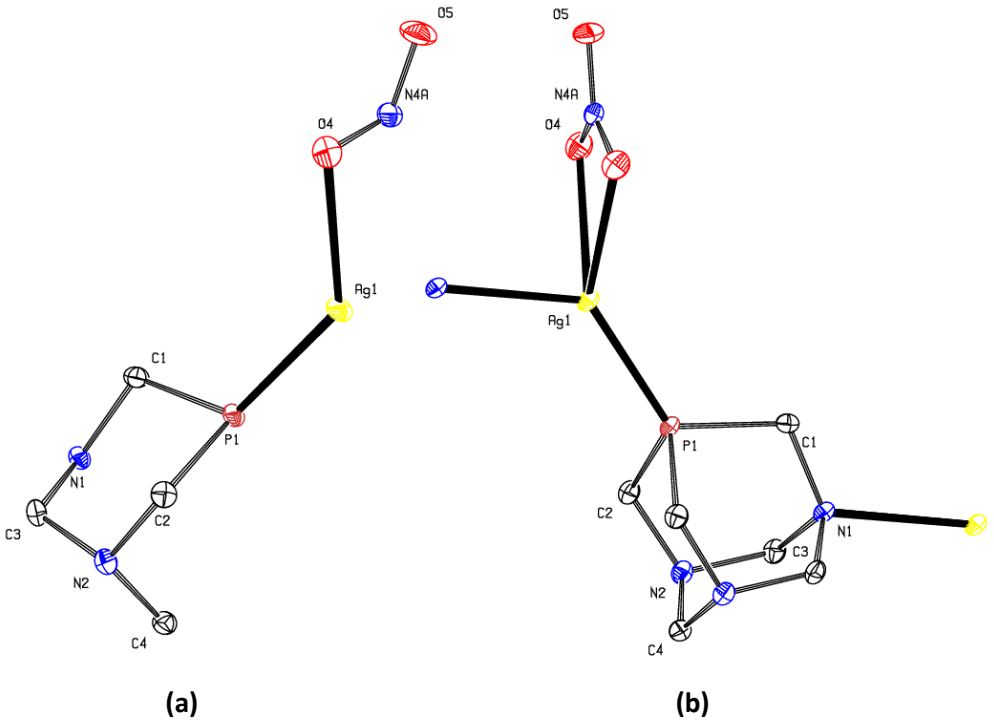

Figure 30: *ORTEP* diagram for (a) the asymmetric unit and a (b) repeating fragment of **CP_1**. All hydrogen atoms have been omitted for clarity and ellipsoids are drawn at 50% probability level.

CP_1 crystallizes in a monoclinic *Cm* space group. Figure 30(a) shows the asymmetric unit of **CP_1** and it contains the unit $[Ag(PTA)_{7/10}(NO_3)_{3/4}]$. The equivalent atoms that complete the molecule are generated by the symmetry code: x, 1-y, z. The *ORTEP* diagram of a repeating fragment of **CP_1** $[Ag(PTA)(NO_3)]_n$ is shown in Figure 30(b) while Table 16 lists the selected bond parameters of **CP_1**. Coordination to the Ag atom is via a P atom and a nitrogen atom of separate PTA molecules and two O atoms of the nitrate anion. The nitrate anion coordinates to the Ag(1) centre in a bidentate fashion and completes a slightly distorted tetrahedral geometry. The bond angles around the Ag(I) centre lie between 87.43(4) to 135.90(3)° and the Ag(1)-P(1), Ag(1)-N(1), Ag(1)-O(4) bond distances are 2.3485(6) Å, 2.3915(17) Å and 2.4672(11) Å, respectively. The Ag-O bond distance, 2.4672(11) Å is significantly longer than the average Ag-O bond distance of 2.393(32) Å for silver(I) complexes containing PTA moieties found in the CSD search. [4b] Similarly the nitrate O(4)-N(4A)-O(4) angle is also slightly smaller [118.69(17)°] compared to that of the other two O-N-O angles [120.64(9)°]. This difference could be as a result of strain caused due to the bidentate coordination mode of the nitrate anion. The N-O distance could imply the lessening of the resonance effect of the nitrate group.

Table 16: Selected bond distances (Å) and angles (°) of **CP_1**

Ag(1)-O(4)	2.4672(11)	Ag(1)-P(1)	2.3485(6)
Ag(1)-N(1)#1	2.3915(17)	N(4A)-O(5)	1.242(2)
N(4A)-O(4)	1.2603(14)	Ag....Ag (within chain)	7.9133(10)
P(1)-Ag(1)-O(4)	135.90(3)	N(1)-Ag(1)-O(4)	87.43(4)
O(5)-N(4A)-O(4)	120.64(9)	O(4)-N(4A)-O(4)	118.69(17)
P(1)-Ag(1)-N(1)#2	129.77(4)	O(5)-N(4A)-O(4)-Ag(1)	-173.33(16)

Symmetry codes: #1 = x, 1-y, z; #2 = x, y, z+1;

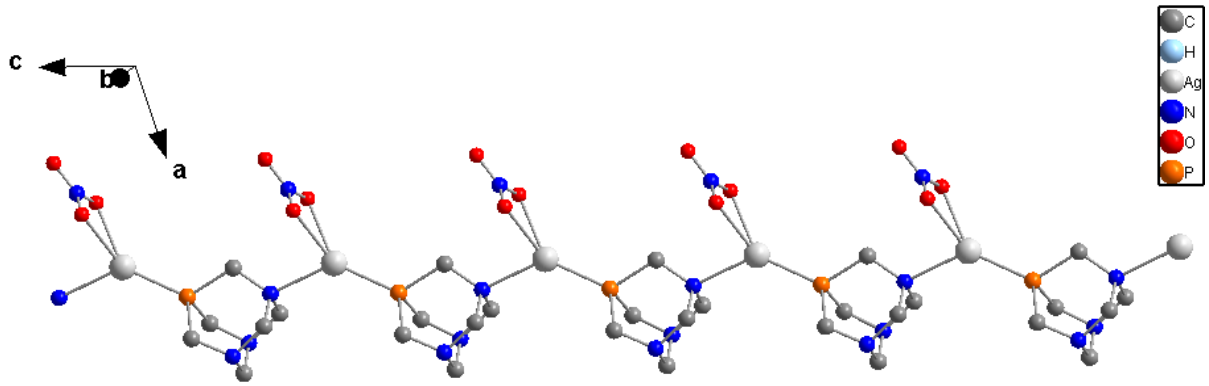

Figure 31: Polymeric representation of **CP_1** viewed along the crystallographic *b*-axis. Hydrogen atoms of the methylene are omitted for clarity

Figure 31 reveals the polymeric representation of **CP_1**. A one dimensional chain-like structure of **CP_1** is observed with a repeating period of 7.9133(10) Å between adjacent Ag(1) atoms which is equivalent to the *c* cell dimension. The coordination polymer propagates along the crystallographic *c*-axis and is through alternating *P*-, *N*- coordination mode of PTA. The bidentate coordination mode of the nitrate anion probably inhibits the formation of two or three dimensional coordination polymer. In the chain, all coordinated nitrate anions, just like the PTA moieties, are perfectly aligned with each other.

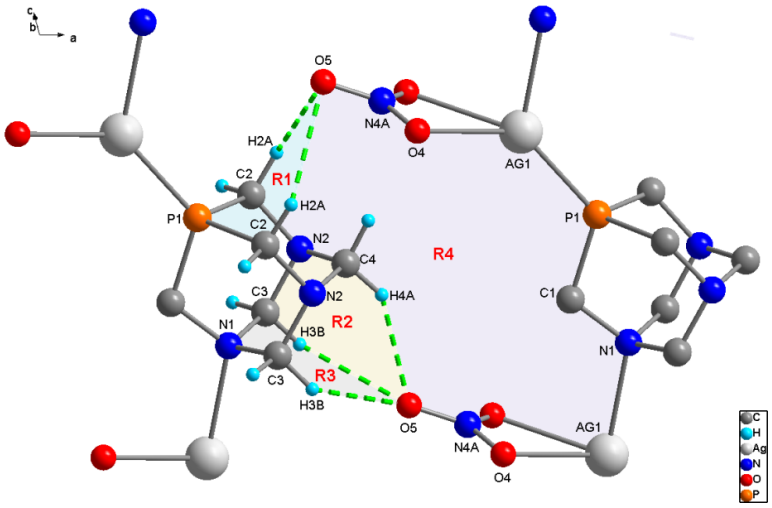

Figure 32: Representation of intermolecular C-H…O hydrogen bonding (shown as dashed green bonds) in **CP**$_1$. R1, R2, R3, and R4 are explained in text.

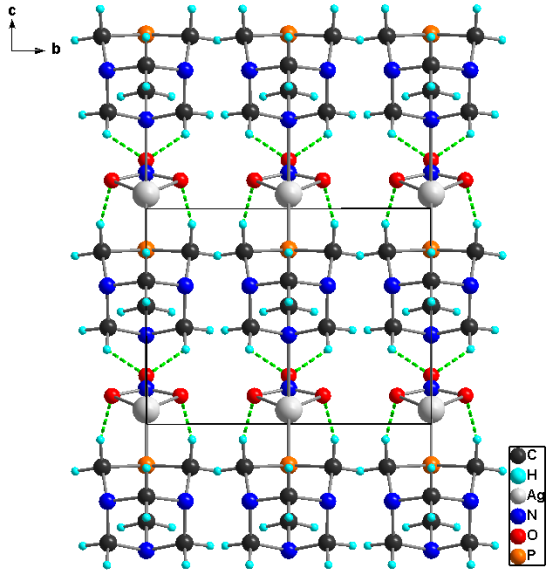

Figure 33: Representation of hydrogen bonding patterns (dashed green lines) present in the crystal packing of **CP$_1$** shown along the crystallographic *a*-axis. The methylene hydrogens that do not exhibit intermolecular hydrogen bonding have been omitted for clarity.

Figure 32 and Figure 33 display the intermolecular hydrogen bonding patterns observed and the crystal packing diagram of **CP$_1$**, respectively while the hydrogen bonding parameters are listed in Table 17. C-H…O hydrogen bonding interactions seem to be predominant in the crystal structure of **CP$_1$** and is between the PTA and the nitrate moieties. Adjacent 1D coordination polymers are connected through a C-H…O hydrogen bonds involving a PTA hydrogen atom and an oxygen atom from the nitrate. This results in the formation of 2D

hydrogen bonded sheets along *ac* face as shown in Figure 33. The hydrogen bonding network contains three 6-member rings R1, R2 and R3 described by the graph-set notation $R_2^1(6)$ and a 16-member ring, R4, that can be described by the graph-set notation $R_2^1(16)$ as shown in Figure 32.

Table 17: Selected hydrogen bonding parameters in **CP_1**

D-H…A	d(D-H)	d(H…A)	d(D…A)	<(DHA)
C(2)-H(2A)…O(5)#1	0.99	2.60	3.432(2)	142
C(3)-H(3B)…O(5)#2	0.99	2.55	3.383(2)	141
C(4)-H(4A)…O(5)#2	0.99	2.41	3.283(2)	147

Symmetry codes: #1 = 1+x,y,z; #2 = 1+x,y,-1+z;

3.1.2.6 Crystal structure of $[Ag(PTA)(\mu^2\text{-}O_2CCH_3)]_n\ 2nH_2O$ (CP_2)

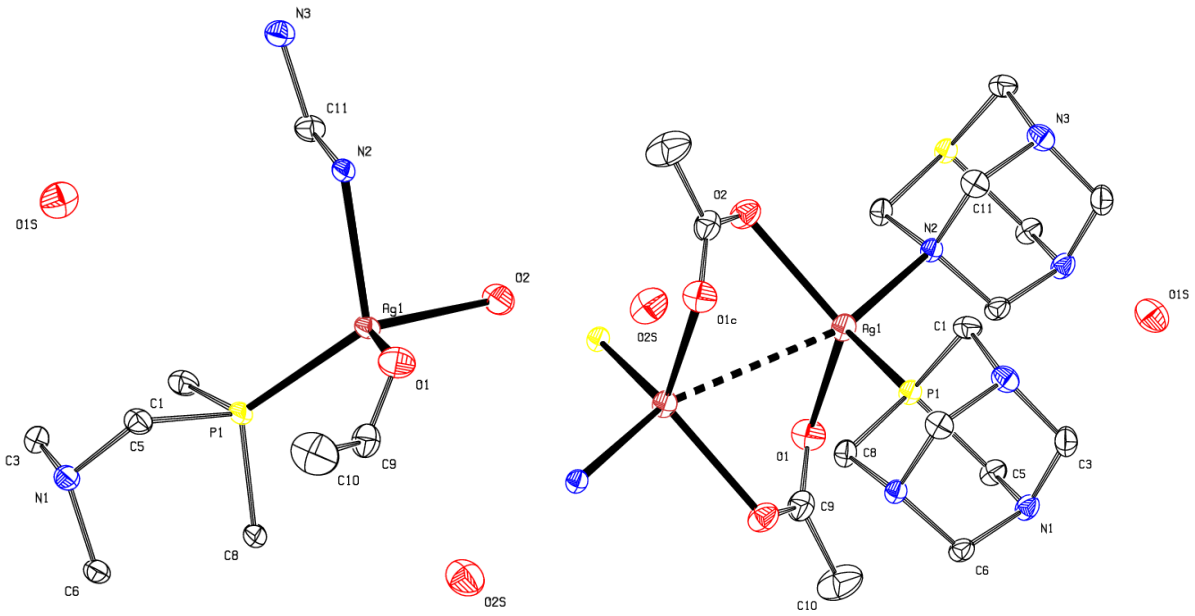

(a) **(b)**

Figure 34: *ORTEP* diagram for (a) the asymmetric unit and (b) a repeating fragment of **CP_2**. All hydrogen atoms have been omitted for clarity and ellipsoids are drawn at 50% probability level

CP_2 crystallizes in the monoclinic *C2/c* space group. The asymmetric unit of **CP_2** contains a unit $[Ag(PTA)(O_2CCH_3)]$ and two water molecules (Figure 34a). The equivalent atoms that complete the molecule are generated by the symmetry code: 1-x, 1-y, 1-z. The *ORTEP* diagram of a repeating fragment is shown in Figure 34(b) while important bond distances and angles are given in Table 18. Coordination to the Ag atom is via a phosphorus atom and a

nitrogen atom of separate PTA molecules and two oxygen atoms from two acetate anions. The two acetate anions bridge the Ag centres in a μ^{2}-O_2 fashion. The silver(I) metal centre has a distorted tetrahedral geometry with the bond angles around the Ag(I) centre ranging from 93.07(4)° to 122.55(3)°. The Ag(1)-P(1), Ag(1)-N(2), Ag(1)-O(1) and Ag(1)-O(2) bond distances of 2.3842(4) Å, 2.3710(12) Å, 2.4444(11) Å and 2.3791(10) Å, respectively. The Ag...Ag separation is 3.0810(2) Å and is shorter than the sum of the van der Waals radii for silver (3.44 Å).[7] The short Ag…Ag probably strain on the carboxylate anion resulting in a slight tilt in the non-planar of the Ag-O-C-O-Ag moieties. The O(2)-C(9)-O(1)-Ag(1) torsion angles is 42.65(17)°.

Table 18: Selected bond distances (Å) and angles (°) of **CP_2**

N(2)-Ag(1)	2.3710(12)	P(1)-Ag(1)	2.3842(4)
O(1)-Ag(1)	2.4444(11)	Ag(1)-Ag(1)#1 (via acetate)	3.0810(2)
O(2)-Ag(1)	2.3791(10)		
N(2)-Ag(1)-O(2)	93.07(4)	P(1)-Ag(1)-O(1)	110.09(3)
N(2)-Ag(1)-P(1)	117.25(3)	O(1)-C(9)-O(2)#1	124.45(14)
O(2)-Ag(1)-P(1)	122.55(3)	O(1)-C(9)-C(10)	117.97(15)
N(2)-Ag(1)-O(1)	93.38(4)	O(2)#1-C(9)-C(10)	117.58(15)
O(2)-Ag(1)-O(1)	115.71(4)	O(2)#2-C(9)-O(1)-Ag(1)	-137.17(14)

Symmetry codes: #1 = 1-x, 1-y, 1-z

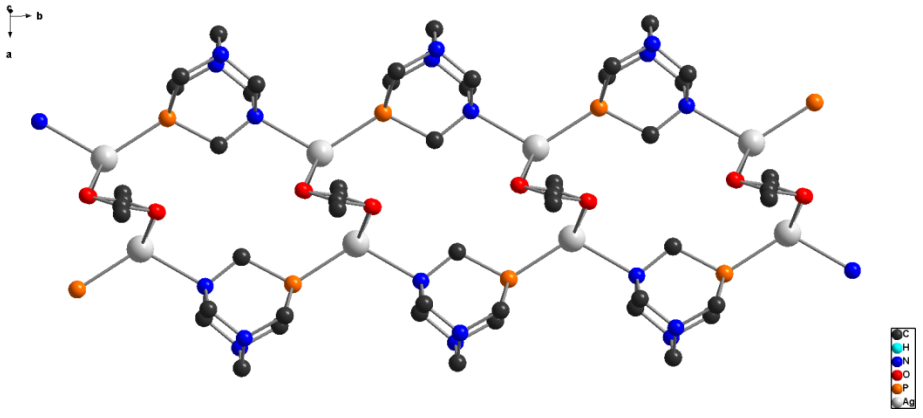

Figure 35: Polymeric representation of **CP_2** rotated along the crystallographic *c*-axis

Figure 35 displays the polymeric representation of **CP_2**. It appears that **CP_2** has a one dimensional skewed ladder-like structure with a repeating distance of 6.8455(3) Å between

adjacent Ag(1) atoms linked by PTA molecules which is equivalent to the '*b*' cell dimension. The alternating *N*-, *P*-coordination to Ag(1) centre forms the strands of the ladder while the acetate anions joining the two strands form the ladder rungs. **CP_2** ladders propagates along the crystallographic *b*-axis.

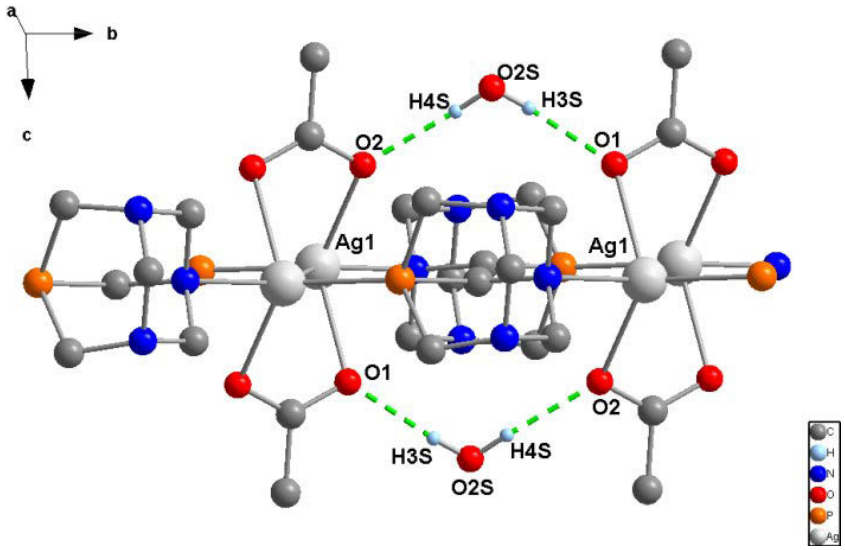

(a)

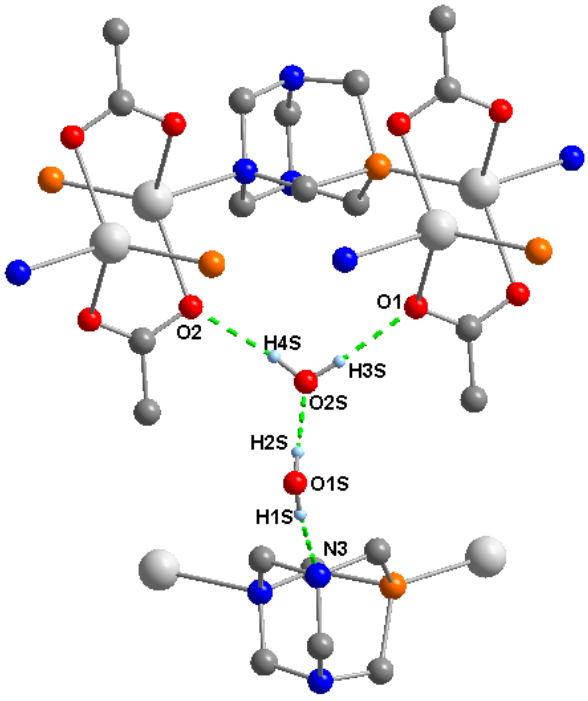

(b)

Figure 36: Hydrogen bonding patterns (shown as dashed green bonds) in **CP_2** (a) forming a ring via O-H…O and (b) forming a 2D supramolecular architecture via O-H…N and O-H…O interactions in **CP_2**

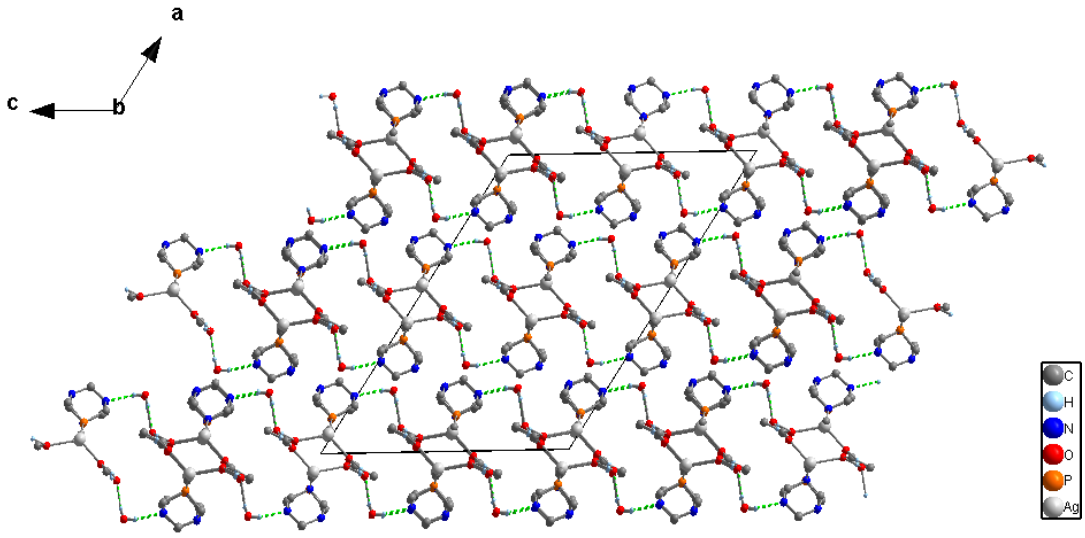

Figure 37: Representation of hydrogen bonding patterns (dashed green lines) present in the crystal packing of **CP_2** shown along the crystallographic b axis. All methylene hydrogen atoms have been omitted for clarity

A number of hydrogen bonds are observed in the crystal structure of **DCC_1**. The hydrogen bonding patterns and the crystal packing diagram of **CP_2** are shown in Figure 36 and 38, respectively while Table 19 lists hydrogen bonding parameters. Both water molecules and the [Ag(PTA)(μ_2-O_2CCH_3)] molecules are involved in intermolecular hydrogen bonding as shown in Figure 37(a). One water molecule with O(2S) links up adjacent bridging acetate groups along the same ladder-like strand through O-H…O hydrogen bonds as shown in Figure 36(a). In doing so, a 12-membered ring described by a $R_4^4(12)$ graph-set notation is formed. The other water molecule with O(1S) links adjacent ladder-like chains O-H…N hydrogen bonds to the first water molecule with O(2S) via O-H…O hydrogen bonds as shown in Figure 36(b). The water molecules sew the adjacent ladder-like chains together through classical O-H…O and O-H…N hydrogen bonds to give 2D hydrogen bonded sheets along the *bc* face as depicted Figure 37.

Table 19: Selected hydrogen bonding parameters in **CP_2**

D-H…A	d(D-H)	d(H…A)	d(D…A)	<(DHA)
O(1S)-H(1S)…N(3)#1	0.82(3)	2.09(3)	2.892(2)	165
O(1S)-H(2S)…O(2S)#2	0.80(3)	2.03(3)	2.823(2)	174
O(2S)-H(3S)…O(1)#3	0.81(3)	1.98(3)	2.7890(18)	175
O(2S)-H(4S)…O(2)#4	0.86(3)	2.02(3)	2.8700(18)	168

Symmetry codes: #1 = ½ -x, ½ -y, 1-z; #2 = x- ½ , $^3/_2$ -y, z- ½; #3 = 1-x, 1-y, 1-z; #4 = x, 1+y, z

3.1.2.7 Crystal structure of $[Ag(PTA)(\mu^1\text{-}O_2CCF_3)]_n$ (CP_3)

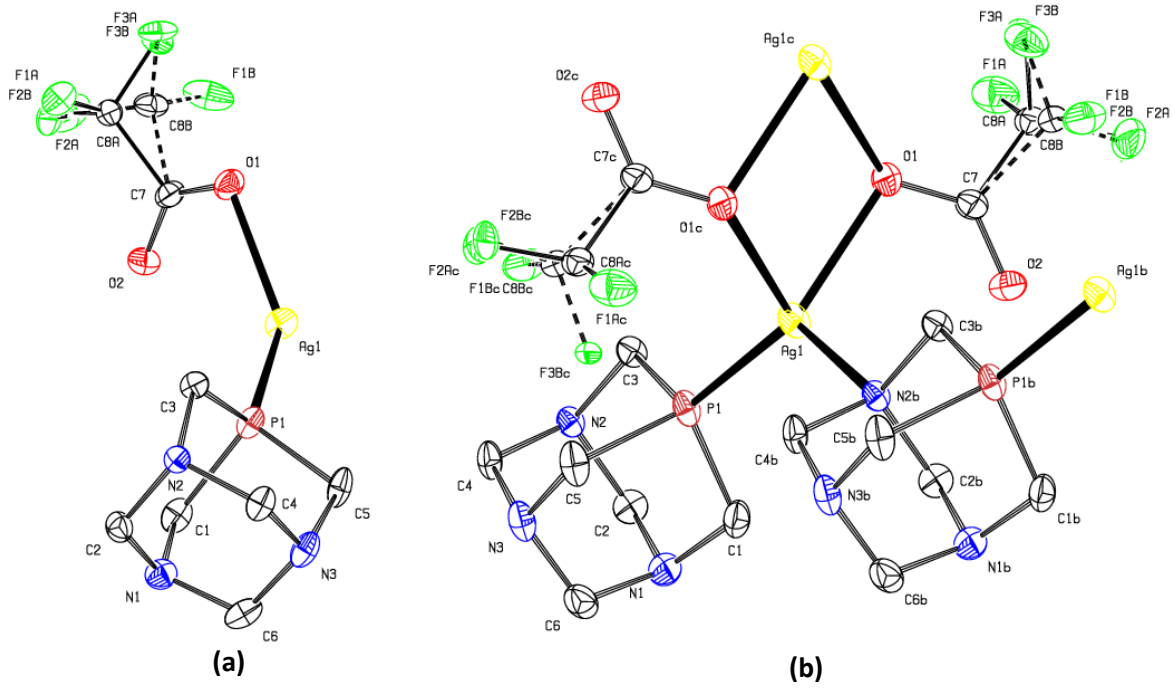

Figure 38: *ORTEP* diagram for (a) the asymmetric unit and (b) a repeating fragment of **CP_3**. All hydrogen atoms have been omitted for clarity and ellipsoids are drawn at 50% probability level

CP_3 crystallizes in the monoclinic $P2_1/c$ space group. Figure 38(a) and (b) shows the asymmetric unit and the *ORTEP* diagram of the repeating unit of **CP_3** respectively while Table 20 lists important bond distances and angles. The asymmetric unit contains the unit $[Ag(PTA)(O_2CCF_3)]$ and the complete molecule is generated by the symmetry codes: x+1, y, z and 1-x, 1-y, 1-z. The repeating unit contains two Ag atoms, four PTA molecules, and two trifluoroacetate molecules. The trifluoroacetate groups are disordered over two positions with the major component having 65% occupancy. The two Ag atoms are in a distorted tetrahedral environment and each is coordinated to a phosphorus atom and a nitrogen atom of two separate PTA molecules and two oxygen atoms of two trifluoroacetate molecules both of which bridge the two Ag centres in a μ^1-O_2 fashion. The bond angles around the Ag centres range between 77.00(14)° and 134.23(11)° with Ag(1)-P(1), Ag(1)-N(2), Ag(1)-O(1) and Ag(1)-O(1)#2 bond distances of 2.3470(13) Å, 2.379(4) Å, 2.324(4) Å and 2.379(4) Å, respectively. The Ag...Ag separation via trifluoroacetate groups is 3.8451(6) Å which is significantly longer than the Ag...Ag separation via the acetate groups in **CP_2**. This separation is longer than the sum of the van der Waals radii for silver (3.44 Å) and cannot therefore be classified as an interaction.[7]

Table 20: Selected bond distances (Å) and angles (°) of **CP_3**

Ag(1)-O(1)	2.324(4)	Ag(1)-O(1)#2	2.584(4)
Ag(1)-P(1)	2.3470(13)	Ag…Ag (within chain)	6.9024(5)
Ag(1)-N(2)	2.379(4)	Ag...Ag (via O_2CCF_3)	3.8451(6)
O(1)-Ag(1)-P(1)	134.23(11)	O(1)-Ag(1)-O(1)#2	77.00(14)
O(1)-Ag(1)-N(2)#1	101.02(14)	P(1)-Ag(1)-O(1)#2	118.80(9)
P(1)-Ag(1)-N(2)#1	121.72(10)	N(2)#1-Ag(1)-O(1)#2	85.51(14)

Symmetry codes: #1 = x+1, y, z; #2 =1-x, 1-y, 1-z

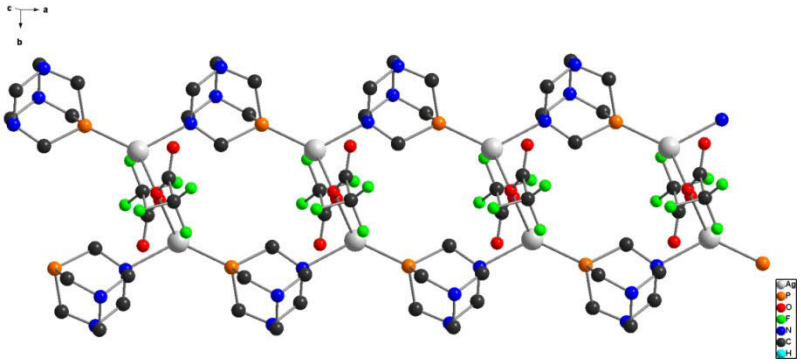

Figure 39: Polymeric representation of **CP_3** along the crystallographic *b*-axis. All methylene hydrogens have been omitted for clarity

Figure 39 displays the polymeric representation of **CP_3**. The crystal structure of **CP_2** and **CP_3** both contain two Ag atoms, two bridging acetate ligands and two PTA. **CP_3** has a one dimensional ladder-like structure similar to that of **CP_2** with a repeating period of 6.9024(5) Å between adjacent Ag(1) atoms linked by PTA molecules which is equivalent to the length of the '*a*' dimension of the cell. The PTA groups display an alternating *P*-, *N*-coordination mode and this forms the strands whilst the trifluoroacetate groups joins the two PTA-based strands by bridging two Ag centres on each of the strands in a μ^1-O_2 fashion to form the rungs of the ladder.

The overall structures of **CP_3** and **CP_4** are comparable to other silver-PTA based coordination polymers in literature in which carboxylates have been used as the anion.[1a] Lis *et al.* reported coordination polymers in which the arylcarboxylates were used as ancillary ligands.[1a] The carboxylate groups in **CP_3** and **CP_4** display two different bridging modes via one oxygen atom or through two oxygen atoms as shown in Figure 40. Adaptation of either mode could possibly be as a consequence of a mixture of electronic and steric properties.

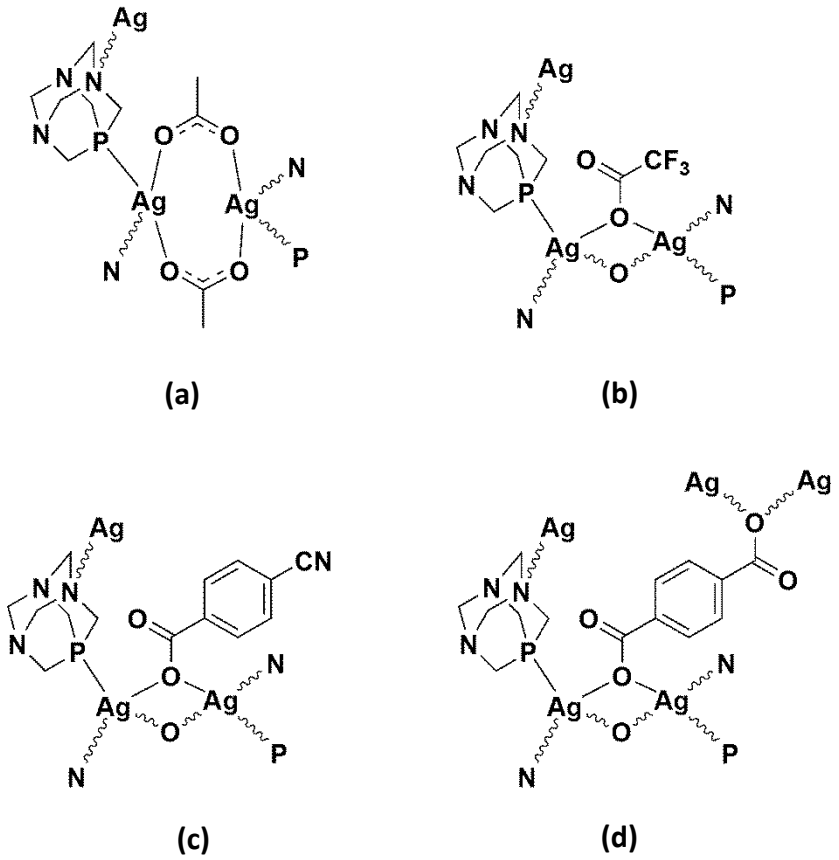

Figure 40: Ag-PTA coordination polymers bearing different carboxylate ancillary ligands

The coordination mode of the acetate group used in **CP_3** is such that the two metal centres are bridged in a μ^2- fashion to the oxygen atoms of the ancillary ligand to separate metal centres as shown in Figure 40(a). On the other hand, the coordination mode of the trifluoroacetate as shown in Figure 40(b) and the arylcarboxylate groups as shown in Figure 40(c) and (d) are in a μ^1- fashion to the single oxygen of the ancillary ligand coordinating to two separate metal centres; thus bridging the two metal centres.

Table 21: Ag...Ag separations in different Ag-PTA coordination polymers with different carboxylate ancillary ligands

Compound	**Bridging mode**	**Ancillary ligand used**	**Ag…Ag distance/Å**	**Reference**
CP_2	μ^2-O_2	$-O_2CCH_3$	3.0810(2)	This work
CP_3	μ^1-O_2	$-O_2CCF_3$	3.8451(6)	This work
$[Ag(C_8H_4NO_2)(PTA)]_n .5nH_2O$	μ^1-O_2	$-O_2C(C_6H_4)CN$	3.5699(4)	[1a]
$[Ag_2(C_8H_4O_2)(PTA)_2]_n .2nH_2O$	μ^1-O_2	$-O_2C(C_6H_4)CO_2-$	3.5408(3)	[1a]

Interestingly the distance between the two silver atoms that are μ^2- bridged as in the case of the acetate bridge, seem to be significantly shorter than the Ag…Ag distances in the μ^1-bridged Ag(I) centres as shown in Table 21. The silver atoms in **CP_3** lie flat with the O1-Ag1-O1-Ag1 bridging plane whilst the silver atoms in **CP_2** lie 1.5405 Å out of the O1-O2-O1-O2 bridging plane. From these findings, it seems that the coordination mode of the carboxylate group to the Ag(I) metal centre is dependent on the nature of the carboxylic acid derivative; whilst the Ag…Ag distance depends on the bridging mode of the carboxylate group.

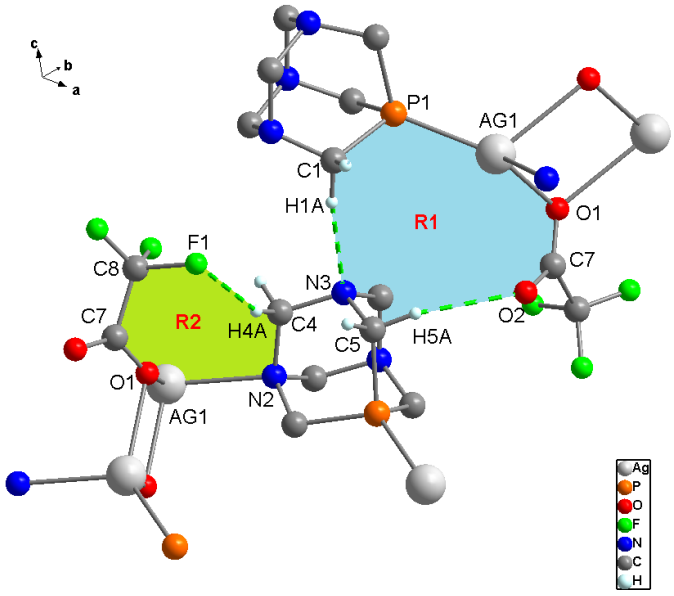

Figure 41: Hydrogen bonding network (shown as dashed green bonds) observed in **CP_3**. R1 and R2 represent graph-set descriptions $\boldsymbol{R_2^2(10)}$ and $\boldsymbol{R_1^1(8)}$, respectively

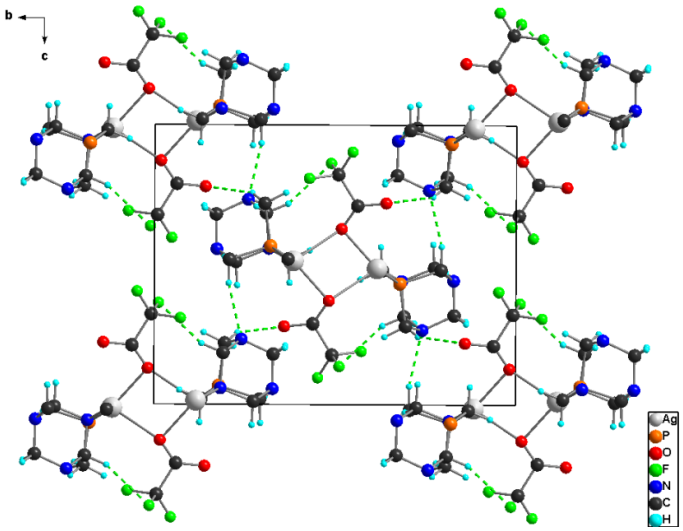

Figure 42: Representation of hydrogen bonding patterns (dashed green lines) present in the crystal packing of **CP_3** shown along the crystallographic *a*-axis

Table 22 lists the hydrogen bonding parameters observed in the crystal structure of CP_3 while Figure 41 andFigure 42 respectively depict the hydrogen bonding patterns and the crystal packing diagram of **CP_3**. Three types of non-classical hydrogen bonding interactions seem to be predominant in **CP_3**. C-H…O hydrogen bonds connect the trifluoroacetate anions to PTA groups from different ladders. C-H…N hydrogen bonds link neighbouring ladders together through the nitrogen atom of PTA and the H atom of PTA of the neighbouring ladder. C-H…O and C-H…N hydrogen bonds form chains that run along the *bc* face to give a 3D supramolecular architecture as shown in Figure 42. The C-H…O and C-H…N hydrogen bonds results in hydrogen bonding networks that give a 10-membered ring, R1, described by the graph-set notation $R_2^2(10)$ shown in Figure 41. C-H…F intramolecular interactions exist between the hydrogen atom of PTA groups and the fluorine atom of the trifluoroacetate group along the same ladders. This results in the formation of a ring, R2, described by the graph-set notation $R_1^1(8)$ as shown in Figure 41.

Table 22: Selected hydrogen bonding parameters in **CP_3**

D-H…A	d(D-H)	d(H…A)	d(D…A)	<(DHA)
C(1)-H(1A)…N(3)#1	0.99	2.41	3.382(7)	165
C(4)-H(4A)…F(1)#2	0.99	2.51	3.444(8)	158
C(5A)-H(5A)…O(2)#3	0.99	2.47	3.391(7)	155

Symmetry codes: #1 = x, ½ -y, z- ½ ; #2 = -x, 1-y, 1-z; #3 = x, ½ -y, ½ +z

3.1.2.8 Crystal structure of $[Ag(O)(PTA)]_n[ClO_4]_n$ (CP_4)

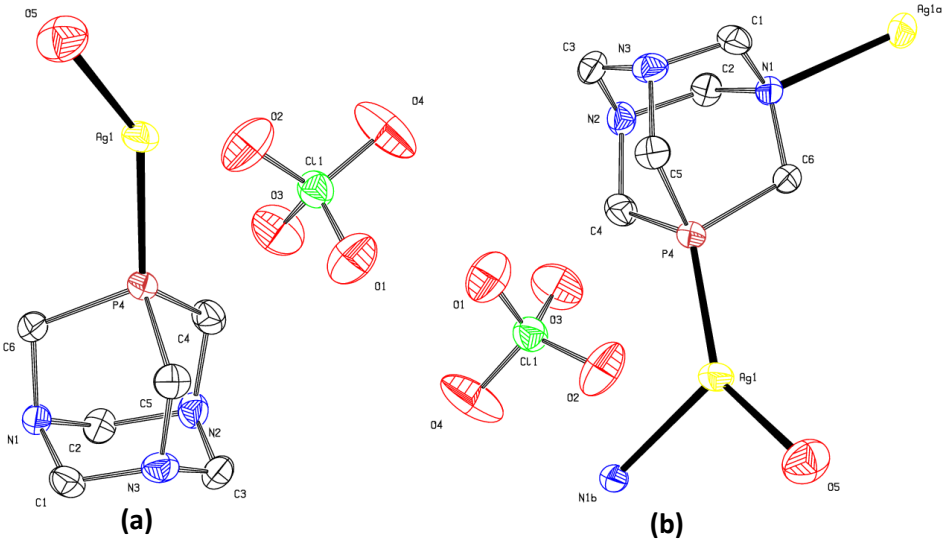

Figure 43: *ORTEP* diagram for (a) the asymmetric unit and (b) a repeating fragment of **CP_4**. All hydrogen atoms have been omitted for clarity and ellipsoids are drawn at 50% probability level

CP$_4$ crystallizes in the orthorhombic $P2_12_12_1$ space group. The asymmetric unit together with the repeating unit of **CP$_4$** is shown in Figure 43 while the important bond distances and angles are listed in Table 23. In the asymmetric unit we have a [Ag(O)(PTA)] unit and an uncoordinated perchlorate anion making **CP$_4$** a complex salt. The equivalent atoms that complete the molecule are generated by the symmetry code: -x, y+ ½ , $^3/_2$ -z. The Ag atom coordinates to a phosphorus atom and a nitrogen atom of two separate PTA molecules and an oxygen atom resulting in a distorted trigonal planar geometry. The bond angles around the metal centre lie between 102.09(10)° and 143.72(8)° while the Ag(1)-P(4), Ag(1)-N(1)#1, Ag(1)-O(5) bond distances of 2.3565(7) Å, 2.438(2) Å and 2.221(3) Å, respectively. two PTA molecules and an oxygen atom.

Table 23: Selected bond parameters of **CP$_4$**

Bond distances/Å		**Bond angles/ °**	
Ag(1)-N(1)#1	2.438(2)	P(4)-Ag(1)-O(5)	143.72(8)
Ag(1)-P(4)	2.3565(7)	N(1)-Ag(1)-O(5)#1	102.09(10)
Ag(1)-O(5)	2.221(3)	P(4)-Ag(1)-N(1)#1	114.03(5)

Symmetry codes: #1 = -x, y+ ½ , $^3/_2$ -z

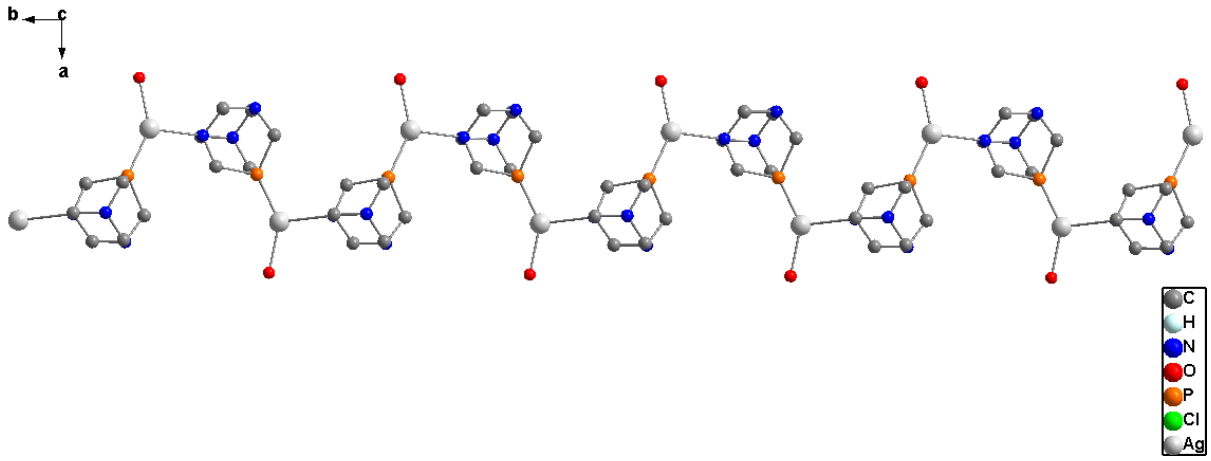

Figure 44: Polymeric representation of **CP$_4$** along the crystallographic *c*-axis

Figure 44 shows the polymeric representation of **CP$_4$**. The coordination polymer has 1D zig-zag molecular architecture with a repeating period of 10.889 Å between adjacent Ag atoms which is equivalent to the *b*-axis dimension of the cell. The polymer grows along the crystallographic *b*-axis which is made possible by the alternating *P*-, *N*- coordination mode of

PTA. The coordinated oxygen atom has a non-bridging coordination mode and inhibits the growth of the polymer in lateral directions.

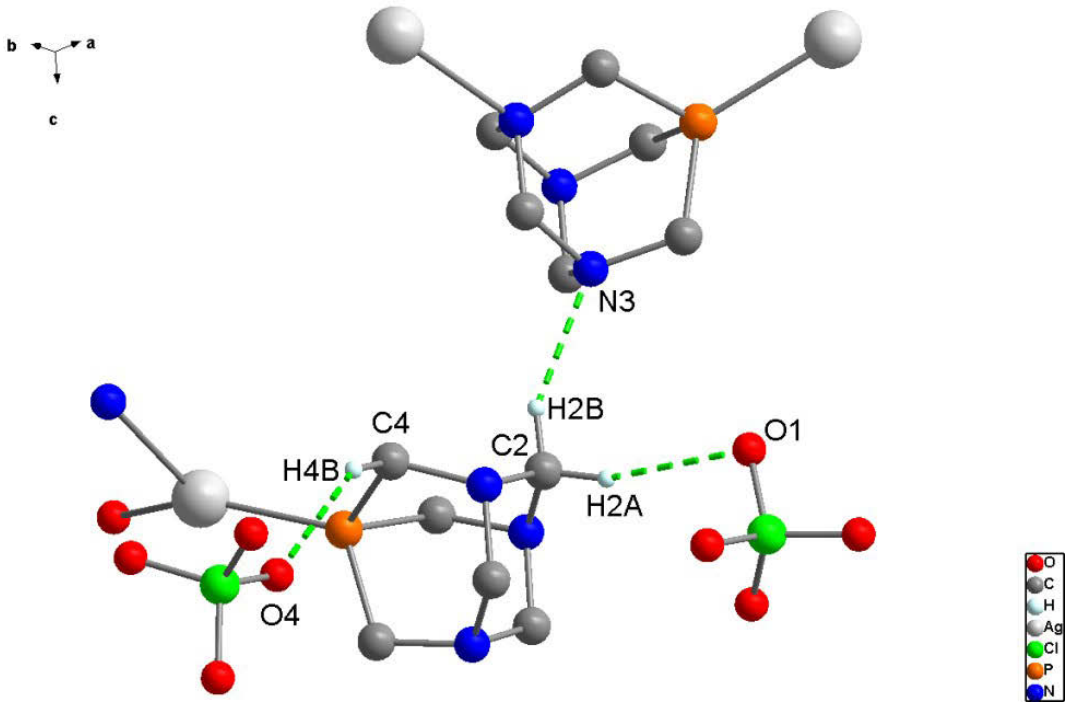

Figure 45: C-H…O hydrogen bonding patterns (shown as dashed green bonds) in **CP_4**

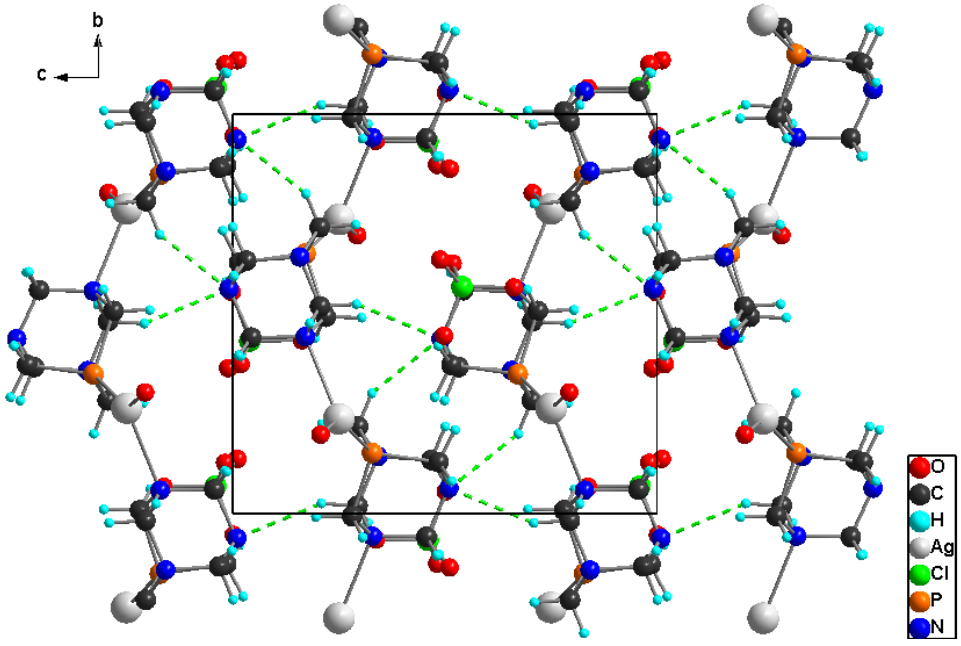

Figure 46: Representation of hydrogen bonding patterns (dashed green lines) present in the crystal packing resulting in the formation of a 3D supramolecular architecture via C-H…N and C-H…O hydrogen bonds in **CP_4** shown along the crystallographic *a*-axis

Figure 45 and Figure 46 show the hydrogen bonding patterns and the crystal packing diagram of **CP_4**, respectively while the hydrogen bonding parameters are listed in Table 24. The type of hydrogen bonding interactions that are predominant in **CP_4** appear to be the C-H…N and C-H…O hydrogen bonds. The C-H…N hydrogen bonds links neighbouring zig-zag coordination polymers. The perchlorate molecules are involved in the C-H…O hydrogen bonding which, together with the C-H…N hydrogen bonds, form a 3D supramolecular structure as shown in Figure 46.

Table 24: Selected hydrogen bonding parameters in **CP_4**

D-H…A	d(D-H)	d(H…A)	d(D…A)	<(DHA)
C(2)-H(2A)…O(1)#1	0.99	2.51	3.450(4)	159
C(2)-H(2B)…N(3)#2	0.99	2.54	3.451(3)	152
C(4)-H(4B)…O(4)#3	0.99	2.54	3.429(4)	149

Symmetry codes: #1 = 1-x, y- ½, $^3/_2$-z; #2 = ½ -x, 1-y, z- ½; #3 = ½ -x, 2-y, ½ +z

3.1.2.9 Crystal structure of $[Ag(\mu_2\text{-PTA})(PTA)(H_2O)]_n(ClO_4)_n$ (CP_5)

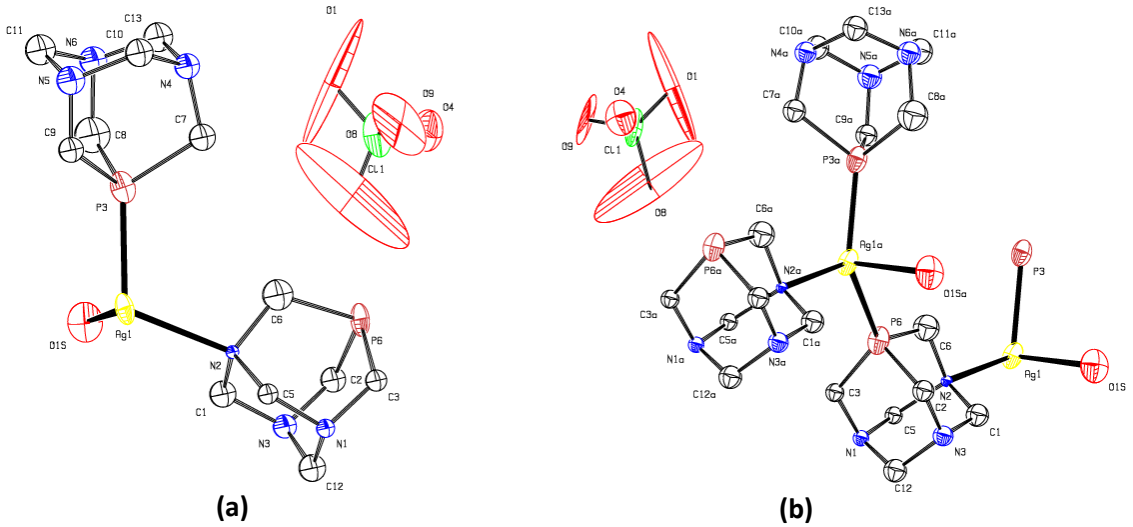

Figure 47: *ORTEP* diagram for (a) the asymmetric unit and (b) a repeating fragment of **CP_5**. All hydrogen atoms have been omitted for clarity and ellipsoids are drawn at 50% probability level.

CP_4 crystallizes in the orthorhombic $P2_12_12_1$ space group. The asymmetric unit of **CP_5** which contains the unit $[Ag(PTA)_2(H_2O)]$ and an uncoordinated perchlorate anion as shown in Figure 47(a). The disorder of the perchlorate ion could not be resolved. The equivalent atoms that complete the molecule are generated by the symmetry code: x+1, y, z. The

ORTEP diagram of a repeating fragment of **CP$_5$** is shown in Figure 47(b). Important bond distances and angles are listed in Table 25. The repeating unit contains one Ag metal center with one aqua and three PTA ligands in the coordination sphere that are counter balanced by a perchlorate ion. The coordination to the Ag atom is via two phosphorus atoms and a nitrogen atom of separate PTA molecules and an oxygen atom of the aqua group to give a distorted tetrahedral geometry. The bond angles around the Ag(I) centre lie between 93.07(4)° to 122.55(3)° with Ag(1)-P(6)#1, Ag(1)-P(3), Ag(1)-N(2) and Ag(1)-O(1S) bond distances of 2.400(6) Å, 2.435(6) Å, 2.400(14) Å and 2.58(2) Å, respectively.

Table 25: Selected bond distances (Å) and angles (°) of **CP$_5$**

Ag(1)-P(6)#1	2.400(6)	Ag(1)-O(1S)	2.58(2)
Ag(1)-N(2)	2.400(14)	Ag(1)-P(3)	2.435(6)
P(6)#1-Ag(1)-N(2)	114.8(3)	P(6)#1-Ag(1)-O(1S)	94.1(5)
P(6)#1-Ag(1)-P(3)	132.2(2)	N(2)-Ag(1)-O(1S)	89.6(6)
N(2)-Ag(1)-P(3)	112.0(4)	P(3)-Ag(1)-O(1S)	95.4(4)

Symmetry codes: #1 = x+1, y, z

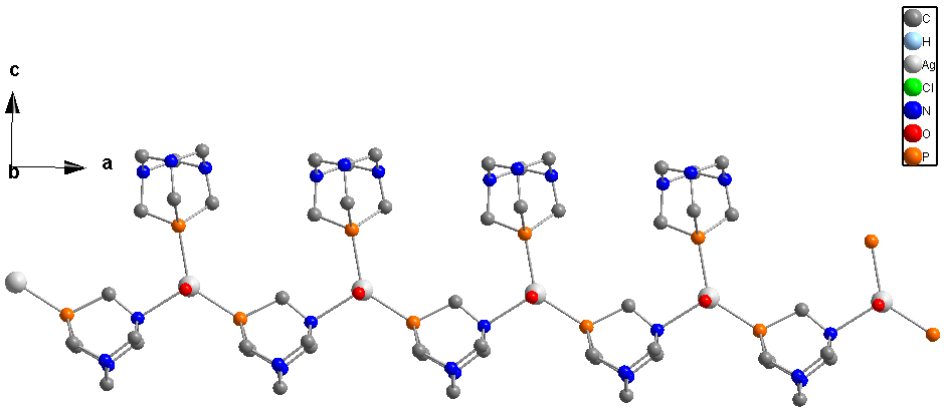

Figure 48: Polymeric representation of **CP$_5$** viewed along the crystallographic *b*-axis

CP$_5$ has a 1D structure with lateral PTA branches and a repeating distance of 6.846(5) Å between adjacent Ag(1) atoms, equivalent to the length of the '*a*' dimension of the cell as shown in Figure 48. The PTA groups coordinates in two ways. The PTA groups in **CP$_5$** coordinate to the metal centre in an alternating P and N atoms on either sides of one PTA and through P atom only of the lateral PTA. The PTA coordinates through the phosphorus atom only and forms lateral branches along the coordination polymer. The combination of the *P*-

and *P*-, *N*- coordination modes observed in **CP$_5$** results in a unique *P*-, *P'*-,*N*- coordination mode of PTA.

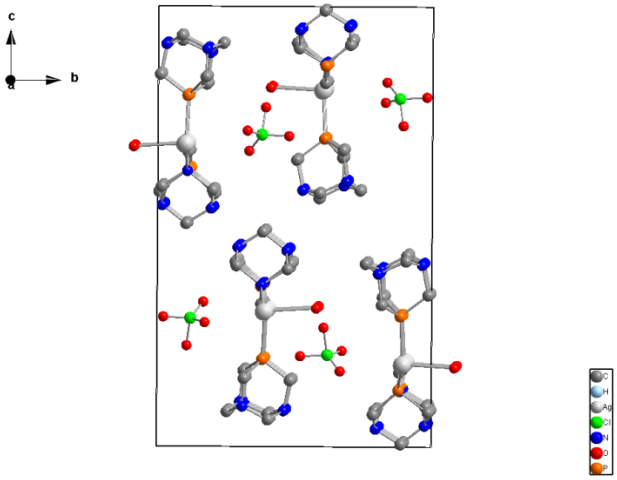

Figure 49: Crystal packing diagram of **CP$_5$** viewed along the crystallographic *a*-axis

Figure 49 shows the crystal packing diagram of **CP$_5$**. There seems to be an alternating orientation of the branch-like coordination polymers with the perchlorate anions positioned in between the strands. The coordinated oxygen atom and the perchlorate anion are not fully resolved due to the poor x-ray quality crystals that were harvested.

3.1.2.10 Crystal structure of [Ag(PTA)(H$_2$O)]$_n$(NO$_3$)$_n$ (CN$_1$)

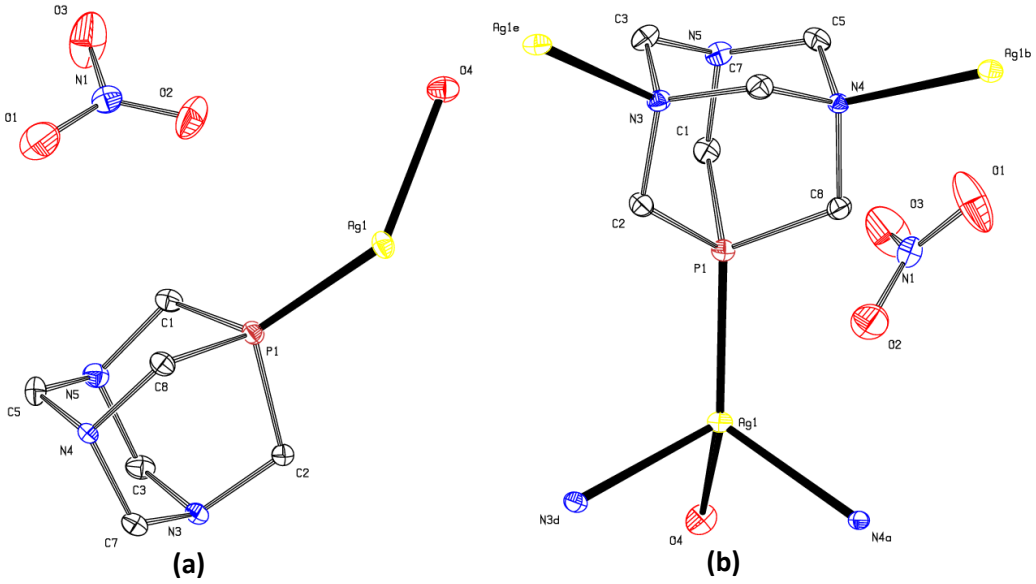

Figure 50: *ORTEP* diagram for (a) the asymmetric unit and (b) a repeating fragment of **CN$_1$**. All hydrogen atoms have been omitted for clarity and ellipsoids are drawn at 50% probability level

CN_1 crystallizes in the orthorhombic *Pbca* space group. Figure 50(a) shows the asymmetric unit of **CN_1** which contains a unit [Ag(PTA)(H_2O)] and an uncoordinated nitrate anion. The complete molecule is generated by the symmetry codes: ½ -x, y- ½ ,z and 1-x, y- ½ , $^3/_2$ -z. Figure 50(b) shows the repeating unit of CN_1 while important bond parameters are listed in Table 26. The repeating unit consists of one Ag atom, three PTA moieties, a coordinated water molecule and an uncoordinated nitrate anion. The coordination to the Ag atom is via a phosphorus atom and two nitrogen atoms of three separate PTA molecules including an oxygen atom of the aqua group. **CN_1** is a salt complex in which the Ag atom has a distorted tetrahedral geometry with bond angles around the metal centre lying between 88.97(5) and 132.09(4)°. The Ag(1)-P(1), Ag(1)-N(4), Ag(1)-N(3) and Ag(1)-O(4) bond distances of 2.3691(7) Å, 2.4323(15) Å, 2.4518(16) Å and 2.3603(15) Å, respectively.

Table 26: Selected bond distances (Å) and angles (°) **CN_1**

Ag(1)-O(4)	2.3603(15)	Ag(1)-N(4)#1	2.4323(15)
Ag(1)-P(1)	2.3691(7)	Ag(1)-N(3)#2	2.4518(16)
O(4)-Ag(1)-P(1)	132.09(4)	O(4)-Ag(1)-N(3)#2	88.97(5)
O(4)-Ag(1)-N(4)#1	90.72(5)	P(1)-Ag(1)-N(3)#2	113.89(4)
P(1)-Ag(1)-N(4)#1	119.49(4)	N(4)-Ag(1)-N(3)#2	105.60(5)

Symmetry codes: #1 = 1-x, y- ½ , $^3/_2$ -z; #2 = ½ -x, y- ½ ,z; #3 = ½ -x, y+ ½ ,z; #4 = 1-x, y+ ½ , $^3/_2$-z

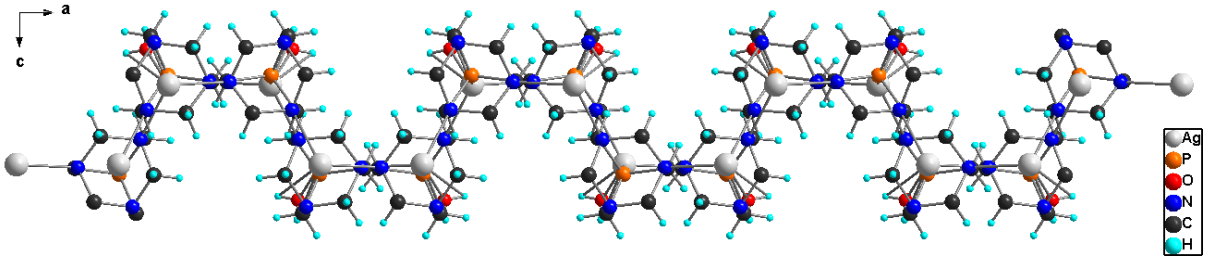

Figure 51: Polymeric representation of **CN_1** along the crystallographic *b*-axis. The nitrate anions are omitted for clarity

Figure 51 depicts the polymeric representation of **CN_1**. The coordination network is two dimensional and forms corrugated sheets when viewed down the *b* axis. The PTA uses *P*-, *N*-, *N'*- in the growth of the polymer in the *ab* plane.

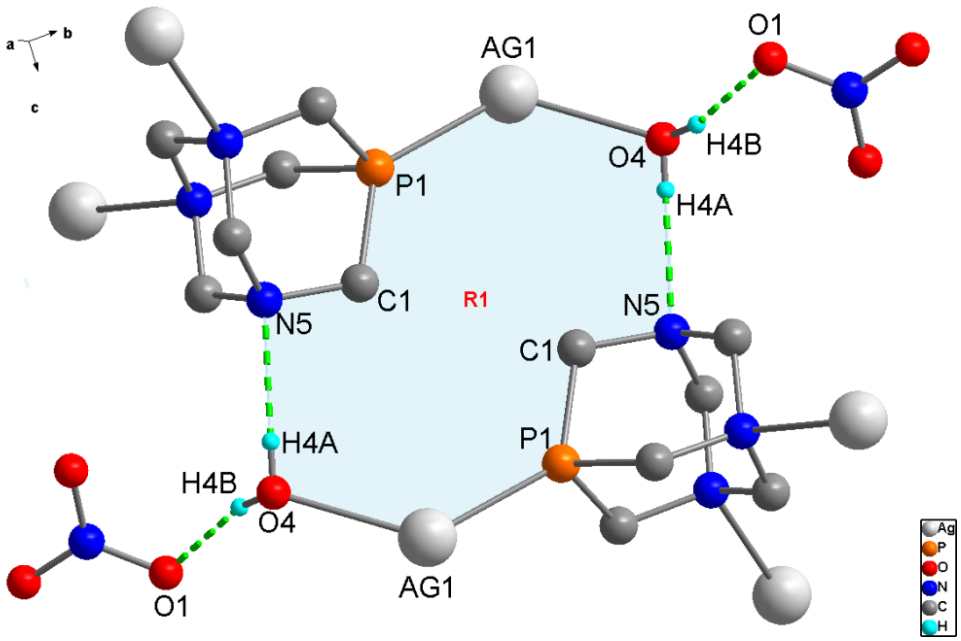

Figure 52: Water molecules forming rings via O-H…O hydrogen bonding (shown as dashed green bonds) in $\mathbf{CN_1}$. R1 is explained in text.

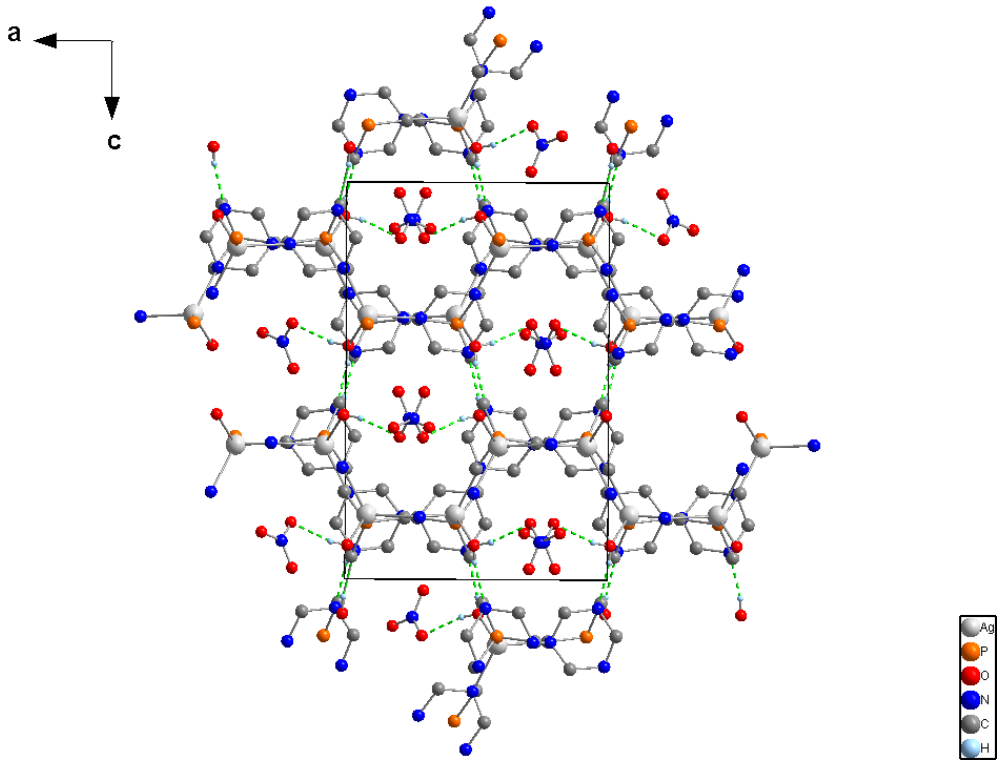

Figure 53: Representation of hydrogen bonding patterns (dashed green lines) present in the crystal packing of $\mathbf{CN_1}$ shown along the crystallographic *b*-axis. All methylene hydrogen atoms have been omitted for clarity

Table 27 lists the hydrogen bonding parameters observed in the crystal structure of $\mathbf{CN_1}$ while Figure 52 and Figure 53 show the hydrogen bonding patterns and the crystal packing diagram of $\mathbf{CN_1}$. Classical O-H…N and O-H…O hydrogen bonds appear to be predominant in

packing of molecules. One of the hydrogen atoms of the water moiety links up with the nitrogen atom of the PTA moiety on the adjacent corrugated sheets through O-H…N hydrogen bonds. In linking the corrugated sheets in this manner, 12-member rings (R1) that can be described by the graph-set notation $R_2^2(12)$ are formed as shown in Figure 52. The O-H…N hydrogen bonds sews the together the 2D corrugated sheets of **CN_1** to form a 3D supramolecular structure as shown in Figure 53. The other hydrogen atom of the water moiety joins with the oxygen atom of the uncoordinated nitrate anion via O-H…O hydrogen bonds. This localizes the nitrate anions in the hexagonal cavities of the stacked 2D corrugated sheets as shown in Figure 53.

Table 27: Selected hydrogen bonding parameters in **CN_1**

D-H…A	d(D-H)	d(H…A)	d(D…A)	<(DHA)
O(4)-H(4A)...N(5)#1	0.75	2.13	2.8695	169
O(4)-H(4B)...O(1)#2	0.81	2.02	2.8072	166

Symmetry codes: #1 = 1+x, y, z; #2 = x - ½, 1+y, ½ -z;

3.1.2.11 Crystal structure of $[Ag_2(PTA)_2(H_2O)]_n(O_3SCF_3)_{2n}$ (CN_2)

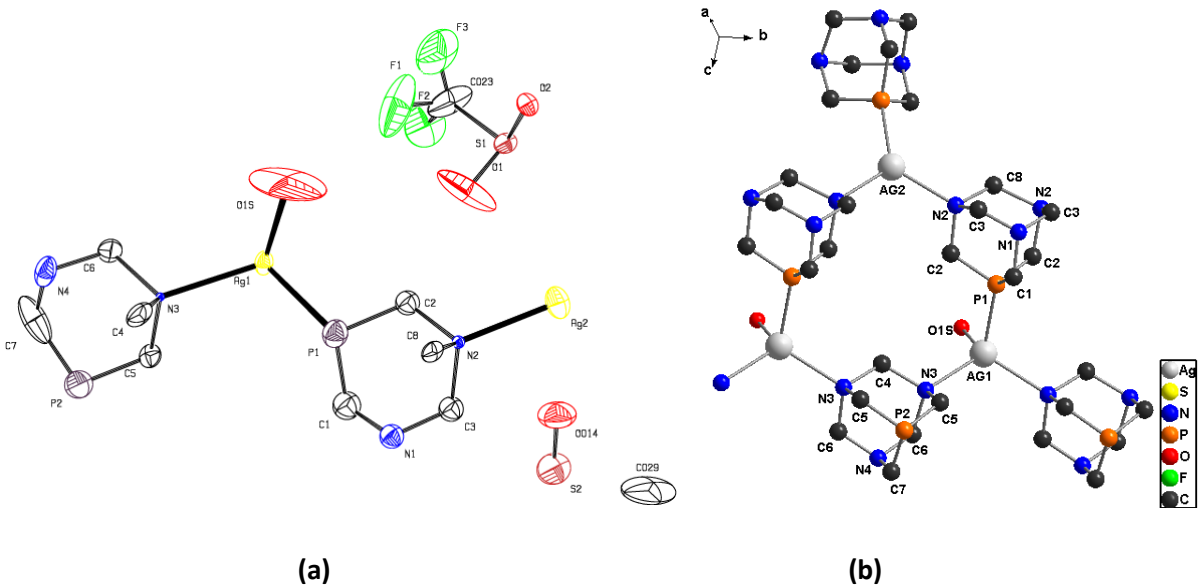

(a) **(b)**

Figure 54: (a) *ORTEP* diagram for the asymmetric unit with thermal ellipsoids drawn at 50% probability level and (b) a repeating fragment of **CN_2** with the triflate anions omitted for clarity. All hydrogen atoms have also been omitted for clarity

CN_2 crystallizes in the orthorhombic *Pnma* space group. Figure 54(a) and (b) show the asymmetric unit and repeating unit of **CN_2**, respectively and Table 28 lists important bond parameter of **CN_2**. The asymmetric unit contains a unit $[Ag_2(PTA)_{1.4}(O)]$ and two uncoordinated triflate anions. The disorder around the triflate ions could not be resolved. The repeating unit consists of two Ag atoms, two PTA moieties, a coordinated water molecule and two uncoordinated triflate anions. The two Ag atoms have different coordination environments and geometries. Coordination to the Ag(1) atom is via a phosphorus atom and two nitrogen atoms of three separate PTA moieties including an oxygen atom of the coordinated water moiety. Ag(1) has a distorted tetrahedral geometry with bond angles around the metal centre lying between 96(2)° and 114.7(2)°. The Ag(1)-P(1), Ag(1)-N(3), and Ag(1)-O(1S) bond distances are 2.390(5) Å, 2.396(5) Å, and 2.30(4) Å , respectively. Coordination to the Ag(2) atom is via a phosphorus atom and two nitrogen atoms of three separate PTA moieties. The geometry around the Ag(2) is slightly distorted trigonal planar as seen in the bond angles around the metal centre lying between 114.2(3) and 122.87(14)°. The Ag(2)-P(2) and Ag(2)-N(2) bond distances are 2.400(7) Å and 2.337(6) Å , respectively.

Table 28: Selected bond distances (Å) and angles (°) of **CN_2**

Ag(1)-O(1S)	2.30(4)	Ag(2)-N(2)	2.337(6)
Ag(1)-P(1)	2.390(5)	Ag(2)-N(2)#2	2.337(6)
Ag(1)-N(3)	2.396(5)	Ag(2)-P(2)#3	2.400(7)
Ag(1)-N(3)#1	2.396(5)		
O(1S)-Ag(1)-P(1)	96(2)	N(3)-Ag(1)-N(3)#1	114.7(2)
O(1S)-Ag(1)-N(3)	110.1(10)	N(2)-Ag(2)-N(2)#2	114.2(3)
P(1)-Ag(1)-N(3)	112.19(13)	N(2)-Ag(2)-P(2)#3	122.87(14)
O(1S)-Ag(1)-N(3)#1	110.1(10)	N(2)#2-Ag(2)-P(2)#3	122.87(14)
P(1)-Ag(1)-N(3)#1	112.20(13)		

Symmetry codes: #1 = x, ½ -y, z; #2 = x, $^3/_2$ -y,z; #3 = x+ ½ , y+1, $^3/_2$ -z

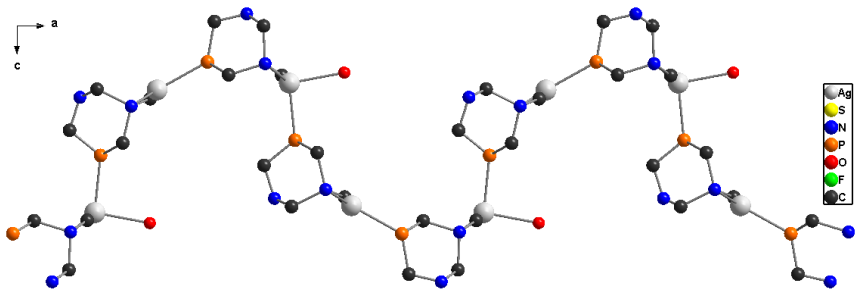

Figure 55: Polymeric representation of **CN_2** as viewed down the crystallographic *b*-axis. The triflate anions have been omitted for clarity

Figure 55 depicts the polymeric representation of **CN_2**. The coordination network has a 2D corrugated sheet molecular architecture which extends along the *ab* plane. All the PTA moieties exhibit an alternating *P*-, *N*-, *N'*- coordination mode causing the coordination network to propagate in a two dimensional manner. The coordination environments of the Ag atoms seem to occur at an alternating sequence in a zig-zag pattern.

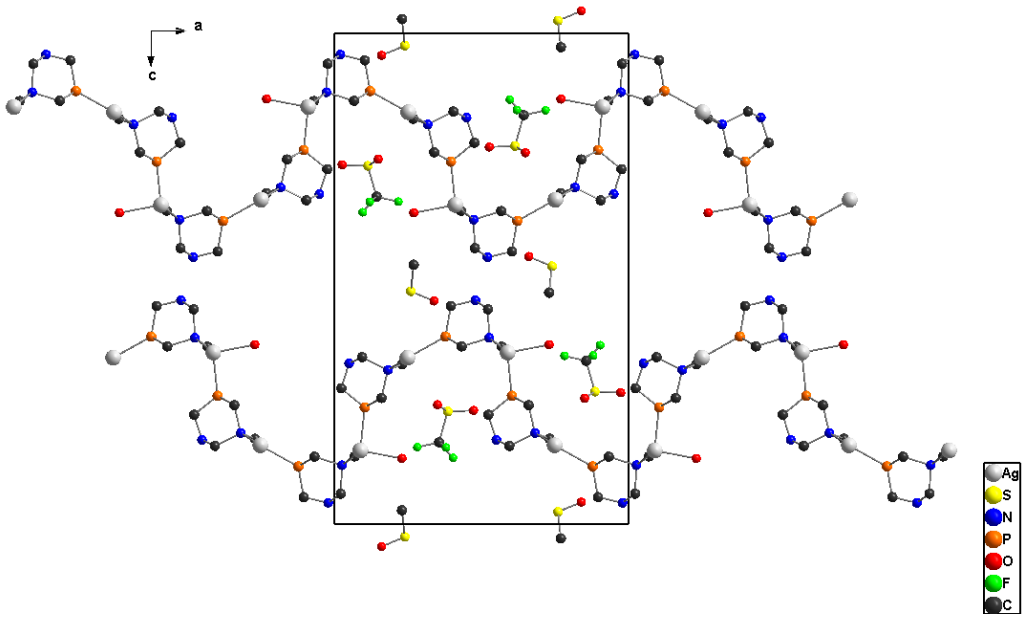

Figure 56: Crystal packing diagram of CN_2 viewed along the crystallographic *b* axis

Figure 56 shows the crystal packing diagram of **CN_2**. The 2D corrugated sheet-like coordination networks are stacked in similar manner as those in **CN_1**. The coordinated oxygen atom and the triflate anions are not fully resolved due to the poor x-ray quality and for this reason hydrogen bonding could not be accurately determined.

3.1.2.12 Crystal structure of $[Ag_2(PTA)_2(H_2O)(NO_3)]_n[(NO_3)(4\text{-}NP)(H_2O)]_n\,(CN_3)$

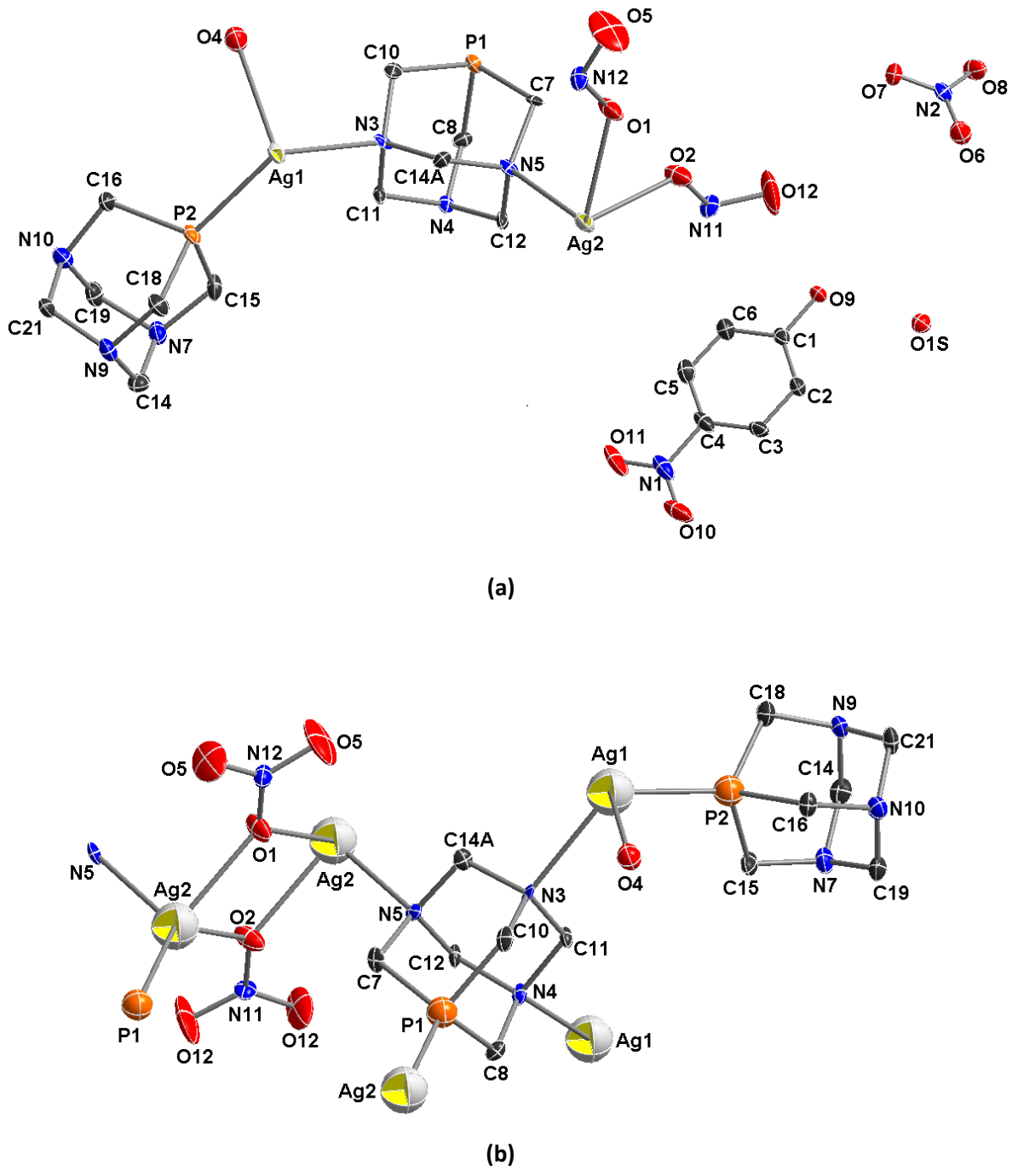

Figure 57: Ellipsoid plot for (a) the asymmetric unit and (b) a repeating fragment of $\mathbf{CN_5}$. All hydrogen atoms have been omitted for clarity and ellipsoids are drawn at 50% probability level.

$\mathbf{CN_5}$ crystallizes in the orthorhombic *Aba*2 space group. Figure 57 shows ORTEP diagrams of the asymmetric unit and the repeating unit of $\mathbf{CN_5}$ while the important bond distances and

angles are listed in Table 29. The asymmetric unit consists of the unit $[Ag_2(PTA)_2(NO_3)_{1.5}(H_2O)]$, an uncoordinated nitrate anion, a 4-nitrophenol molecule and a water molecule, making **CN_5** a salt complex as shown in Figure 57(a). The repeating unit of **CN_5** reveals two Ag(I) centres which have different coordination environments. Coordination to Ag(1) is through a phosphorus atom and two nitrogen atoms of three separate PTA molecules and an oxygen atom of the coordinated water molecule. Ag(1) has a distorted tetrahedral geometry environment with the bond angles around the metal centre lying between 87.2(2) and 138.32(18)°. The Ag(1)-P(2), Ag(1)-N(3), Ag(1)-N(4) and Ag(1)-O(4) bond distances are 2.3740(18) Å, 2.476(7) Å, 2.346(7) Å, and 2.565(6) Å , respectively. The coordination environment of the silver atom Ag(2) has a phosphorus atom and a nitrogen atom of two separate PTA molecules and two oxygen atoms of two separate nitrate molecules resulting in a distorted tetrahedral geometry. The bond angles lie between 69.9(2)° and 134.79(17)°. The Ag(2)-P(2), Ag(2)-N(5), Ag(2)-O(1) and Ag(2)-O(2) bond distances are 2.3239(15) Å, 2.406(5) Å, 2.368(7) Å and 2.366(6) Å , respectively. The coordinated nitrate molecules bridges the two Ag(2) metal centres in a μ^1 fashion and results in a Ag…Ag separation of 3.880(2) Å which is longer than the sum of the van der Waals radii for silver (3.44 Å) cannot be classified as an interaction.[7]

Table 29: Selected bond distances (Å) and angles (°) of **CN_5**

P(2)-Ag(1)	2.3740(18)	P(1)-Ag(2)#3	2.3239(15)
O(4)-Ag(1)	2.565(6)	O(1)-Ag(2)	2.368(7)
N(3)-Ag(1)	2.476(7)	O(2)-Ag(2)	2.366(6)
N(4)-Ag(1)#1	2.346(7)	N(5)-Ag(2)	2.406(5)
N(4)#4-Ag(1)-P(2)	138.32(18)	P(1)#5-Ag(2)-O(2)	134.34(16)
N(4)#4-Ag(1)-N(3)	101.86(18)	P(1)#5-Ag(2)-O(1)	134.79(17)
P(2)-Ag(1)-N(3)	117.80(17)	O(2)-Ag(2)-O(1)	69.9(2)
N(4)#4-Ag(1)-O(4)	89.9(2)	P(1)#5-Ag(2)-N(5)	124.62(13)
P(2)-Ag(1)-O(4)	103.56(14)	O(2)-Ag(2)-N(5)	87.35(17)
N(3)-Ag(1)-O(4)	87.2(2)	O(1)-Ag(2)-N(5)	86.91(17)

Symmetry codes: #1 = -x+ $^3/_2$, y, z- ½ ; #3 = x-1, y, z; #4 = $^3/_2$-x, y, z+ ½ ; #5 = x+1, y, z

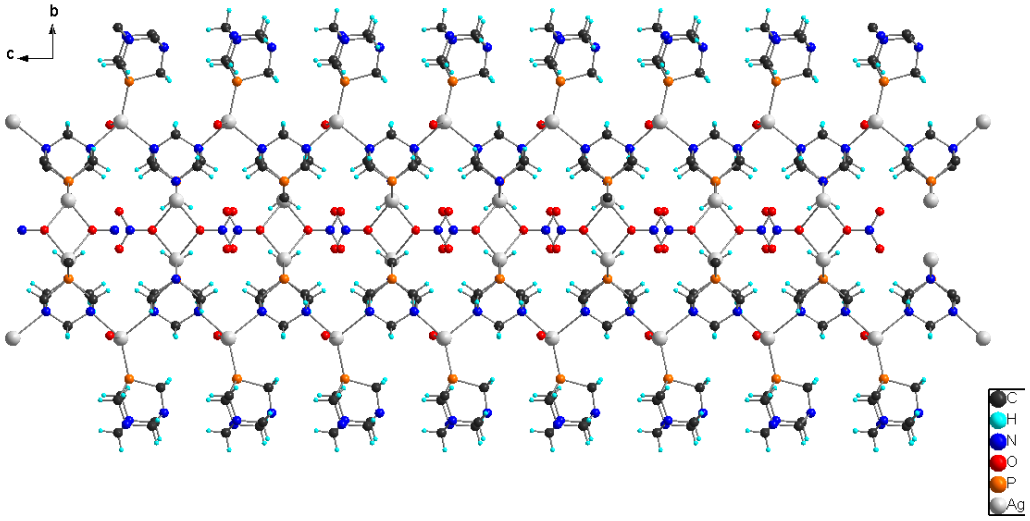

Figure 58: Polymeric representation of $\mathbf{CN_5}$ viewed down the crystallographic *a*-axis. Molecules in the outer coordination sphere have been omitted for clarity

Figure 58 shows the polymeric representation of $\mathbf{CN_5}$ as viewed down the *a* axis. The overall molecular architecture of $\mathbf{CN_5}$ appears to be 2D sheet-like coordination network that grows along the crystallographic axes *a* and *c*. The PTA molecules in $\mathbf{CN_5}$ have different coordination modes. In some PTA molecules a *P*-, *N*-, *N'*-, *N''*- coordination mode is observed which links to four Ag metal centres and facilitates the growth of the polymer. In the other PTA molecules a *P*- coordination mode is observed.

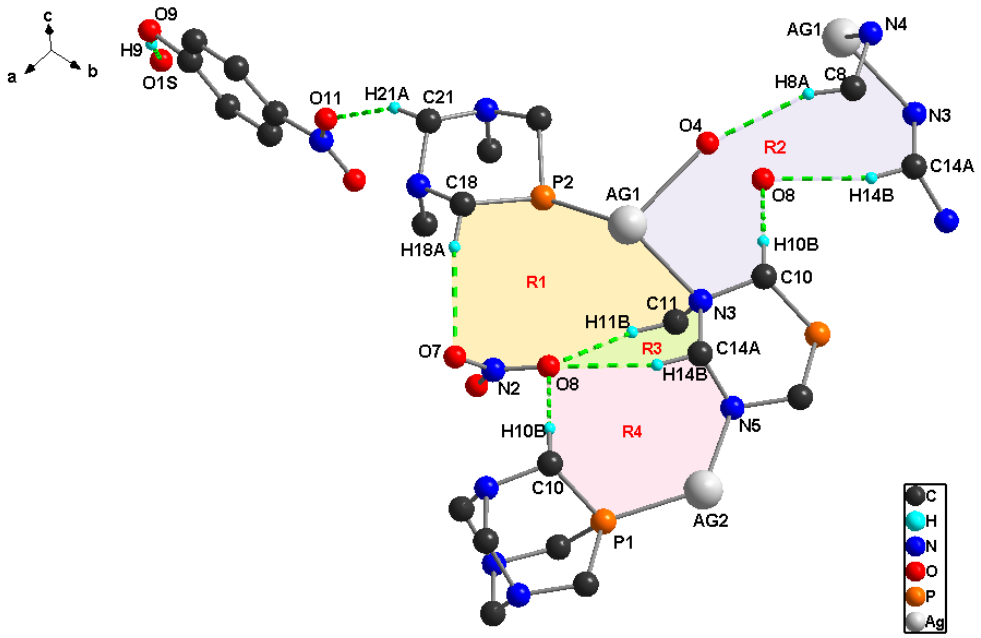

Figure 59: Hydrogen bonding network observed in $\mathbf{CN_5}$ (shown as dashed green bonds). R1, R2, R3 and R4 represent graph-set descriptions $\boldsymbol{R_2^2(10)}$, $\boldsymbol{R_3^2(13)}$, $\boldsymbol{R_2^1(6)}$ and $\boldsymbol{R_2^2(12)}$, respectively

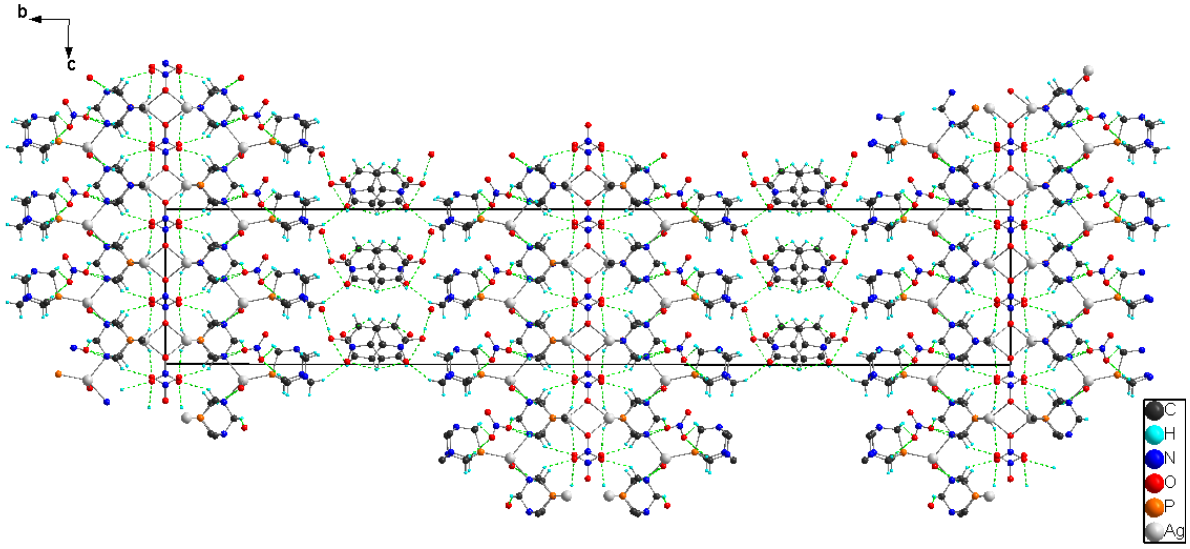

Figure 60: Representation of hydrogen bonding patterns (dashed green lines) present in the crystal packing of **CN_5** shown along the crystallographic *a*-axis. All methylene hydrogen atoms have been omitted for clarity

Table 30 lists the hydrogen bonding parameters observed in the crystal structure of **CN_5** while Figure 59 and Figure 60 depicts the hydrogen bonding patterns observed and the crystal packing diagram of **CN_5**, respectively. The classical O-H…O and the non-classical C-H…O hydrogen bonds are present in **CN_5**, of which the latter dominates. The hydrogen atoms of the PTA moieties link with oxygen atoms of the uncoordinated nitrate molecule through C-H…O hydrogens bonds. In linking the molecules in this manner, a 10-membered ring (R1), a 13-membered ring (R2), a 6-membered ring (R3) and an 8-membered ring (R4) described by the graph-set notations $R_2^2(10)$, $R_3^2(13)$, $R_2^1(6)$ and $R_2^2(12)$ respectively are formed as shown in Figure 59. The hydrogen atoms of the PTA moieties also link with the oxygen atoms of the nitro group of the 4-nitrophenol molecule through C-H…O hydrogen bonds and the hydroxyl group of the 4-nitrophenol molecule links with the oxygen atom of the uncoordinated water molecule as shown in Figure 59. The 4-nitrophenol and the water molecules are positioned in between the stacked layers of the 2D sheets of **CN_5** whilst the uncoordinated nitrate molecules appear to be embedded with the 2D sheet-like molecules as shown in Figure 60. The intermolecular O-H…O and C-H…O hydrogen bonds do not sew the 2D sheet-like molecules together to form a 3D supramolecular structure.

Table 30: Selected hydrogen bonding parameters in CN_5

D-H…A	d(D-H)	d(H…A)	d(D…A)	<(DHA)
O(9)-H(9)...O(1S)	0.84	1.76	2.596(9)	170
C(8)-H(8A)...O(4)#1	0.99	2.51	3.457(10)	159
C(10)-H(10B)...O(8)#2	0.99	2.47	3.427(11)	163
C(11)-H(11B)...O(8)#3	0.99	2.41	3.314(9)	151
C(14A)-H(14B)...O(8)#3	0.99	2.55	3.402(10)	145
C(18)-H(18A)...O(7)#3	0.99	2.45	3.427(10)	168
C(21)-H(21A)...O(11)#4	0.99	2.41	3.324(12)	154

Symmetry codes: #1 = 1/2-x,y,-1/2+z; #1-x,1-y,z; #3 = 2-x,1-y,z; #4 = 1/2-x,y,-1/2+z

3.2 Reactions of PTAMeI with various silver(I) salts

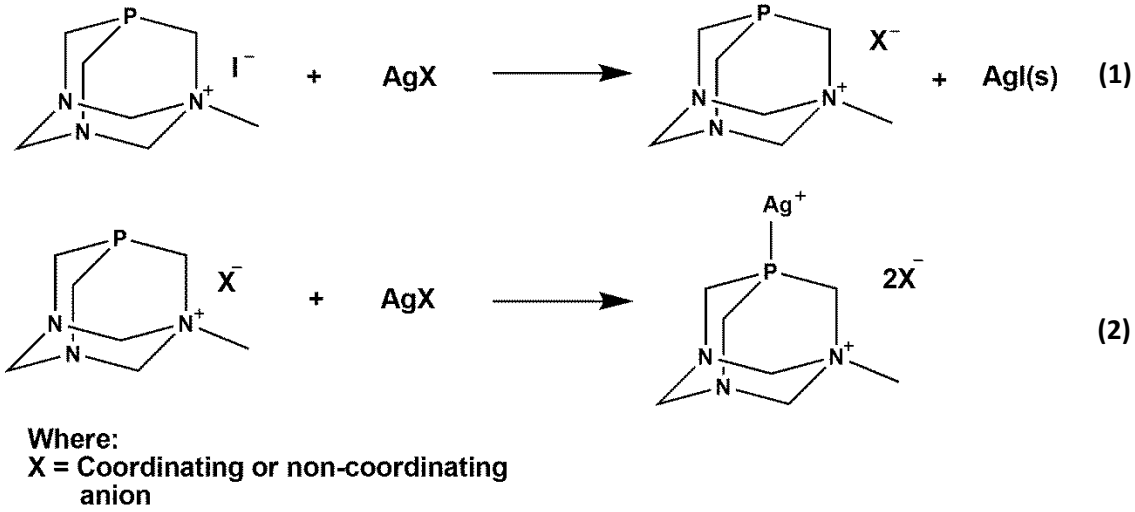

Silver(I) coordination compounds containing nitrogen methylated-PTA have not been reported in literature. In this work we attempted to synthesize coordination polymers of Ag(I) and PTAMeI. The compounds we synthesized are organic salts containing halide counterions. Their syntheses involved anion exchange reactions whereby the silver(I)iodide was precipitated out as shown in Equation 1 above. Filtration of the reaction mixture afforded a clear colourless solution and the further addition of the silver salt resulted in the formation of novel coordination compounds **m-CP$_1$**, **m-CP$_2$**, **m-CP$_3$** and **m-CP$_4$** as shown in equation 2 above. The reactions were performed in the dark to avoid the photodecomposition of silver(I)iodide to produce elemental silver and diatomic iodine.

We have used water soluble silver(I) salts to perform the anion exchange reactions. The anions used are ClO_4^- (for **m-CP$_1$**), NO_3^- (for **m-CP$_2$**), $O_2CCF_3^-$ (for **m-CP$_3$**) and $O_3SCF_3^-$ (for **m-CP$_4$**). The products were obtained in low yields and this may be attributed to the reaction of silver(I)iodide with PTAMe to form an insoluble by-product before the isolation of the desired product.

3.2.1 Spectroscopic analysis of Ag-PTAMe coordination compounds

We have performed solution ^1H and ^{31}P NMR studies of uncomplexed PTAMeI and the synthesized Ag-PTAMe complexes. From these studies we observe that methylation takes place primarily on one nitrogen atom of the PTA as opposed to the phosphorus atom. This causes a decrease in the molecular symmetry of the PTA moiety when compared to the parent compound. Hence in the ^1H NMR spectrum of PTAMeI in D_2O, the methylene protons of PTAMeI were observed to be non-equivalent and diastereotropic.

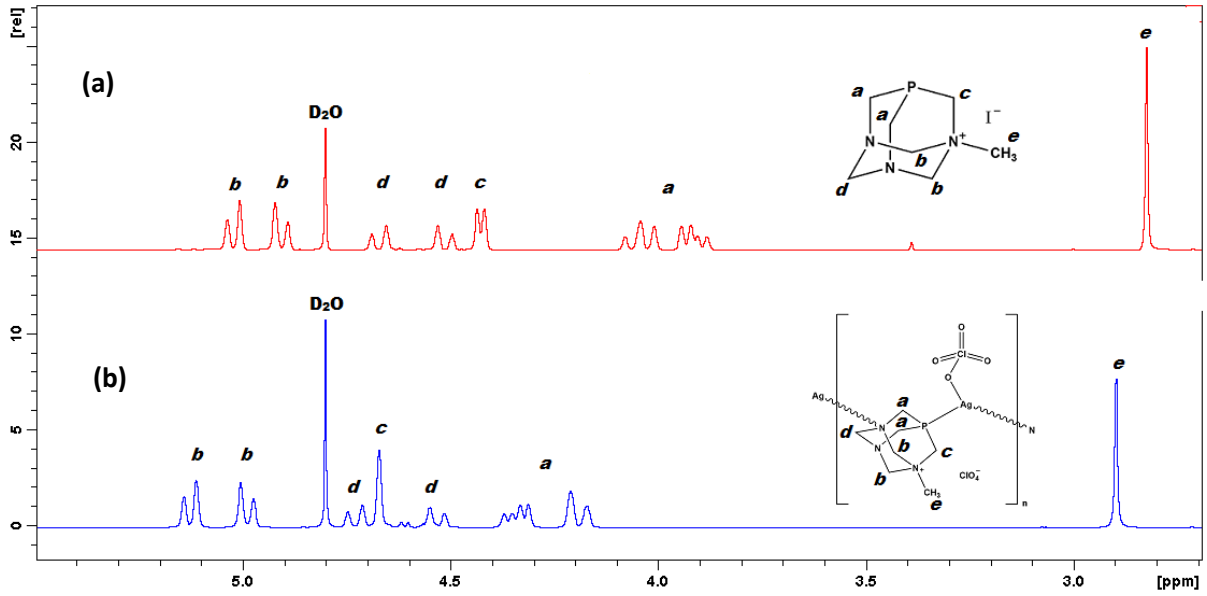

Figure 61: ^1H NMR spectrum of (a) free PTAMeI in D_2O and (b) **m-CP$_1$**

Figure 61(a) and (b) shows the ^1H NMR spectrum of PTAMeI and **m-CP$_1$**, respectively. The N-CH_2-N^+ protons of PTAMeI appear as two separate doublets resonating at 5.02 and 4.91 ppm with $^2J_{HH}$ = 11.9 Hz. The N-CH_2-N protons resonate at 4.67 and 4.51 ppm and appear as two separate doublets with identical $^2J_{HH}$ values of 11.9 Hz. The P-CH_2-N^+ protons are observed as a doublet at 4.43 ppm with $^2J_{PH}$ = 6.7 Hz and the P-C**H$_2$**-N protons appear as two

separate multiplets which are caused by the overlapping doublets that resonate at 4.04 and 3.91 ppm. Finally the methyl protons on the alkylated nitrogen are observed as a singlet resonating at 2.82 ppm. The ^{1}H NMR spectrum of **m-CP$_1$** is different from that of the free ligand even though the methylene protons still appear to be non-equivalent and diastereotropic. The N-C**H**$_2$-N$^+$ protons of **m-CP$_1$** still appeared as two separate doublets but resonate slightly downfield at 5.16 and 5.00 ppm with slightly increased coupling constants of 14.2 Hz and 14.0 Hz, respectively. The separation between the N-C**H**$_2$-N protons increase from 0.16 ppm (for PTAMeI) to 0.22 ppm (for **m-CP$_1$**) and the protons resonate more downfield at 4.76 and 4.55 ppm signifying that the N-C**H**$_2$-N protons have become even more non-equivalent. This was also observed for silver-PTA coordination polymers and suggests that coordination via the PTAMe's nitrogen atom to the silver(I) metal centre has been achieved in silver-PTAMe coordination compounds. The P-C**H**$_2$-N$^+$ protons also shifts downfield from 4.43 to 4.72 ppm but the signal changes from a doublet with $^{2}J_{PH}$ = 6.7 Hz to a singlet. This suggests that the phosphorus atom of the PTAMe unit is coordinated to the Ag metal, in a similar manner to what is observed for the Ag-PTA coordination compounds. The P-C**H**$_2$-N protons appear as two separate multiplets which are caused by overlapping doublets that resonate at 4.04 and 3.91 ppm. Finally the methyl protons were observed as a singlet resonating at 2.82 ppm.

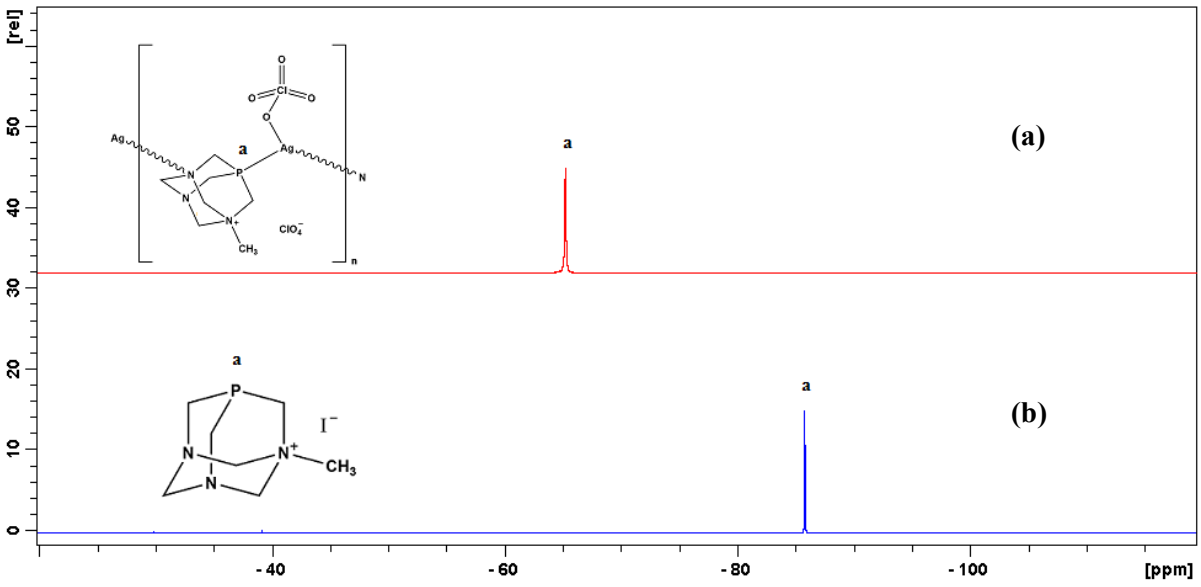

Figure 62: ^{31}P NMR of (a) **m-CP$_1$** and (b) PTAMeI

The ^{31}P NMR spectrum of PTAMeI is shown in Figure 62(b). The peak for phosphorus appears as a sharp singlet resonating at δ -85.76 ppm. Figure 62(a) shows the ^{31}P NMR

spectrum of **m-CP$_1$** which is a representative spectrum of the Ag-PTAMe coordination compounds and the peak for phosphorus resonates at a much higher frequency of δ = -65.20 ppm and appears as a broad singlet.

Table 31: Characteristic NMR spectroscopic data for Ag(I)-PTAMe coordination compounds

Compound	δ (s, 2H,P-C**H**$_2$-N$^+$, ^{1}H)	δ (d, 2H, N-C**H**$_{2(eq)}$-N, ^{1}H)	δ (d, 3H, N-C**H**$_{2(ax)}$-N, ^{1}H)	δ (P, ^{31}P)
m-CP$_1$	4.72	5.00 ($J_H{}^A{}_H{}^B$ = 12.1 Hz)	5.16 ($J_H{}^B{}_H{}^A$= 11.6 Hz)	-65.2
m-CP$_2$	4.43	4.89 ($J_H{}^A{}_H{}^B$ = 11.6 Hz)	4.99 ($J_H{}^B{}_H{}^A$= 11.4 Hz)	-65.2
m-CP$_3$	4.70	4.89 ($J_H{}^A{}_H{}^B$ = 11.6 Hz)	5.07 ($J_H{}^B{}_H{}^A$= 11.4 Hz)	-68.4
m-CP$_4$	4.70	4.98 ($J_H{}^A{}_H{}^B$ = 12.0 Hz)	5.14 ($J_H{}^B{}_H{}^A$= 12.1 Hz)	-65.3

Table 31 lists characteristic peaks observed in the ^{1}H and ^{31}P NMR for all the Ag-PTAMe coordination compounds. The variation of the anion from perchlorate to nitrate to trifluoroacetate to triflate, seem not to affect the chemical shifts of the peaks.

The IR spectra of all the silver(I)-PTAMe coordination compounds exhibit similar features with typical vibrations due to the anions and PTAMe ligands. Characteristic bands between 2942 cm^{-1} and 2988 cm^{-1}, and between 1100 cm^{-1} and 900 cm^{-1} are associated with *ν*(C-H) and *ν*(C-X; whereby X = P and N) vibrations within the PTAMe ligands, respectively. **m-CP$_1$** and **m-CP$_2$** both contain a coordinated methanol molecules; hence broad *ν*(O-H) vibrational bands appear between 3500 cm^{-1} and 3200 cm^{-1} which is associated with the extensive O-H…O hydrogen bonding interactions between the methanol molecule and the respective uncoordinated anion.[1c] The presence of the anion moieties in **m-CP$_1$**, **m-CP$_2$**, **m-CP$_3$** and **m-CP$_4$** is confirmed by the occurrence of *ν*(ClO_4) vibrational bands between 1036 cm^{-1} and 1018 cm^{-1}, *ν*(NO_3) vibrational band at 1291 cm^{-1}, n intense peak at 1675 cm^{-1} which is attributed to the *ν*(C=O) vibration band and peaks at 1243 cm^{-1} associated with *ν*(S=O) vibrational band. The *ν*(S-O) vibrational band is observed at 1019 cm^{-1}, respectively.

Table 32: Summary of events from the thermal analysis of silver(I)-PTAMe coordination compounds

Compound	**Anion**	**Solvent**	**Temperature/°C**	
			Loss of solvent[a]	**Decomposition[b]**
m-CP$_2$	NO_3	CH_3OH	161	194
m-CP$_3$	O_2CCF_3	-	-	202

[a] Endothermic event; [b] Exothermic event

The thermal stability of the synthesized silver(I)-PTAMe coordination compounds were studied by a simultaneous thermogravimetric and differential scanning calorimetry analysis and the results are summarized in Table 32. **m-CP$_3$** contains no solvent molecules whereas **m-CP$_2$** does. This is observed in the loss of the coordinated methanol molecule at 160 °C which occurs as an endothermic event with ΔH = 33.6 kJ mol^{-1}. Both **m-CP$_2$** and **m-CP$_3$** appear to be thermally stable up to temperatures of 190 °C despite the loss of coordinated methanol molecule which occurs in m-CP$_2$. Decomposition of the Ag-PTAMe complexes occurs as an exothermic event between 194 °C and 204 °C. The Ag-PTAMe complexes of **m-CP$_2$** and **m-CP$_3$** appear to be thermally less stable than the Ag-PTA complexes of **CP$_1$** and **CP$_3$** which were synthesized using the same silver(I) salt precursors $AgNO_3$ and AgO_2CCF_3, respectively.

3.2.2 Crystal structure analysis of Ag-PTAMe coordination compounds

This section outlines in detail the molecular crystal structures of and the hydrogen bonding patterns present in **m-CP$_1$**, **m-CP$_2$** and **m-CP$_3$**. The discussion of this section is centred around the influence of the N-methylated PTA (PTAMe) on the molecular architecture of silver-PTAMe coordination compounds.

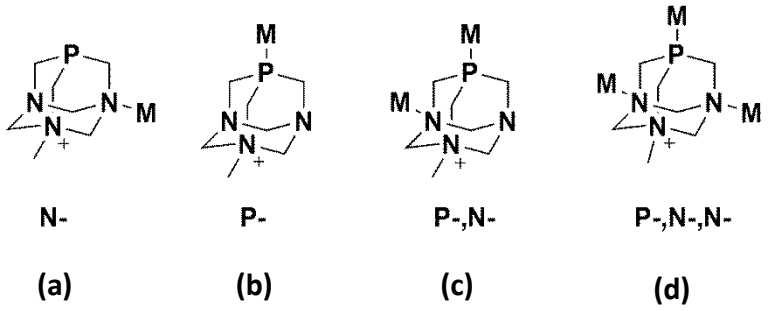

Figure 63: Possible coordination modes of PTAMe

Figure 63 shows all the possible coordination modes of PTAMe to metal centres. Both **m-CP$_1$** and **m-CP$_2$** appear to be linear 1D coordination polymers that have an alternating *P*-,*N*-coordination mode of PTA as shown in Figure 63(c). The main difference in the two coordination polymers is mainly in the different oxy-anions used which ClO_4^- and NO_3^- for coordination compounds **m-CP$_1$** and **m-CP$_2$**, respectively. On the other hand, **m-CP$_3$**

appears to have a coiled 1D molecular architecture with *P*- coordination mode of PTA as shown in Figure 63(b).

3.2.3.1 Crystal structure of $[Ag(\mu_2\text{-PTAMe})(ClO_4)(CH_3OH]_nClO_4$ (m-CP_1)

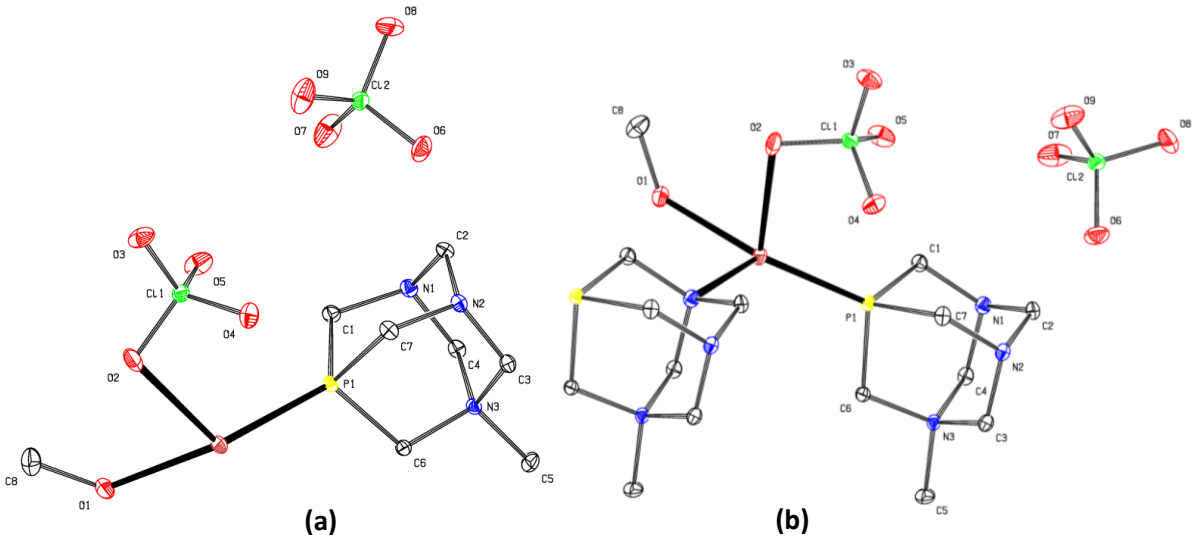

Figure 64: *ORTEP* diagram for (a) the asymmetric unit and (b) a repeating fragment of **m-CP_1**. All hydrogen atoms have been omitted for clarity and ellipsoids are drawn at 50% probability level

m-CP_1 crystallizes in the orthorhombic *Pna2₁* space group. Figure 64(a) and (b) shows the *ORTEP* diagram of the asymmetric unit and the repeating unit of **m-CP_1** while Table 33 lists important bond angles and distances. The asymmetric unit contains the unit $[Ag(ClO_4)(CH_3OH)(PTAMe)]$ and an uncoordinated perchlorate anion making **m-CP_1** a complex salt. The equivalent atoms that complete the molecule are generated by the symmetry code: x, y, z+1. In the repeating unit shown in Figure 64(b), the Ag atom is coordinated to a phosphorus atom and nitrogen atom of separate PTAMe moieties, an oxygen atom of the methanol moiety and another oxygen atom of the perchlorate molecule. The silver metal centre has a distorted tetrahedral geometry with the bond angles around the Ag(I) atom lie between 82.88(6)° and 138.92(4)°. The Ag(1)-P(1), Ag(1)-N(1), Ag(1)-O(1) and Ag(1)-O(2) bond distances are 2.3755(5) Å, 2.4789(18) Å, 2.3203(13) Å and 2.5606(15) Å, respectively.

Table 33: Selected bond distances (Å) and angles (°) of **m-CP$_1$**

N(1)-Ag(1)#1	2.4789(18)	O(2)-Ag(1)	2.5606(15)
O(1)-Ag(1)	2.3203(13)	P(1)-Ag(1)	2.3755(5)
O(1)-Ag(1)-P(1)	138.92(4)	O(1)-Ag(1)-O(2)	82.97(4)
O(1)-Ag(1)-N(1)#2	90.73(5)	P(1)-Ag(1)-O(2)	114.29(3)
P(1)-Ag(1)-N(1)#2	126.83(4)	N(1)-Ag(1)-O(2)#2	82.88(6)

Symmetry codes: #1 = x, y, z+1; #2 = x, y, z-1

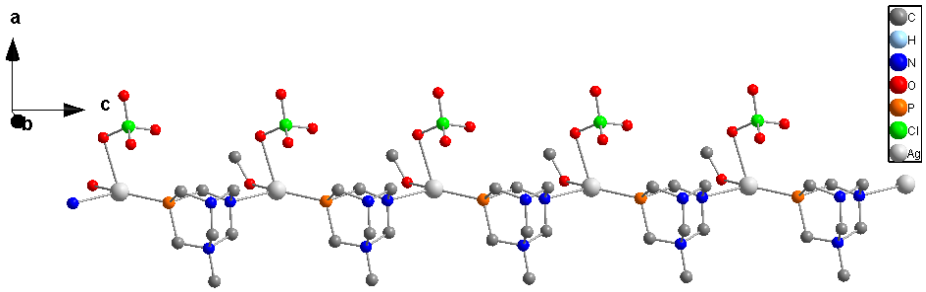

Figure 65: Polymeric representation of **m-CP$_1$** rotated along the crystallographic *b* axis

Figure 65 shows the coordination chain of **m-CP$_1$** which has a linear 1D chain-like structure with a repeating Ag to Ag distance of 7.1173(2) Å equivalent to the '*c*' cell dimension. PTAMe is coordinated to Ag through *P*-, *N*- coordination mode and forms the backbone of the of the propagating chain. The coordinated perchlorate and the methanol moieties, just like the PTAMe moieties, are perfectly aligned with each other.

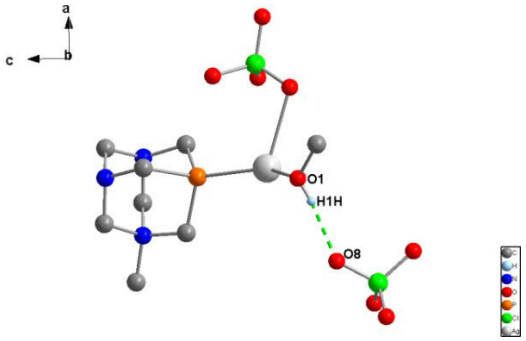

Figure 66: Intermolecular O-H…O hydrogen bonding between the uncoordinated perchlorate and methanol (dashed green lines) in **m-CP$_1$**. All methylene and methyl hydrogen atoms have been omitted for clarity.

Figure 66 depicts the O-H…O hydrogen bonding present in **m-CP$_1$**. In the crystal structure of **m-CP$_1$**, the coordinated methanol acts as a hydrogen donor [O(1)- H(1H) 0.80 Å] and links with the uncoordinated perchlorate which acts as the hydrogen acceptor [H(1H)…O(8) 1.95 Å]. The donor-acceptor distance is 2.750 Å and the O(1)-H(1H)…O(8) angle is 172°. Other intermolecular interactions that contribute to stabilizing the crystal lattice are listed in Table 34 while Figure 67: andFigure 68 shows the intermolecular C-H…O hydrogen bonding network and the crystal packing diagram of **m-CP$_1$**, respectively.

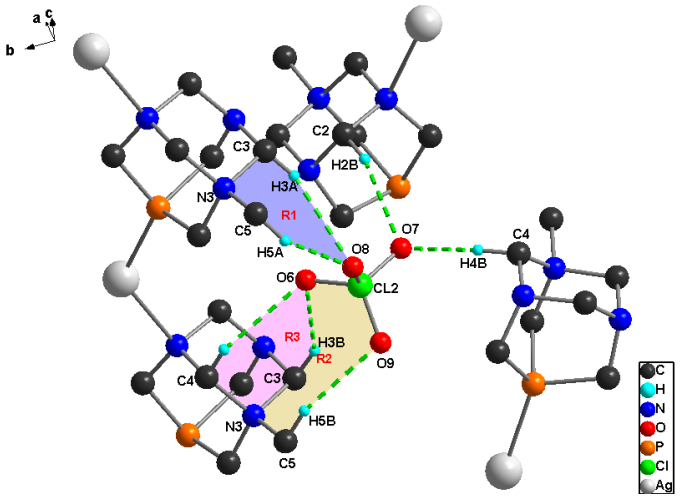

Figure 67: Intermolecular C-H…O hydrogen bonding network observed in **m-CP$_1$**. R1, R2 and R3 represent graph-set descriptions $R_2^1(6)$, $R_2^2(12)$ and $R_2^1(6)$, repectively

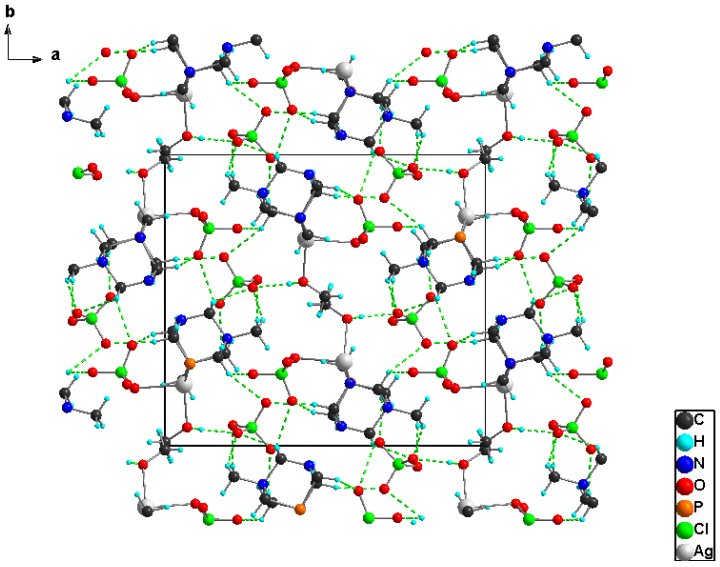

Figure 68: Representation of hydrogen bonding patterns forming a three dimensional supramolecular structure of **m-CP$_1$** shown along the crystallographic *c*-axis

The PTAMe molecules link up with oxygen atoms of the uncoordinated perchlorate molecule through C-H…O hydrogens bonds. In linking the molecules in this manner, a six membered ring, an eight membered ring and another six membered ring that can be described by the graph-set notations $R_2^1(6)$, $R_2^2(12)$ and $R_2^1(6)$ are formed as depicted in Figure 67: labelled R1, R2, and R3, respectively. The oxygen atom of the uncoordinated perchlorate molecule links up with PTAMe moieties of separates 1D molecules via C-H…O hydrogen bonding to form a 3D supramolecular structure as shown as Figure 68.

Table 34: Selected hydrogen bonding parameters in **m-CP$_1$**

D-H…A	d(D-H)	d(H…A)	d(D…A)	<(DHA)
C(2)-H(2B)...O(7)	0.99	2.54	3.490(2)	161
C(3)-H(3A)...O(8)#1	0.99	2.56	3.490(2)	144
C(3)-H(3B)...O(6)#2	0.99	2.53	3.396(3)	146
C(4)-H(4A)...O(6)#2	0.99	2.55	3.418(3)	146
C(4)-H(4B)...O(7)#3	0.99	2.54	3.433(2)	151
C(5)-H(5A)...O(8)#1	0.99	2.48	3.356(3)	148
C(5)-H(5B)...O(9)#2	0.99	2.47	3.393(2)	157

Symmetry codes: #1 = 1-x, 2-y, z- ½; #2 = 1-x, 2-y, ½ +z; #3 = x- ½, ^{3}/$_2$ -y, z

3.2.3.2 Crystal structure of [Ag(μ_2-PTAMe)(NO_3)(CH_3OH)]$_n$(NO_3)$_n$ (m-CP$_2$)

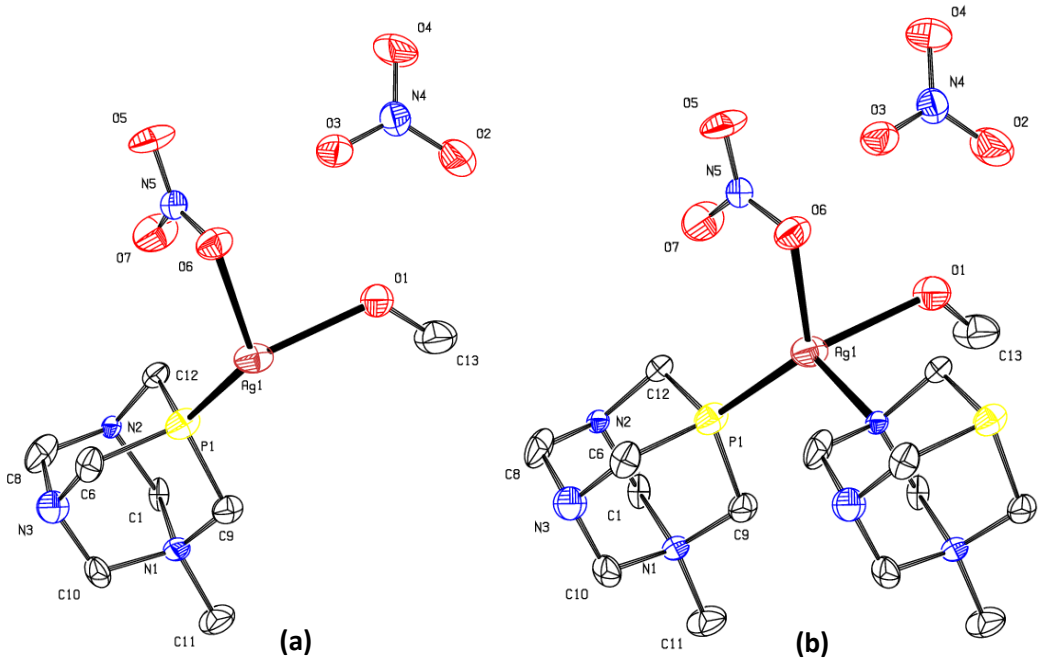

Figure 69: *ORTEP* diagram for (a) the asymmetric unit and (b) a repeating fragment of **m-CP$_2$**. All hydrogen atoms have been omitted for clarity and ellipsoids are drawn at 50% probability level.

Coordination compound **m-CP$_2$** crystallizes in the orthorhombic $P2_12_12_1$ space group. Figure 69(a) and (b) show the thermal ellipsoid plot of the asymmetric unit and the repeating unit of **m-CP$_2$** while the important bond parameters are listed in Table 35. The asymmetric unit consists of the unit [Ag(NO_3)(CH_3OH)(PTAMe)] and an uncoordinated nitrate anion making **m-CP$_2$** a salt complex. The repeating unit contains one Ag atom, two PTAMe molecules, a methanol molecule, and two nitrate molecules, one coordinating and the other non-coordinating. The coordination to the Ag atom is via a phosphorus atom and nitrogen atom of separate PTAMe moieties, an oxygen atom of the methanol molecule and another oxygen atom of the nitrate molecule. The silver metal centre has a distorted tetrahedral geometry with bond angles around the Ag(I) atom lying between 85.1(3)° and 131.9(2)°. The Ag(1)-P(1), Ag(1)-N(2), Ag(1)-O(1) and Ag(1)-O(6) bond distances are 2.344(2) Å, 2.434(6) Å, 2.341(9) Å and 2.447(7) Å, respectively.

Table 35: Selected bond parameters of **m-CP$_2$**

O(1)-Ag(1)	2.341(9)	P(1)-Ag(1)	2.344(2)
O(6)-Ag(1)	2.447(7)	Ag(1)-N(2)#1	2.434(6)
O(1)-Ag(1)-P(1)	131.9(2)	O(1)-Ag(1)-O(6)	85.1(3)
O(1)-Ag(1)-N(2)#1	89.7(3)	P(1)-Ag(1)-O(6)	127.81(19)
P(1)-Ag(1)-N(2)#1	118.95(14)	N(2)#1-Ag(1)-O(6)	91.2(2)

Symmetry codes: #1 = x+1, y, z

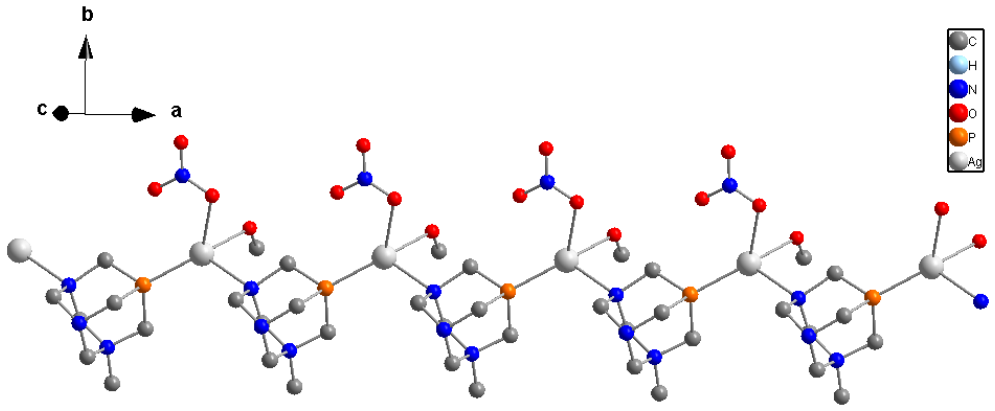

Figure 70: Polymeric representation of **m-CP$_2$** rotated along the crystallographic *c*-axis

Figure 70 depicts the polymeric representation of **m-CP$_2$**. The coordination polymer has a 1D chain-like structure with a repeating period of 7.1173(2) Å between two Ag atoms which

is equivalent to the '*a*' dimension of the unit cell. The polymer propagates along the crystallographic *a*-axis; which is made possible by the alternating *N*-, *P*-coordination mode of PTA and this forms the backbone of the polymer.

The structure of the polymer and coordination environment of Ag(I) atoms in **m-CP$_2$** is similar to that of **m-CP$_1$.** In both cases, the crystal system is orthorhombic, both are one dimensional cationic coordination polymers with anions balancing the charged polymer and that one of the oxy-anion is coordinated to the Ag(I) metal centre along with the solvent molecule. The difference between the two polymeric compounds is that **m-CP$_1$** has a space group of $Pna2_1$ and grows along the crystallographic *c*- axis, whilst **m-CP$_2$** has a space group of $P2_12_12_1$ and grows along the crystallographic *a*-axis.

Table 36: Selected hydrogen bonding parameters in **m-CP$_2$**

D-H…A	d(D-H)	d(H…A)	d(D…A)	<(DHA)
C(6)-H(6A)...O(5)#1	0.99	2.56	3.4572(8)	151
C(9)-H(9A)...O(2)#2	0.99	2.30	3.1888(7)	149
C(9)-H(9B)...O(3)#3	0.99	2.45	3.2754(7)	140
C(10)-H(10A)...O(5)#4	0.99	2.52	3.4311(8)	153
C(10)-H(10B)...O(7)#1	0.99	2.40	3.3316(8)	156
C(11)-H(11C)...O(4)#1	0.99	2.52	3.4495(8)	159
C(13)-H(13A)...O(4)#3	0.99	2.51	3.3427(8)	143

Symmetry codes: #1 = x, 1+y, z; #2 = x- ½, ³⁄₂ -y, -z; #3 = x -1, y, z; #4 = 1+x, 1+y, z

Table 36 lists the hydrogen bonding parameters observed in the crystal structure of **m-CP$_2$** while Figure 71 andFigure 72 shows the hydrogen bonding patterns observed and the crystal packing diagram of **m-CP$_2$**, respectively. The hydrogen atom of the PTAMe moiety link up with oxygen atoms of the coordinated nitrate molecules through C-H…O hydrogens bonding to form a 10-membered ring and an 8-membered ring that are described by the graph-set notations $R_2^1(10)$ and $R_2^1(8)$ as depicted in Figure 71 (R1 and R2, respectively). The hydrogen atoms of the methyl group of the methanol moiety interacts with the oxygen atoms of the uncoordinated nitrate molecule which are linked up with and hydrogen atoms of PTAMe moieties of separate 1D chain-like coordination polymers through C-H…O hydrogen bonds. This forms other 10-membered and 8-membered rings that are described by the

graph-set notations $R_2^1(10)$ and $R_2^1(8)$ as shown in Figure 71 as R3 and R4, respectively. The C-H…O hydrogen bonding interactions between the PTAMe groups and the nitrate moieties sew the neighbouring 1D chain-like coordination polymers together to form stacked 2D corrugated sheet-like supramolecular structures as shown in Figure 72.

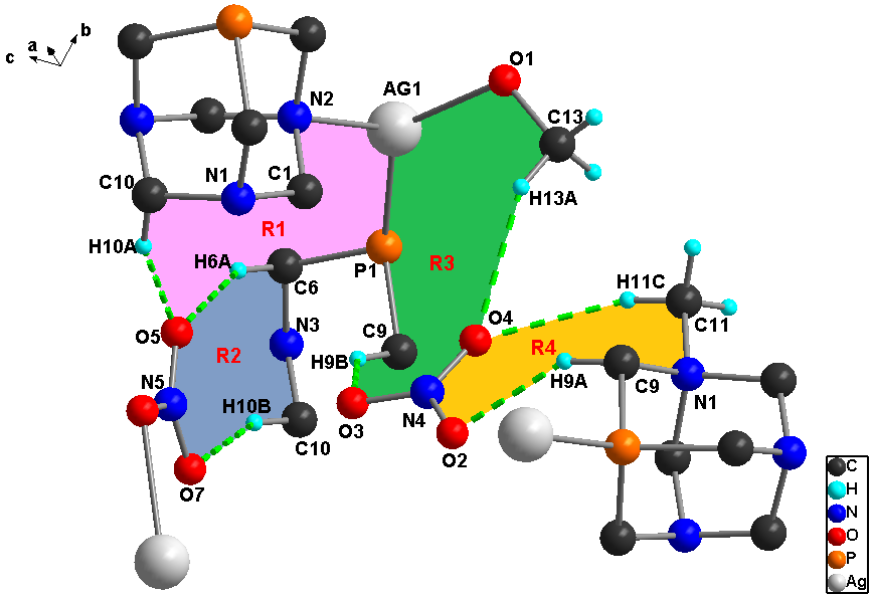

Figure 71: Hydrogen bonding network observed in **m-CP$_2$**. R1, R2, R3 and R4 represent graph-set descriptions $R_4^4(16)$ and $R_6^6(20)$, repectively.

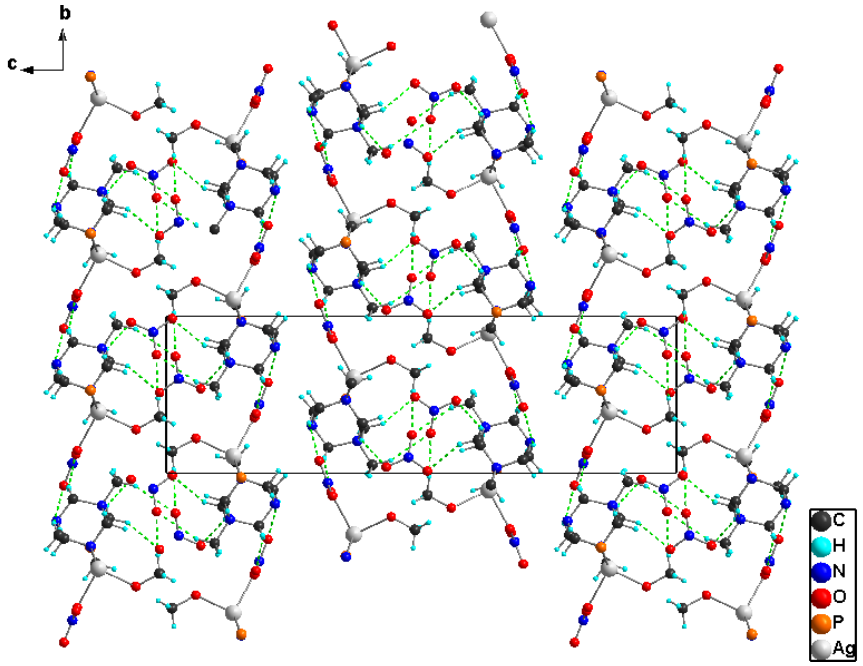

Figure 72: Representation of hydrogen bonding patterns forming stacked two dimensional supramolecular molecules of **m-CP$_2$** shown along the crystallographic *a*-axis

3.2.3.3 Crystal structure of $[Ag_2(\mu^2\text{-}O_2CCF_3)(\mu^1\text{-}O_2CCF_3)(PTAMe)]_n$ (m-CP_3)

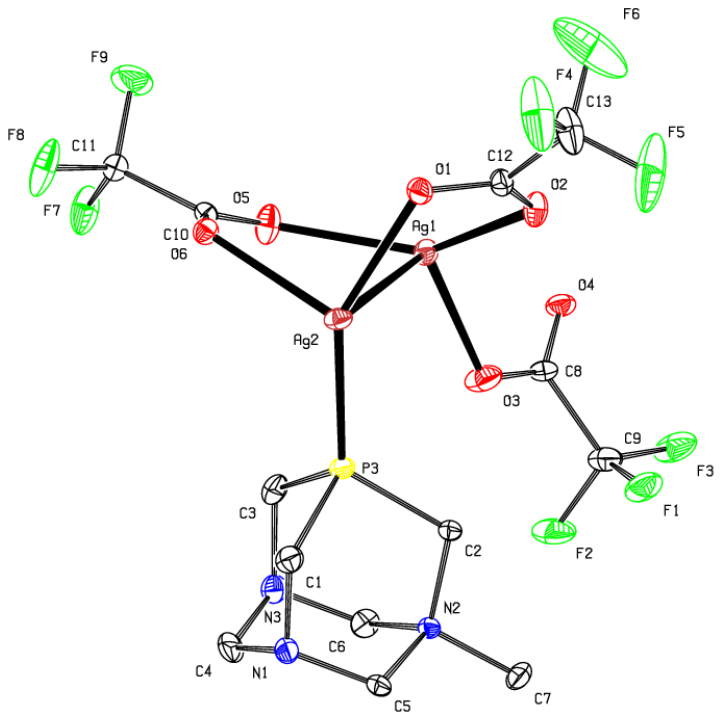

(a)

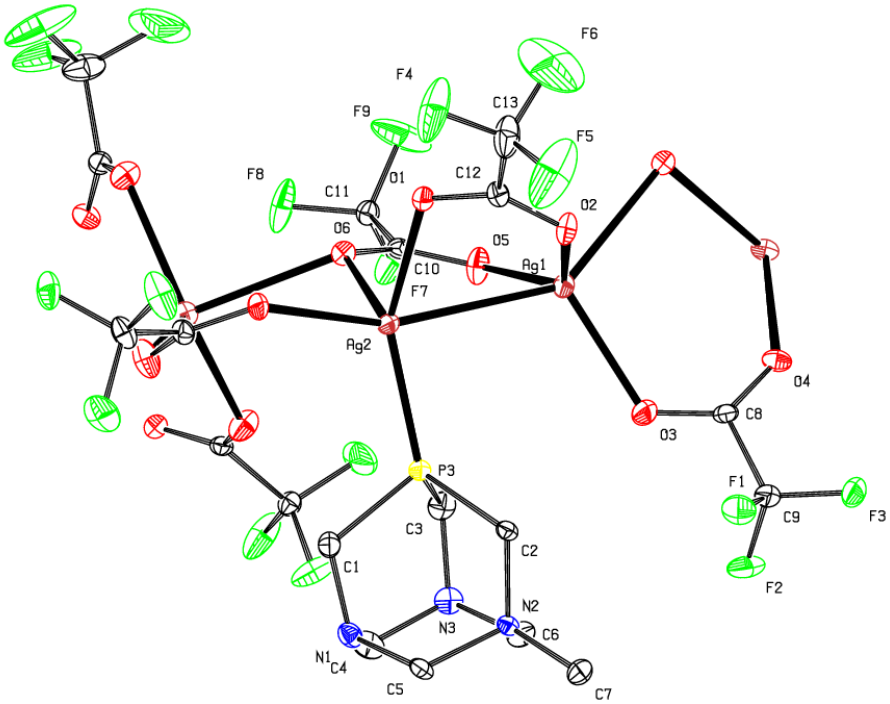

(b)

Figure 73: *ORTEP* diagram for (a) the asymmetric unit and (b) a repeating fragment of **m-CP_3**. All hydrogen atoms have been omitted for clarity and ellipsoids are drawn at 50% probability level.

The asymmetric unit of **m-CP$_3$** is shown in Figure 73(a) and it contains a unit [Ag_2(PTAMe)(O_2CCF_3)$_3$]. Figure 73(b) show the *ORTEP* diagram of a repeating unit while Table 37 lists important bond angles and distances of **m-CP$_3$**. The complete molecule is generated by the symmetry code: x, 1-y, z+ ¼. The repeating unit contains three Ag atoms, one PTAMe molecule, and four trifluoroacetate molecules. Figure 73(b) also reveals that the Ag atoms have different coordination environments. Ag(1) is coordinated to oxygen atoms of three separate trifluoroacetate molecules and has a distorted tetrahedral geometry. The bond angles around the Ag(I) atom lie between 109.35(5)° and 135.75(5)°. The Ag(1)-O(2), Ag(1)-O(3), Ag(1)-O(5) and Ag(1)-O(6) bond distances are 2.3645(14) Å, 2.3205(14) Å, 2.3123(14) Å and 2.607(3) Å, respectively. Ag(2) is coordinated to a phosphorus atom of a PTAMe molecule and oxygen atoms of three separate trifluoroacetate molecules. Ag(2) has a distorted tetrahedral geometry with the bond angles around the Ag(2) centre lying between 82.60(5)° and 147.79(3)°. The Ag(2)-P(3), Ag(2)-O(1), Ag(2)-O(4) and Ag(2)-O(6) bond distances are 2.3298(5) Å, 2.2769(14) Å, 2.4034(12) Å and 2.3189(13) Å, respectively. The trifluoroacetate molecules have two bridging modes, μ^1-O_2 and μ^2-O_2, which appear to be in alternating segments throughout the coordination polymer. In the two bridging modes μ^1-O_2 and μ^2-O_2, the Ag…Ag separations are 3.8237(2) Å and 2.94092(19) Å. The latter is shorter than the sum of the van der Waals radii for silver (3.44 Å); signifying that the existence of silver-silver interactions.

Table 37: Selected bond parameters of **m-CP$_3$**

O(2)-Ag(1)	2.3645(14)	O(4)-Ag(2)	2.4034(12)
O(3)-Ag(1)	2.3205(14)	O(6)-Ag(2)#1	2.3189(13)
O(5)-Ag(1)	2.3123(14)	P(3)-Ag(2)	2.3298(5)
O(6)-Ag(1)	2.607(3)	O(1)-Ag(2)	2.2769(14)
O(5)-Ag(1)-O(3)	112.91(6)	O(6)#2-Ag(2)-P(3)	111.73(4)
O(5)-Ag(1)-O(2)	109.35(5)	O(1)-Ag(2)-O(4)	94.94(5)
O(3)-Ag(1)-O(2)	135.75(5)	O(6)#2-Ag(2)-O(4)	96.33(5)
O(1)-Ag(2)-O(6)#2	82.60(5)	P(3)-Ag(2)-O(4)	111.10(3)
O(1)-Ag(2)-P(3)	147.79(3)		

Symmetry codes: #1 = x, 1-y, z+ ¼; #2 = 1-x, y, z- ¼

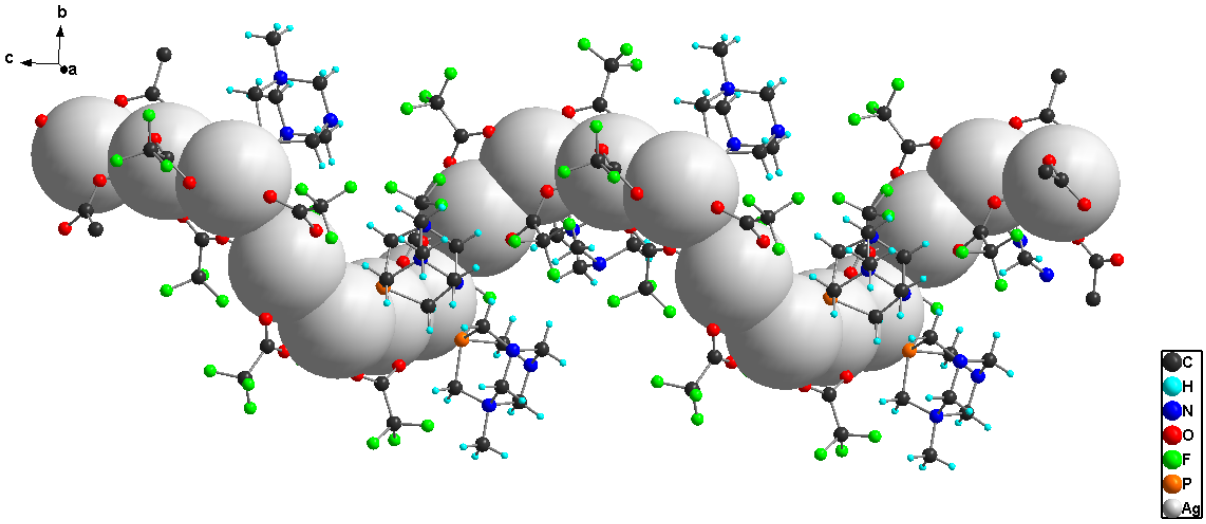

Figure 74: Polymeric representation of m-CP_3 rotated along the crystallographic *a*-axis. The Ag atoms are represented in the space-filling model

Figure 74 shows the polymeric representation of **m-CP_3**. The coordination polymer has a 1D coil-like molecular structure propagating along the crystallographic *c*-axis. The growth of the polymer is caused by the alternating μ^1-O and μ^2-O_2 bridging modes of the trifluoroacetate groups. **m-CP_3** has a spiral backbone with the PTAMe exhibiting a *P*- coordination mode.

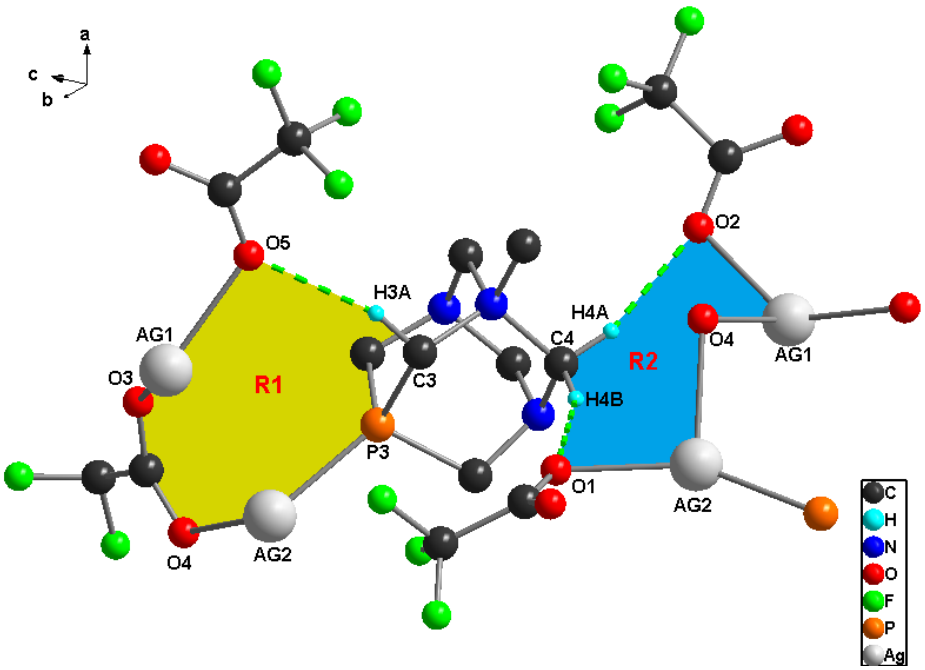

Figure 75: C-H…O hydrogen bonding network observed in **m-CP_3**. R1 and R2 represent graph-set descriptions $R_1^1(9)$ and $R_2^2(8)$, repectively.

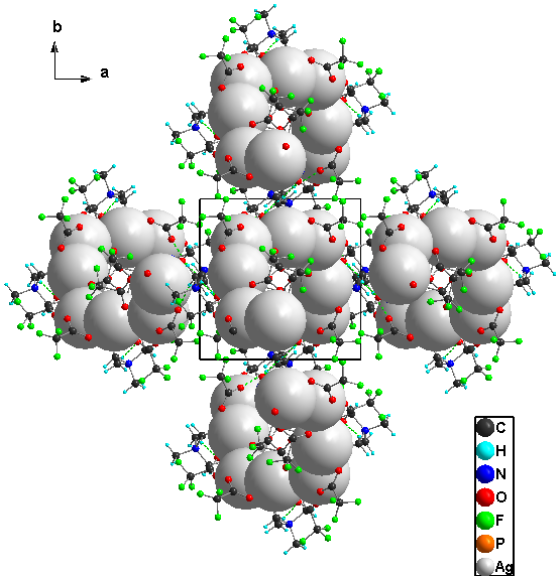

Figure 76: Representation of hydrogen bonding patterns forming a three dimensional supramolecular structure of **m-CP$_3$** shown along the crystallographic *c*-axis**.** Ag atoms are displayed in the space-filling model

Table 38 lists the selected hydrogen bonding parameters in **m-CP$_3$** while Figure 75 andFigure 76 depicts the hydrogen bonding patterns and the crystal packing diagram, respectively. The hydrogen atom of the PTAMe moiety link ups with an oxygen atom of the trifluoroacetate moiety through intramolecular C-H…O hydrogen bonds. This forms a nine membered ring that can be described by the graph-set notation $R_1^1(9)$ as shown in Figure 75 as R1. The hydrogen atoms of the PTAMe moieties also link up with oxygen atoms of two separate trifluoroacetate moieties of a neighbouring coil-like coordination polymer through intermolecular C-H…O hydrogen bonds. In linking the molecules in this manner, an eight membered ring is formed and can be described by the graph-set notation $R_2^2(8)$ depicted in Figure 75 as R2. The PTAMe molecules not only take part in intramolecular hydrogen bonding but they are also involved in intermolecular hydrogen bonding. The latter sews the neighbouring 1D coil-like molecules together to form a 3D supramolecular structure as shown in Figure 76.

Table 38: Selected hydrogen bonding parameters in **m-CP$_3$**

D-H…A	d(D-H)	d(H…A)	d(D…A)	<(DHA)
C(3)-H(3A)...O(5)#1	0.99	2.30	3.192(2)	149
C(4)-H(4A)...O(2)#2	0.99	2.29	3.249(2)	164
C(4)-H(4B)...O(1)#3	0.99	2.46	3.395(2)	157

Symmetry codes: #1 = x, 1+y ,z; #2 = x- ½ , ^{3}/$_2$-y, -z; #3 = x-1, y, z; #4 = x+1, y+1, z

3.3 References

[1] a) A. Lis, M. F. t. C. Guedes da Silva, A. M. Kirillov, P. Smoleński and A. J. L. Pombeiro, *Crystal Growth & Design* **2010**, *10*, 5244-5253; b) A. M. Kirillov, S. W. Wieczorek, M. F. C. Guedes da Silva, J. Sokolnicki, P. Smoleński and A. J. L. Pombeiro, *Crystal Engineering Communicatio* **2011**, *13*, 6329; c) P. Smolenski, S. W. Jaros, C. Pettinari, G. Lupidi, L. Quassinti, M. Bramucci, L. A. Vitali, D. Petrelli, A. Kochel and A. M. Kirillov, *Dalton Transactions*, **2013**, *42*, 6572-6581.

[2] F. Tisato, L. Crociani, M. Porchia, P. D. Bernardo, F. Endrizzi, C. Santini and R. Seraglia, *Rapid Communications in Mass Spectrometry* **2013**, *27*, 2019-2027.

[3] M. P. Nadler in *Thermal degradation study of IM7/DMBZ-15 high temperature composite by TGA/FTIR (U)*, *Vol.* (Ed. C. F. Markarian), Naval Air Warfare Center Weapons Division China Lake, CA 93555-6100, China Lake,, **2003**.

[4] a) CSD version 5.35 updates (May 2014); b)C.C.D. Centre in *Vista - A Program for the Analysis and Display of Data Retrieved from the CSD*, *Vol.* Cambridge Crystallographic Data Centre, England, **1994**; c) I. J. Bruno, J. C. Cole, P. R. Edgington, M. Kessler, C. F. Macrae, P. McCabe, J. Pearson and R. Taylor, *Acta Crystallographica Section B* **2002**, *58*, 389-397.

[5] a) M. Porchia, F. Benetollo, F. Refosco, F. Tisato, C. Marzano and V. Gandin, *Journal of Inorganic Biochemistry* **2009**, *103*, 1644-1651; b) A. M. Kirillov, P. Smoleński, M. F. C. Guedes da Silva and A. J. L. Pombeiro, *European Journal of Inorganic Chemistry* **2007**, *2007*, 2686-2692.

[6] É. Fournier, A. Decken and Pierre D. Harvey, *European Journal of Inorganic Chemistry* **2004**, *2004*, 4420-4429.

[7] C. A. Hollis, S. R. Batten and C. J. Sumby, *Crystal Growth & Design* **2013**, *13*, 2350-2361.

Chapter 4

4 Conclusion

The synthesis of Ag-PTA and Ag-PTAMe coordination compounds using various silver(I) salts was successfully confirmed using spectroscopy and spectrometry techniques. Studies on solution and solid state characterization of Ag-PTA and Ag-PTAMe coordination compounds have been done using a variety of methods such as NMR, IR, ESI-MS, TGA/DSC and SC-XRD.

4.1 Solution NMR studies of Ag-PTA and Ag-PTAMe coordination compounds

The N-C**H**$_2$-N protons observed in the ^{1}H NMR results exhibited AB type spin as a consequence of the hydrogen bonding interactions with D_2O and the coordination of Ag onto the nitrogen atoms of PTA. In the latter case, the N-C**H**$_2$-N protons became more non-equivalent and this is observed for Ag-PTA coordination polymers and coordination networks. The P-C**H**$_2$-N protons of Ag-PTA coordination compounds have $^2J_{P\text{-}H}$ values which are lower than that of free PTA. This implied that the phosphorus atom of PTA is coordinated to the Ag metal. This is supported by the change in the chemical shift of the phosphorus peak to higher frequencies observed in the ^{31}P NMR spectra. The phosphorus peak also appears as a broad singlet with suppression of Ag-P spin-spin coupling which is typical of silver monophosphine coordination compounds. The ^{13}C NMR results showed no significant information with regards to coordination of PTA onto silver atom except for cases whereby the presence of the anion is evident. The variation of the anion has an effect on the NMR results and this could be based on the electronic properties of the anion.

The ^{1}H NMR results of Ag-PTAMe coordination compounds revealed that PTAMe has a decreased molecular symmetry of the PTA moiety when compared to the parent compound and that the methylene protons of PTAMe are non-equivalent and diastereotropic. The separation between the diastereotropic N-C**H**$_2$-N protons increased and resonated more

downfield, signifying that the N-C**H**$_2$-N protons have become even more non-equivalent. This suggests that coordination via the PTAMe's nitrogen atom to the silver(I) metal centre has been achieved in silver-PTAMe coordination compounds. The P-C**H**$_2$-N$^+$ protons resonated further downfield and appeared as a singlet. The peak for phosphorus in ^{31}P NMR results resonated at a much higher frequency and appeared as a broad singlet. This suggests that the phosphorus atom of the PTAMe unit is coordinated to Ag metal as observed for the Ag-PTA coordination compounds. The variation of the anion appears to have no effect on the solution NMR results of Ag-PTAMe coordination compounds.

4.2 IR and ESI-MS studies of Ag-PTA and Ag-PTAMe coordination compounds

The IR spectra of all Ag-PTA and Ag-PTAMe coordination compounds exhibited related features with typical vibrations due to the anions and the main ligand; therefore IR results provided evidence for the presence of the anion and the main ligand in the coordination compounds.

ESI-MS results contained m/z peaks that were attributed to the product despite the fragmentation of the polymeric species and formation of multiple charged ionic species with either solvent, sodium or potassium adducts.

4.3 Thermal property studies of Ag-PTA and Ag-PTAMe coordination compounds

Some new findings that arose from the thermal property studies (TGA and DSC) include:

- Dihydrated coordination compounds (**DCC$_1$** and **CP$_2$**) experience the loss of water molecules at 78 °C and 70 °C, respectively. The loss of water molecules in both **DCC$_1$** and **CP$_2$** occured as endothermic events with ΔH values of 172 kJ mol^{-1} and 92.5 kJ mol^{-1}, respectively. **CN$_1$** contains a coordinated water molecule which was lost at a higher temperature (121 °C).

- Ag-PTA coordination compounds are thermally stable up to approximately 210 °C and beyond this threshold an exothermic event occurs which is attributed to the decomposition of the Ag-PTA complex and the loss of PTA. Similar TGA and DSC profiles were obtained for Ag-PTAMe coordination compounds although they decomposed at a lower temperature range (194-202 °C).

4.4 Solid state structural analysis of Ag-PTA and Ag-PTAMe coordination compounds

The use SC-XRD aided in the investigation of the influence of anions on the topology of molecular architectures with a detailed look at hydrogen bonding, weak intermolecular interactions and co-crystallization in silver(I)-PTA and silver(I)-PTAMe complexes. The various overall structures of Ag-PTA and Ag-PTAMe are summarized in Table 39 from which general trends were observed.

Table 39: Overall structures of Ag-PTA and Ag-PTAMe compounds containing various anions

Ag-PTA complexes	Anion	Overall structure
DCC_1	CN^-	Discrete complex
DCC_2	CO_3^-	Discrete complex
CP_1	NO_3^-	1D linear coordination polymer
CP_2	$O_2CCH_3^-$	1D ladder-like coordination polymer
CP_3	$O_2CCF_3^-$	1D ladder-like coordination polymer
CP_4	ClO_4^-	1D zig-zag coordination polymer
CP_5	ClO_4^-	1D branched coordination polymer
CN_1	NO_3^-	2D corrugated sheet-like network
CN_2	$O_3SCF_3^-$	2D corrugated sheet-like network
CN_3	NO_3^-	2D planar sheet-like network
Ag-PTAMe compounds		
m-CP_1	ClO_4^-	1D linear coordination polymer
m-CP_2	NO_3^-	1D linear coordination polymer
m-CP_3	$O_2CCF_3^-$	1D coil-like coordination polymer

Ag-PTA and Ag-PTAMe compounds containing carboxylate anions tend to result in polymeric structures with the carboxylate group having either μ^1-O_1 or μ^2-O_2 bridging modes which resulted in the formation of 1D ladder-like or coil-like structures. The nitrate anion displayed a wide variety of coordination modes which led to the formation of 1D linear coordination polymers and 2D sheet-like networks. For Ag-PTA complexes, triflate and perchlorate anions displayed very weak coordination abilities; hence they are present in the outer coordination sphere. The crystal structures of Ag-PTA and Ag-PTAMe coordination

compounds contained iintermolecular hydrogen bonding interactions. These interactions played a vital role in completing the lattice stabilization and formation of multi-dimensional supramolecular architectures.

4.5 Recommendations and future work

Most of Ag-PTA and Ag-PTAMe compounds contain free, uncoordinated nitrogen atoms which can be used to introduce a second metal to the compound to form heterometallic coordination entities. The synthesized compounds can also be investigated for their anti-microbial activity since silver compounds are well known for their biological activity.